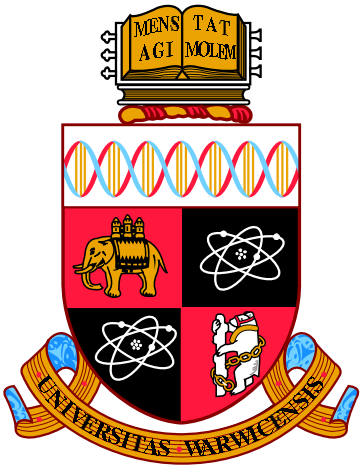

Wave turbulence in Rotating and Non-rotating Magnetohydrodynamics

by

Nicholas Kiran Bell

Thesis

Submitted to the University of Warwick

for the degree of

Doctor of Philosophy

Mathematics Institute

September 2018

THE UNIVERSITY OF WARWICK

Contents

List of Figures

Acknowledgments

Firstly, I would like to thank my PhD supervisor Sergey Nazarenko for his exemplary guidance and support over the last few years in addition to his continued hospitality and generosity. I cannot mention every person with whom I have had useful conversations over the last four years, but special thanks go to my collaborators Vladimir Grebenev and Sergey Medvedev.

The numerous conferences and international trips have been some of the most enjoyable aspects of my PhD. These would not have been nearly as enjoyable without the company of Jonathan Skipp and Adam Griffin, so thanks to them.

I would like to thank my Mum, Dad and brother for all they have done for me and for their constant support. Finally, I would like to express my gratitude to Cathy for all of her love and for always giving me something to look forward to after a day studying turbulence.

Declarations

This thesis is submitted to the University of Warwick as per the requirements for the degree of Doctor of Philosophy. It has not been submitted for a degree at another institution. I declare that the work contained within is my own except where stated otherwise.

Chapters 1 and 2 contain no original work but provide context and foundational understanding of wave turbulence and magnetohydrodynamics. Chapter 3 is original work by myself, Vladimir Grebenev, Sergey Medvedev and Sergey Nazarenko published in [6]. Chapter 4 is original work by myself and Sergey Nazarenko and is published in [7]. The beginning of Chapter 5 follows and reproduces work by Galtier [24]. From Section 5.3.3 onwards, the work is my own. This is currently being prepared for publication.

Abstract

In this thesis Magnetohydrodynamics (MHD) is considered within the framework of wave turbulence (WT). I open with an introduction to MHD and turbulence theory before providing the fundamental theory for WT - including a worked example of the main steps in a WT derivation.

In non-rotating MHD, the system exhibits Alfvén waves. A WT theory for Alfvén waves is well known and results in a prediction for the wave action spectrum in a steady state, $n(k_\perp) \sim k_\perp^{-3}$. In the first part of this thesis, the evolution of the spectrum preceding the formation of the steady state is studied. It is postulated that the evolution of the spectrum proceeds as a three step process. In the first stage, the spectrum forms a front which propagates from small to large wave numbers. In the second stage there is a reflected wave from large to small wavenumbers which leaves the KZ spectrum in its wake.

The first stage of the development of the KZ spectrum is studied here first. This stage is understood to occur via self-similar solutions of the kinetic equation. In infinite capacity systems such as MHD, the self-similarity is of the second kind. In this case, the similarity can not be fixed by conservation laws as for the first kind, but is instead found from the solution of an eigenvalue solution. The problem is reformulated into a nonlinear eigenvalue problem which is investigated analytically and numerically.

Next the second stage is investigated. Again the solution is expected to be self-similar in nature. However now the similarity is fixed neither by conservation laws or by solving a nonlinear eigenvalue problem. Instead they are determined by imposed asymptotics at one end of the similarity interval. These solutions are studied numerically by devising a numerical method to find the correct form of the spectrum at this stage.

The final part of this thesis concerns rotating MHD turbulence. First the theory is introduced including the weak and strong turbulence predictions. These are then compared with numerical simulations of the governing equations. Finally the kinetic equation is examined to discuss coupling of waves.

Chapter 1

Introduction

1.1 Magnetohydrodynamics

Magnetodydrodynamics (abbreviated to MHD from herein) is the study of the dynamics of electrically conducting fluids in the presence of a magnetic field. Such a framework has proven useful in describing a wide range of astrophysical fluids including accretion disks, planetary cores and the solar wind. The field of MHD descends from the 1972 work of Hannes Alfvén [2] for which he was awarded the Nobel Prize in 1970. In his original letter he identified the magnetohydrodynamical waves which take his name and which form the basis for much of this thesis. These Alfvén waves propagate in the direction of the magnetic field at a speed known as the Alfvén velocity given by $v_A = B_0/\sqrt{4\pi\rho_0}$ and the oscillations occur transverse to the magnetic field. In the definition of the Alfvén velocity, B_0 is the background magnetic field and ρ_0 is the uniform density. Alfvén made his discovery while studying sunspots. He noticed that the current and the magnetic field present in the plasma comprising the sunspot must influence the motion of the plasma. From this observation and some simplifications of the physics (homogeneous magnetic field, infinite conductivity, permittivity and permeability of one), Alfvén combined Maxwell's equations of electromagnetism with the equations of motion. Thus MHD was born.

Despite the later impact of Alfvén's work, it was not immediately accepted. The lack of experimental evidence supporting the existence of Alfvén waves was one obstacle to recognition. The theoretical derivation of the waves was performed in the ideal limit of infinite conductivity. In the opposite limit of zero conductivity, the fluid motion will simply have no impact on the magnetic field. These limits can be considered here in terms of the non-dimensional Lundquist number $S = 4\pi v_A L\sigma/c^2$ where L is a typical length scale and σ is the conductivity of the fluid.

The appearance of the length scale is explained by the Biot-Savart law in which the magnetic field induced by a current is proportional to the size of the region. In the perfect limit of infinite conductivity (and infinite Lundquist number) the magnetic field is said to be "frozen" into the the fluid such that the magnetic field and the fluid move with one another. High Lundquist numbers are ubiquitous amongst astrophysical plasmas, but replicating them in laboratories was initially challenging and thus producing the conditions for Alfvén waves was difficult.

Early experiments were performed by Lundquist [43] with mercury. However, due to the low conductivity of mercury the Lundquist number in the experiments was unable to surpass unity. This limitation rendered pronounced Alfvén waves impossible, although interactions between the magnetic field and the hydrodynamic motion were observed, giving credence to Alfvén's methodology if not his outcome. In 1954, Bo Lehnert managed to produce Alfvén waves using liquid sodium at a Lundquist number of 40 [39]. Due to the still modest Lundquist number, his waves were strongly damped but they still retained satisfactory agreement with the Alfvén wave theory.

The equations derived by Alfvén are now known as the MHD equations. The MHD equations may be derived by combining Maxwell's equations, Ohm's Law, a gas law and the equations of mass continuity and motion of a regular fluid. Doing so requires making some assumptions on the plasma which leads to three conditions of applicability [66]:

1. The plasma must be strongly collisional so that the time scale on which collisions occur is shorter than any other characteristic time scale of the system and so the particles are in a state close to the Maxwell-Boltzman distribution.

2. The resistivity due to these collisions is small, so that typically the magnetic diffusion occurs over a longer time than any other time scale.

3. Length scales must be longer than the ion skin depth (the depth in a plasma to which radiation can penetrate) and the Larmor radius perpendicular to the field (the radius of the circular motion of the ions), so that Landau damping is ignored. Also, time scales must be longer than the ion gyration time (the time taken for ions to rotate).

If one or more of these conditions is broken, then a more complicated description of the plasma must be used.

One example of an extension to the MHD considered in this thesis would be Hall MHD. The key difference between the various regimes of MHD is found in

Ohm's law. Ohm's law states that the current density ($\boldsymbol{j}$) is proportional to the total electric field and may be written as

$$\boldsymbol{j} = \sigma(\boldsymbol{E} + \boldsymbol{v} \times \boldsymbol{B}). \tag{1.1}$$

Under conditions 1-3 above, this version of Ohm's law is sufficient. However at length scales shorter than the ion skin depth and time scales shorted than the ion gyration time, it is necessary to consider a generalised Ohm's law in which a 'three-fluid' model of electrons, protons and ions are considered. This will not be discussed in detail here as it is outside of the scope of this thesis, but repeating the derivation of MHD using this generalised Ohm's law results in an extra term in the equations known as the Hall term. Physically, the Hall term decouples the ion and electron motions and introduces two new wave modes into the system; the whistler waves and Hall drift waves.

The full set of equations; comprising of an induction equation for the magnetic field, a momentum equation for the fluids velocity and the continuity equation which enforces incompressibility, can be written in the following form:

$$\left(\frac{\partial}{\partial t} + \boldsymbol{v} \cdot \nabla\right) \boldsymbol{v} = -\nabla P_* + \boldsymbol{b} \cdot \nabla \boldsymbol{b} + \nu \nabla^2 \boldsymbol{v} \tag{1.2}$$

$$\left(\frac{\partial}{\partial t} + \boldsymbol{v} \cdot \nabla\right) \boldsymbol{b} = \boldsymbol{b} \cdot \nabla \boldsymbol{v} + \eta \nabla^2 \boldsymbol{b}, \tag{1.3}$$

$$\nabla \cdot \boldsymbol{v} = \nabla \cdot \boldsymbol{b} = 0 \tag{1.4}$$

where P_* is the total pressure, ν is the viscosity, η is the magnetic diffusivity, $\boldsymbol{b} = \boldsymbol{B}/\sqrt{4\pi\rho_0}$ is the Alfvén velocity and ρ_0 is the uniform density of the fluid. The Alfvén velocity is the phase velocity of the Alfvén wave [11] and therefore these equations provide a natural framework in which to consider Alfvén wave turbulence, as will be done in the first part of this thesis. There exist three inviscid invariants within these equations [82], namely; the total energy

$$E^T = \frac{1}{2}\langle v^2 + b^2 \rangle, \tag{1.5}$$

the cross-helicity

$$H^C = \langle \boldsymbol{v} \cdot \boldsymbol{b} \rangle \tag{1.6}$$

and the magnetic helicity

$$H^M = \langle \boldsymbol{\mathcal{A}} \cdot \boldsymbol{b} \rangle. \tag{1.7}$$

Unlike in hydrodynamics, MHD supports a number of different types of waves in addition to the Alfvén waves already discussed. A simple but often relevant case is one in which a homogeneous plasma is embedded in a large scale mean field $\boldsymbol{B}_0$. Considering sufficiently small perturbations and linearising the equations, waves with three different dispersion relations are possible; Alfvén waves, fast magnetosonic waves and slow magnetosonic waves. Of these three types of waves, only the Alfvén waves are incompressible whereas the other two are compressible. Since our attention is focussed on incompressible plasmas, the Alfvén wave is of primary importance. Indeed under certain conditions, the two magnetosonic waves collapse onto Alfvén waves. The dispersion relation for Alfvén waves is found to be

$$\omega^2 = \omega_{\mathrm{A}}^2 = k_{\parallel}^2 b_0^2. \tag{1.8}$$

Alfvén waves propagate along the mean field $\boldsymbol{B}_0$, either in the same direction or opposing the field at a speed corresponding to the Alfvén velocity. For calculations involving waves, it is convenient to rewrite the MHD equations in terms of Elsässer fields [17]:

$$\boldsymbol{z}^s = \boldsymbol{v} + s\boldsymbol{b} \tag{1.9}$$

with $s = \pm 1$. A particularly useful property of these variables is that $\boldsymbol{z}^{-1}$ describes Alfvén waves propagating in the direction of $\boldsymbol{B}_0$ and $\boldsymbol{z}^{+1}$ describes Alfvén waves propagating opposite to $\boldsymbol{B}_0$. In these variables the induction and momentum equations can be combined leading to

$$\partial_t \boldsymbol{z}^s \mp \boldsymbol{B}_0 \cdot \nabla \boldsymbol{z}^s + \boldsymbol{z}^{-s} \cdot \nabla \boldsymbol{z}^s = -\nabla P_* \tag{1.10}$$

where the viscosity has been neglected. An interesting property can be observed from Equation (1.10). The nonlinear term permits no self-coupling between co-propagating waves but only cross-coupling between $\boldsymbol{z}^{-1}$ and $\boldsymbol{z}^{+1}$. This interaction between counter-propagating waves only, is an atypical property which ensures that the wave turbulence approach is applicable despite the fact that Alfvén waves break the general condition that waves are dispersive in wave turbulence[27].

1.2 Turbulence

1.2.1 General Turbulence

Turbulence concerns itself with the random, chaotic motion of fluids. The study of turbulence as a rigorous discipline emanates from at least 1883 and Osborne

Reynolds' famous experiments of turbulent flow [69]. Reynolds demonstrated that there are the two regimes of fluids; the steady laminar one and the turbulent one. He correctly identified the effects of fluid velocity, pipe diameter and viscosity on the transition from laminar to turbulent flow and characterised this using a non-dimensional number now known as the Reynolds number. Flows with a Reynolds number above some critical value would become turbulent whilst those below would remain laminar. The Reynolds number is still regarded as fundamental to the study of turbulence.

Even before mathematical descriptions of turbulence, the existence of chaotic fluids was recognised. In the 1500's Leonardo da Vinci produced sketches of turbulent flows showing the "eddies" present. Such eddies are characteristic of turbulent fluids. Their importance was outlined by Lewis Fry Richardson [70] and summarised by the following rhyme:

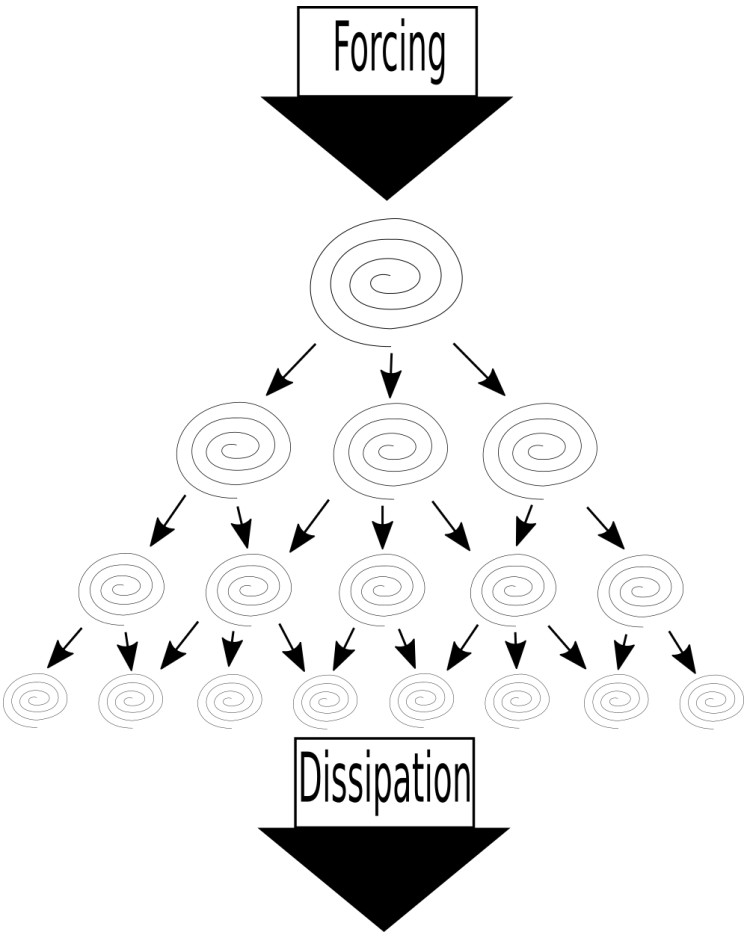

Figure 1.1: Diagrammatic representation of the Richardson Cascade. Energy is transferred from large scale to small scale until it is dissipated by the viscosity.

Big whirls have little whirls
that feed on their velocity.
Little whirls have lesser whirls
and so on to viscosity.

The idea illustrated by this rhyme is that energy is transferred across length scales from large to small eddies which continue to transfer the energy to even smaller ones. The energy, which is initially input to the system by large scale forcing, is eventually dissipated at the smallest scales by the viscosity. A diagrammatic representation is shown in Figure 1.1.

The most important discovery in the history of turbulence was by Andrei Kolmogorov and Alexander Obukhov in their now famous 1941 papers [35, 63]. Kolmogorov and Obukhov studied the Richardson cascade quantitatively. For this,

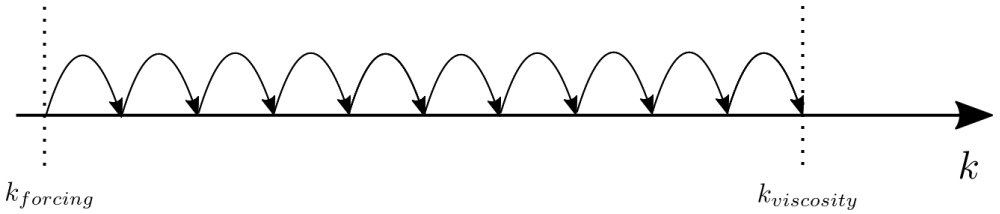

Figure 1.2: The Richardson Cascade in Fourier space. Energy is transferred from small to large wavenumbers.

the cascade is best thought of in Fourier space as in Figure 1.2. In Fourier space, the energy cascades from small wavenumbers to larger ones. Kolmogorov and Obukhov introduced the idea of an inertial range which is far from both the energy source and the energy sink, i.e. $k_{forcing} \ll k \ll k_{viscosity}$. In the inertial range, the properties of the turbulence depend only upon the energy flux and not on the details of the forcing or dissipation. This assumption follows from the one that the Richardson cascade is local, meaning that energy is transferred between eddies of similar size only.

The inertial range hypothesis allows the derivation of the one-dimensional energy spectrum $E^{(1D)}(k)$. This energy spectrum gives the amount of energy at a given wavenumber k. According to the Richardson cascade, energy is first injected into the systems at $k \sim k_{in}$ which then cascades across the inertial range at the transfer rate ϵ_t before finally being removed at the dissipation scale $k \sim k_\nu$. For stationary turbulence a constant energy flux is assumed

$$\epsilon_{in} = \epsilon_t = \epsilon_\nu \equiv \epsilon. \tag{1.11}$$

Energy is only exchanged between modes with wavenumbers of the same order of magnitude since the energy transfer is assumed to be local. Consider the average difference of velocity δv_l between two points a distance l apart. Labelling each eddy with the subscript n, the energy contained within each eddy is given by the band-integrated Fourier spectrum:

$$E_n \simeq \delta v_n^2 \simeq \int_{k_n}^{k_{n+1}} E_k \mathrm{d}k. \tag{1.12}$$

The time taken for the transfer of energy between two neighbouring scales is given by the eddy turnover time

$$\tau_n \sim l_n / \delta v_n. \tag{1.13}$$

The energy flux between the eddies can then be written as

$$E_n/\tau_n \sim \delta v_n^3/l_n \sim \epsilon, \tag{1.14}$$

which leads to the following relation

$$\delta v_n \sim \epsilon^{1/3} l_n^{1/3}. \tag{1.15}$$

Equations (1.12) and (1.14) are consistent only if

$$E_k = C\epsilon^{2/3} k^{-5/3}, \tag{1.16}$$

where $C \sim 1.6$ is called the Kolmogorov constant. This is known as the Kolmogorov-Obukhov spectrum and is one of the key results from Kolmogorov's influential works on turbulence. Equation (1.16) relies upon the assumption of self-similarity and is derived phenomenologically, with the Kolmogorov constant determined experimentally. Rigorous mathematical derivations are rare in turbulence due to the inherent complexity of the governing equations. One finding which can be derived rigorously is Kolmogorov's celebrated 4/5-law, often regarded as the strongest result in turbulence.

It may seem surprising that the strongest result in turbulence is nearly 80 years old. The reason for the slow progress in the field of turbulence is the lack of closure in the equations describing the statistical properties. In statistical mechanics a *moment* is a measure of the shape of a set of points, in this case representing the energy. The energy spectrum is the first moment but there exist an infinite number. The difficulty with these moments is that lower order moments depend upon higher order moments and no closure exists for general turbulence. This makes analytical treatment of general turbulence impossible without introducing an artificial closure.

Despite eddies being the fundamental structures in both the Richardson cascade and the Kolmogorov-Obukhov spectrum, both ideas remain fundamental for the wave turbulence theory since similar cascade states and spectra are typical for wave turbulence. In wave turbulence however, energy is transferred between waves rather than eddies.

1.2.2 Wave turbulence

Wave turbulence (WT) can be broadly defined as the "*out-of-equilibrium statistical mechanics of random nonlinear waves*" [55]. Generally speaking, WT concerns itself with waves which are weakly nonlinear and dispersive. The waves in WT take on

the role that eddies play in general turbulence displaying similar cascade states.

The history of WT goes back to Rudolph Peierls in 1929 who derived a wave kinetic equation for phonons in anharmonic crystals [64]. Early papers on WT focussed on the derivation of kinetic equations and finding solutions describing the thermodynamic equilibria. The WT ideas were applied both to plasma physics [20, 80] and water waves [10, 9, 32, 33]. It was not until 1965 when a new type of solution was found by Vladimir Zakharov corresponding to a constant energy flux through scales [83]. These solutions are analogous to the Kolmogorov spectrum, Equation 1.16 and are aptly named the Kolmogorov-Zakharov (KZ) spectra. Since the discovery of these solutions WT has been applied to a wide range of physical systems including water surface gravity and capillary waves [3, 4], inertial waves in rotating hydrodynamics [21, 8, 50], waves in superfluid helium [36, 44], waves in Bose-Einstein condensates [16, 58], and many other wave systems. MHD provides a rich zoo of linear waves, and thus wave turbulence theories are natural to derive. Indeed, Alfvén wave turbulence in incompressible MHD has been studied extensively [27, 26, 47, 54], furthermore theories for electron MHD [25] and Hall MHD [22] have been developed.

Unlike general turbulence, WT contains a natural asymptotic closure [9] which allows for an analytical treatment. The asymptotic closure arises as a result of the weakly nonlinear nature of the waves and their dispersive character. These two factors ensure that there is a separation of time scales between the short linear time scale and the longer nonlinear time scale. This separation of time scales then results in the closure used to derive expressions for the statistical moments. The success of the WT theory is that all long-time statistical behaviour can be calculated from a set of core particle densities $n(\boldsymbol{k}, t)$ and it allows the derivation of a closed kinetic equation for the evolution of this density.

1.2.3 Wave turbulence in MHD

MHD systems naturally contain a rich variety of linear waves. In a weakly nonlinear plasma, waves are the fundamental structures as in all WT theories. However, even as we depart from the weakly nonlinear condition, MHD waves may continue to coexist alongside eddies with the dynamics impacted on by both [23]. Formulating WT theories for MHD waves therefore offers great insights into the systems for which it describes. However, arriving at an Alfvén wave turbulence theory was not trivial since the waves are non-dispersive *i.e* the frequency of the waves is proportional to the wavenumber.

The scaling of the energy spectrum is an important property of both wave

turbulence and strong turbulence and so it is important to discuss the various proposals for the scaling in MHD. The Iroshnikov-Kraichnan [34, 37] picture of MHD turbulence proposes that the *Alfvén effect*, in which only counter propagating Alfvén waves interact, modifies the Kolmogorov scaling. Due to both Alfvén wave interactions and eddy distortion affecting the dynamics, there are two timescales to consider. These will be discussed here following Dobrowolny *et al,* [15]. Considering the equations in the Elsässer form (1.10), the time taken for two wave packets to interact is called the Alfvén time

$$\tau_A \sim 1/v_A. \tag{1.17}$$

This is much shorter than the eddy turnover time

$$\tau_l \sim 1/\delta z_l^{\mp}. \tag{1.18}$$

The variation in amplitude of a vortex or wave packet δz^+ due to one collision with an oppositely propagating wave packet δz^- is found from Equation (1.10) as

$$\mathrm{d}z^{\pm} \sim \tau_A \delta z^{\pm} \delta z^{\mp}/l \tag{1.19}$$

The stochastic nature of such interactions means that after N interactions, the variation in amplitude will be

$$\Delta z^{\pm} \sim \sqrt{N}\mathrm{d}z^{\pm}. \tag{1.20}$$

A considerable modification to the amplitude can be considered to have occurred once the variation is of the same order as the initial amplitude, *i.e.*

$$\Delta z^{\pm} \sim \delta z^{\pm}, \tag{1.21}$$

which using Equations (1.19) and (1.20) gives

$$N \sim \left(\frac{l}{\delta z^{\mp}}\right)^2 \tau_A^{-2}, \tag{1.22}$$

giving an energy-transfer time of

$$T_l \sim N\tau_A \sim (\tau_l^{\pm})^2/\tau_A. \tag{1.23}$$

Using this timescale in place of Equation (1.13) and continuing with the arguments

for deriving the Kolmogorov spectrum, one arrives at the Iroshnikov-Kraichnan (IK) spectrum for MHD turbulence

$$E_k = C_{IK}(\epsilon v_A)^{1/2} k^{-3/2}, \tag{1.24}$$

where C_{IK} is a constant which is expected to be different from C_K.

Both the Kolmogorov spectrum and the Iroshnikov-Kraichnan spectrum assume isotropy in their phenomenology. This means that the energy spectrum is independent of direction, or in other words modes in all directions are equally excited. The presence of a mean magnetic field has a strong effect on the turbulent properties and it is expected that rather than being isotropic, MHD turbulence should be anisotropic such that small-scale modes are primarily excited in the direction perpendicular to the magnetic field $k_\perp \gg k_\parallel$ [11].

Anisotropy was included in the Alfénic turbulence theory developed by Goldreich and Sridhar [76, 29]. In a series of two papers they considered both weak and strong wave turbulence. The two regimes can be distinguished by comparing the time period of the linear waves and the nonlinear terms. In weak wave turbulence, nonlinear effects are sub-dominant to the effects of the linear waves. Thus the linear wave period should be much shorter than the nonlinear turnover timescale:

$$\tau_l \ll \tau_{NL}. \tag{1.25}$$

I shall show later how this fact can be manipulated to allow analytical treatment of weak turbulence. Weak wave turbulence is characterised by interactions between resonant waves. Goldreich and Sridhar postulated that the 3-wave interactions which were generally accepted in Alfvén wave turbulence were empty. They therefore argue that the weak wave turbulence arises from 4-wave interactions. This was disputed by Galtier *et al* [27] who showed that the 3-wave interactions were in fact non-empty leading to the currently accepted theory for weak Alvén wave turbulence. For the discussion in this introduction it is sufficient just to note the derived energy spectrum for the stationary state

$$E(k_\parallel, k_\perp) = f(k_\parallel) k_\perp^{-2}. \tag{1.26}$$

The method with which this is derived is outlined in Chapter 2.

In order to study strong Alfvénic turbulence, Goldreich and Sridhar consid-

ered a so called *critically balanced* state between the two time scales:

$$\tau_l \sim \tau_{NL}. \tag{1.27}$$

Considering Equation (1.10), these time scales at scale l in incompressible MHD can be estimated as

$$\tau_l \sim \frac{1}{k_\parallel B_0} \qquad \text{and} \qquad \tau_{NL} \sim \frac{1}{k_\perp z_l}, \tag{1.28}$$

wit the linear time scale coming trivially from the dispersion relation of Alfvén waves, and the nonlinear time scale from assuming that the cascade occurs predominately in the perpendicular direction such that

$$k_\perp \gg k_\parallel \tag{1.29}$$

and then analysing the dimension of the nonlinear term against the time derivative. Balancing the two timescale we find that

$$z_l \sim B_0 \frac{k_\parallel}{k_\perp}. \tag{1.30}$$

Repeating the Kolmogorov derivation with $\tau_{tr} \sim \tau_l \sim \tau_{NL}$ then leads to

$$\epsilon \sim \frac{z_l^2}{\tau_{tr}} \sim k_\perp z_l^3. \tag{1.31}$$

Combining Equations (1.31) and (1.30) gives the scaling relation of the wavenumber components

$$k_\parallel \sim \frac{\epsilon^{2/3}}{B_0} k_\perp^{2/3}. \tag{1.32}$$

Equations (1.30) and (1.32) can be combined to find the energy spectrum

$$E(k_\perp) \sim \frac{z_l^2}{k_\perp} \sim \epsilon^{2/3} k_\perp^{-5/3}. \tag{1.33}$$

The critical balance argument given here remains a phenomenological one and thus lacks the analytical rigour of the weak wave turbulence approach. However it is useful in its ability to explain the energy spectra when the assumption of weak nonlinearity is not met, as is often the case in physical scenarios.

1.3 Layout of thesis

This thesis covers turbulence in both rotating and non-rotating MHD systems paying particular attention to wave turbulence. Wave turbulence theories have been developed for the non-rotating case [27] and for the rotating case [24]. This thesis builds on both of these works.

In Chapter 2 a primer in wave turbulence theory is provided. The theory will be discussed using a general model equation. This should provide the reader with a firm foundation which will be built upon in the remainder of the thesis.

Chapters 3 and 4 concern non-rotating MHD. Specifically I investigate the formation of the stationary state in Alfvén wave turbulence. This occurs in a two stage process: first there is a self-similar solution which manifests as a propagating front in spectral space; secondly once this front reaches large enough wavenumbers, there is a reflected wave which travels towards small wavenumbers leaving the stationary state in its wake. Chapter 3 will study the first stage whilst the second stage is dealt with in Chapter 4.

In Chapter 5, rotating MHD is studied building on the theoretical framework developed by Galtier [24]. The weak wave turbulence predictions are discussed and a critical balance phenomenology is developed. Both predictions are then compared to numerical simulations of the rotating MHD equations. In the final part, the kinetic equation are discussed highlighting the coupling between different types of wave.

Chapter 2

Weak Wave Turbulence

Weak wave turbulence is a mathematically complex subject. There are numerous sources written which outline the weak wave turbulence theory [55, 84, 9, 61, 60, 19]. For a complete overview of the theory, the reader is directed to the books of Zakharov *et. al.*[84] and Nazarenko [55]. In this chapter the essential concepts will be discussed in order to build the foundation for the remaining thesis.

2.1 Key concepts

2.1.1 Fourier space

Wave turbulence is best represented in Fourier space as this naturally describes waves. Consider a vector field $\boldsymbol{u}(\boldsymbol{x}, t)$ is real space $\boldsymbol{x}$. The three-dimensional forward and inverse Fourier transforms are then

$$\boldsymbol{u}(\boldsymbol{x}, t) = \int_{\mathbb{R}^3} \boldsymbol{A}(\boldsymbol{k}, t) e^{i\boldsymbol{k}\cdot\boldsymbol{x}} \mathrm{d}\boldsymbol{k} \tag{2.1}$$

and

$$\boldsymbol{A}(\boldsymbol{k}, t) = \frac{1}{(2\pi)^3} \int_{\mathbb{R}^3} \boldsymbol{u}(\boldsymbol{x}, t) e^{-i\boldsymbol{k}\cdot\boldsymbol{x}} \mathrm{d}\boldsymbol{x}. \tag{2.2}$$

We can also introduce the interaction representation variables

$$\boldsymbol{a}(\boldsymbol{k}, t) = \boldsymbol{A}(\boldsymbol{k}, t) e^{i\omega_k t}, \tag{2.3}$$

where $\omega_k = \omega(\boldsymbol{k})$ is the frequency of wave vector $\boldsymbol{k}$ given by an appropriate dispersion relation. The interaction representation is used to separate the time scales by transforming the governing equation into variables which do not change in the linear approximation.

2.1.2 Resonant waves

Wave turbulence is the statistical mechanics of random nonlinear waves. Interactions occur between resonant waves. The number of waves involved in the resonant interaction varies depending on the system considered. In an N-wave system the N-wave resonance conditions

$$\omega(\boldsymbol{k}_1) \pm \omega(\boldsymbol{k}_2) \pm \cdots \pm \omega(\boldsymbol{k}_N), \tag{2.4}$$

$$\boldsymbol{k}_1 \pm \boldsymbol{k}_2 \pm \cdots \pm \boldsymbol{k}_N, \tag{2.5}$$

must be matched simultaneously. The plus or minus signs are chosen based on the type of the N-wave process. For example, a three-wave process may be a $2 \to 1$ process in which there will be 2 plus signs and 1 negative sign or it may be a $1 \to 2$ process in which there will be one positive sign and two negative signs. The number N is the minimum number of waves for which such resonance conditions can be matched. In general, systems in which the leading order of nonlinearity is quadratic, interactions occur between three waves. If the nonlinearity is cubic then the interactions occur between four waves and so on. In Alfvén wave turbulence, there has been some debate about the number of resonant waves involved in the interaction. The MHD equations possess a quadratic nonlinearity and so a three waves interaction seems likely. Wave turbulence theory relies on the asymptotic expansion of the fields in powers of the small nonlinearity. Sridhar and Goldreich [76] argued that there is no solution at the leading order and so one must go to the next order to describe Alfvén wave turbulence. In this way, they proposed that Alfvén wave turbulence is characterised by four-wave interactions. Several works were then published in response using phenomenological or rigorous approaches to argue for the nontrivial nature of the three-wave interactions [53, 81, 62]. A full three-wave Alfvén wave turbulence theory was then derived by Galtier *et. al.* in 2000 [27, 26, 57, 28]. It is this three-wave system that is generally accepted now and is the one which is used in this thesis. In the rotating MHD system which is also considered in this thesis, the interactions are also between three resonant waves.

2.1.3 Inviscid invariants and cascades

Inviscid invariants play a crucial role in turbulent systems. These are quantities which are conserved under the absence of dissipation and which are then cascaded in the physical and Fourier spaces. The energy and the momentum are conserved in all wave systems. For all even-order wave interactions (four-wave, six-wave, etc), the

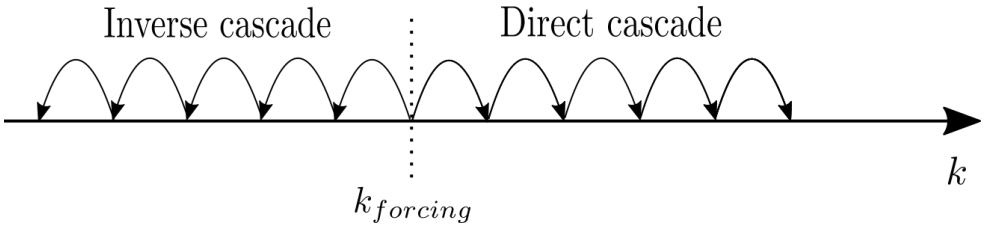

Figure 2.1: Dual cascade behaviour in k-space.

waveaction is also conserved. Additional invariants are also possible. In an infinite homogeneous turbulence, the invariants are infinite and so it only make sense to discuss their spatial density.

As previously discussed, the cascades of the inviscid invariants are of utmost importance. In a system where the only cascading quantity is the energy, the cascade will be from large scales to small scales. In terms of wavenumbers, this means that the energy flux will transfer the energy from small wavenumbers to larger ones. Where additional cascading invariants are present, then the cascade picture is modified. This picture was discovered in two-dimensional flows by Fjørtoft [72]. In this scenario there are two invariants which are transferred in opposite directions, one direct cascade from small to large wavenumbers and one inverse cascade from large to small wavenumbers. This picture can be formed physically if the forcing is at a moderate wavenumber, see Figure 2.1.

In the example of two-dimensional incompressible hydrodynamic turbulence there are two inviscid invariants, the energy density and the enstrophy density. These invariants can be written in terms of the energy spectrum $E(k)$ as follows:

$$E = \frac{\text{Energy}}{\text{Area}} = \frac{1}{2}\langle \boldsymbol{u}^2 \rangle = \int_0^\infty E(k)\mathrm{d}k, \tag{2.6}$$

$$\Omega = \frac{\text{Enstrophy}}{\text{Area}} = \frac{1}{2}\langle \boldsymbol{\omega}^2 \rangle = \int_0^\infty k^2 E(k)\mathrm{d}k, \tag{2.7}$$

where the relationship between vorticity and velocity $\boldsymbol{\omega}_k = i\boldsymbol{k} \times \boldsymbol{u}_k$ has been used. The enstrophy production rate η should be equal to its rate of dissipation in a stationary turbulence state, as is true also of the energy injection rate ϵ. Consider a case where the fluid is forced at k_f and then dissipated at large $k_+ \gg k_f$ and small $k_- \ll k_f$ wavenumbers. Using (2.6) and (2.7), η and ϵ are related by

$$\eta \sim k_f^2 \epsilon. \tag{2.8}$$

The directions of the energy and enstrophy cascades can then be found using a

so called Fjørtoft argument which goes as follows. If the energy is dissipated at k_+ at the same rate as the energy injection rate ϵ, then the enstrophy would be dissipated at a rate $k_+^2\epsilon \gg k_f^2\epsilon \sim \eta$. This is a contradiction since, in a steady state, the enstrophy cannot be dissipated faster than the rate at which it is produced. Therefore the energy must be dissipated at k_- and so there is an inverse energy cascade.

Similarly, assume that enstrophy is dissipated at k_- at the same rate as the enstrophy production rate η. Then the energy would be dissipated at a rate of $\eta/k_-^2 \gg \eta/k_f^2 \sim \epsilon$. Again, the energy cannot be dissipated faster than it is produced and so we have a contradiction. Thus for the enstrophy we must have a direct cascade.

2.1.4 Turbulent spectra

The spectra of the inviscid invariants are the key object studied in turbulence. Such spectra are functions which describe the distribution of the invariant in Fourier space. In particular, one often concentrates on the energy spectrum. The $3D$ energy spectrum is given by

$$E^{(3D)}(\boldsymbol{k}) = \frac{1}{2}\int_{\mathbb{R}^3} \langle \boldsymbol{u}(\boldsymbol{x}) \cdot \boldsymbol{u}(\boldsymbol{x}+\boldsymbol{r})\rangle e^{-i\boldsymbol{k}\cdot\boldsymbol{r}} \frac{\mathrm{d}\boldsymbol{r}}{(2\pi)^3}, \tag{2.9}$$

where the angled brackets indicate an ensemble average. The $3D$ energy spectrum represents the kinetic energy density in $3D$ $\boldsymbol{k}$ space such that

$$\frac{1}{2}\langle \boldsymbol{u}^2\rangle = \int_{\mathbb{R}^3} E^{(3D)}(\boldsymbol{k})\mathrm{d}\boldsymbol{k}. \tag{2.10}$$

We define *isotropic turbulence* as a turbulent system where the energy spectrum is independent of the direction of the wave vector $\boldsymbol{k}$. In an isotropic system, the same information as contained in the $3D$ energy spectrum can be represented by the $1D$ energy spectrum which represents the kinetic energy density over $k = |\boldsymbol{k}|$. The $1D$ spectrum is obtained by integrating $E^{(3D)}$ over the unit sphere in $3D$ $\boldsymbol{k}$-space,

$$E^{(1D)}(k) = 4\pi k^2 E^{(3D)}(k). \tag{2.11}$$

The total kinetic energy is given by

$$\frac{1}{2}\langle \boldsymbol{u}^2\rangle = \int_0^\infty E^{(1D)}(k)\mathrm{d}k. \tag{2.12}$$

In some cases there are external physical effects which affect the isotropy of the system. In Alfvén wave turbulence there is an external magnetic field and in rotating turbulence there is a solid body rotation. For both of these particular cases we can consider the components of the wave vector parallel and perpendicular to either the external magnetic field or the axis of rotation. Call the parallel component $k_\parallel$. The perpendicular component $\boldsymbol{k}_\perp$ is a two-dimensional vector in the plane perpendicular to the magnetic field or the rotation axis. It is then found that there is anisotropization such that the energy spectrum is suppressed in the $k_\parallel$ direction and we have $k_\perp \gg k_\parallel$ where $k_\perp = |\boldsymbol{k}_\perp|$. The spectrum then becomes almost $2D$ in the transverse plane

$$E^{(2D)}(\boldsymbol{k}_\perp) = \frac{1}{2}\int_{\mathbb{R}^2} \langle \boldsymbol{u}(\boldsymbol{x}) \cdot \boldsymbol{u}(\boldsymbol{x}+\boldsymbol{r})\rangle e^{-i\boldsymbol{k}_\perp \cdot \boldsymbol{r}} \frac{\mathrm{d}\boldsymbol{r}}{(2\pi)^2}. \tag{2.13}$$

The $1D$ energy spectrum is then found by integrating over the unit circle

$$E^{(1D)}(k_\perp) = 2\pi k_\perp E^{(2D)}(k_\perp). \tag{2.14}$$

The mathematical formulation of the wave turbulence theory leads to a kinetic equation describing the evolution of the energy (and other invariants) spectrum.

2.1.5 Steady states

The most important result from wave turbulence is the ability to find steady state solutions for the spectra. The simplest of these steady state solutions correspond to the case where there are no fluxes of energy or the other invariants and the system is in thermodynamic equilibrium. These solutions are know as the Rayleigh-Jeans (RJ) spectra. RJ states have been known since the advent of wave turbulence by Peierls [64]. However, the RJ solutions can only be realized in truncated $\boldsymbol{k}$-space systems in absence of forcing and dissipation. They are therefore of limited relevance to WT.

The most important solutions are the Kolmogorov-Zakharov solutions, so called due to their correspondence with the Kolmogorov-Obukhov spectrum of hydrodynamic turbulence and because of their discovery by Zakharov [83]. The KZ solutions are those which correspond to a finite-flux of the invariants and represent exact solutions of the kinetic equation. The KZ solutions are found by applying a conformal transform known as the Zakharov transform to the kinetic equation. For an isotropic turbulence, this transform applies to the integration variables k_1 and

k_2 as:

$$k_1 \to \frac{k^2}{k_1}, \tag{2.15}$$

$$k_2 \to \frac{kk_2}{k_1}. \tag{2.16}$$

However, since magnetized plasmas almost always display anisotropy, a bi-homogeneous conformal transform of a similar type is more appropriate [38]. In order to apply this transform, the plasma must be assumed to be axisymmetric. The bi-homogeneous conformal transform is:

$$k_{1\perp} \to \frac{k_\perp^2}{k_{1\perp}}, \tag{2.17}$$

$$k_{2\perp} \to \frac{k_\perp k_{2\perp}}{k_{1\perp}}, \tag{2.18}$$

$$k_{1\parallel} \to \frac{k_\parallel^2}{k_{1\parallel}}, \tag{2.19}$$

$$k_{2\parallel} \to \frac{k_\parallel k_{2\parallel}}{k_{1\parallel}}. \tag{2.20}$$

After applying this transformation we are able to search for power law solutions of the form $k_\perp^n k_\parallel^m$.

2.2 Worked example

Here I will work through the wave turbulence derivation with the aid of a general example. Consider the inviscid model equation

$$\frac{\partial \boldsymbol{u}}{\partial t} = \mathcal{L}(\boldsymbol{u}) + \epsilon \mathcal{N}(\boldsymbol{u}, \boldsymbol{u}), \tag{2.21}$$

where $\boldsymbol{u}$ is a stationary random variable such as the velocity, $\mathcal{L}$ is a linear operator and $\mathcal{N}$ is a nonlinear operator. The parameter ϵ is small, $0 < \epsilon \ll 1$ such that the nonlinearity is small as per the requirements of weak wave turbulence.

2.2.1 Wave amplitude equation

The first step in the wave turbulence formulation is to Fourier transform equation (2.21) using the 3D direct and inverse Fourier transforms (2.1) and (2.2). The time derivative of $\boldsymbol{u}$ in Fourier space is then

$$\boldsymbol{u}(\boldsymbol{x}, t) = \int_{\mathbb{R}^3} \frac{\partial \boldsymbol{A}(\boldsymbol{k}, t)}{\partial t} e^{i\boldsymbol{k}\cdot\boldsymbol{x}} \mathrm{d}\boldsymbol{k}. \tag{2.22}$$

The linear operator $\mathcal{L}$ is an operator such that the linear waves are solutions in the linear limit. Thus, in the case where $\epsilon = 0$, the equation in Fourier space for the j-component reads

$$\left(\frac{\partial}{\partial t} + i\omega(\boldsymbol{k})\right) A_j(\boldsymbol{k}, t) = 0, \tag{2.23}$$

where $\omega(\boldsymbol{k}) = \omega_k$ is the dispersion relation giving the frequency of the linear waves. Given a specific linear operator in place of $\mathcal{L}$, one can find the dispersion relation from this equation. Assuming that the nonlinearity described by $\mathcal{N}$ is of a quadratic type, the full nonlinear equation in Fourier space for the j-component is

$$\left(\frac{\partial}{\partial t} + i\omega(\boldsymbol{k})\right) A_j(\boldsymbol{k}, t) = \epsilon \iint\limits_{\mathbb{R}^6} \mathcal{H}_{jmn}^{\boldsymbol{k}\boldsymbol{k_1}\boldsymbol{k_2}} A_m(\boldsymbol{k_1}, t) A_n(\boldsymbol{k_2}, t) \delta(\boldsymbol{k} - \boldsymbol{k_1} - \boldsymbol{k_2}) \mathrm{d}\boldsymbol{k_1} \mathrm{d}\boldsymbol{k_2}, \tag{2.24}$$

where $\mathcal{H}$ is a symmetric function in its vector arguments which depends upon the specific nonlinear operator $\mathcal{N}$ and $\delta(\boldsymbol{k} - \boldsymbol{k_1} - \boldsymbol{k_2})$ is the Dirac delta function which is equal to 1 when $\boldsymbol{k} = \boldsymbol{k_1} + \boldsymbol{k_2}$ and 0 everywhere else. Note the following properties of the function $\mathcal{H}$:

$$\mathcal{H}_{jmn}^{\boldsymbol{k}\boldsymbol{k_1}\boldsymbol{k_2}} = \left(\mathcal{H}_{jmn}^{-\boldsymbol{k}-\boldsymbol{k_1}-\boldsymbol{k_2}}\right)^*, \tag{2.25}$$

$$\mathcal{H}_{jmn}^{\boldsymbol{k}\boldsymbol{k_1}\boldsymbol{k_2}} \text{ is symmetric in } (\boldsymbol{k_1}, \boldsymbol{k_2}) \text{ and } (m, n), \tag{2.26}$$

$$\mathcal{H}_{jmn}^{\boldsymbol{0}\boldsymbol{k_1}\boldsymbol{k_2}} = 0, \tag{2.27}$$

where the * indicates the complex conjugate. Now substituting for the interaction representation variables (2.3) we have,

$$\frac{\partial a_j(\boldsymbol{k})}{\partial t} = \epsilon \iint\limits_{\mathbb{R}^6} \mathcal{H}_{jmn}^{\boldsymbol{k}\boldsymbol{k_1}\boldsymbol{k_2}} a_m(\boldsymbol{k_1}) a_n(\boldsymbol{k_2}) e^{-\Omega_{k,k_1k_2}t} \delta_{k,k_1k_2} \mathrm{d}\boldsymbol{k_1} \mathrm{d}\boldsymbol{k_2}, \tag{2.28}$$

where the shorthand notation:

$$\delta_{k,k_1k_2} = \delta(\boldsymbol{k} - \boldsymbol{k_1} - \boldsymbol{k_2}), \tag{2.29}$$

$$\Omega_{k,k_1k_2} = \omega_k - \omega_{k_1} - \omega_{k_2}, \tag{2.30}$$

has been introduced. Equation (2.28) is the wave amplitude equation. The dependence on the small parameter ϵ means that the nonlinearity modifies the wave amplitude slowly in time. The wave amplitude equation suggests a three-wave interaction process which results from the quadratic nonlinearity. This is relevant for most MHD systems.

2.2.2 Wave turbulence statistics

The next step is to derive the statistical description of the wave turbulence properties. In turbulence, averaged quantities are considered and we introduce the ensemble average denoted by angular brackets, $\langle \dots \rangle$. The chaotic nature of turbulent fluids means that repeated experiments may result in wildly different values of a quantity, $U(\boldsymbol{x}, t)$. The ensemble average is used to overcome this difficulty and is defined as the mean value of $U(\boldsymbol{x}, t)$ over infinitely many realizations:

$$\langle U(\boldsymbol{x}, t) \rangle = \lim_{n \to \infty} \frac{1}{n} \sum_{i=1}^{n} U_i(\boldsymbol{x}, t). \tag{2.31}$$

The density tensor $q_{jj'}(\boldsymbol{k'})$ for homogeneous turbulence is defined such that

$$q_{jj'}(\boldsymbol{k'}) \delta(\boldsymbol{k} + \boldsymbol{k'}) = \langle a_j(\boldsymbol{k}) a_{j'}(\boldsymbol{k'}) \rangle. \tag{2.32}$$

Taking the time derivative and using Equation (2.28) we have, for the second-order moment $\langle a_j(\boldsymbol{k}) a_{j'}(\boldsymbol{k'}) \rangle$,

$$\begin{aligned}
&\frac{\partial q_{jj'}(\boldsymbol{k'}) \delta(\boldsymbol{k} + \boldsymbol{k'})}{\partial t} \\
&\quad = \frac{\partial}{\partial t} \langle a_j(\boldsymbol{k}) a_{j'}(\boldsymbol{k'}) \rangle \\
&\quad = \langle \frac{\partial a_j(\boldsymbol{k})}{\partial t} a_{j'}(\boldsymbol{k'}) \rangle + \langle a_j(\boldsymbol{k}) \frac{\partial a_{j'}(\boldsymbol{k'})}{\partial t} \rangle \\
&\quad = \epsilon \iint_{\mathbb{R}^6} \mathcal{H}^{\boldsymbol{k} \boldsymbol{k_1} \boldsymbol{k_2}}_{jmn} \langle a_m(\boldsymbol{k_1}) a_n(\boldsymbol{k_2}) a_{j'}(\boldsymbol{k'}) \rangle e^{-\Omega_{k, k_1 k_2} t} \delta_{k, k_1 k_2} \mathrm{d}\boldsymbol{k_1} \mathrm{d}\boldsymbol{k_2} \\
&\qquad + \epsilon \iint_{\mathbb{R}^6} \mathcal{H}^{\boldsymbol{k'} \boldsymbol{k_1} \boldsymbol{k_2}}_{jmn} \langle a_m(\boldsymbol{k_1}) a_n(\boldsymbol{k_2}) a_{j'}(\boldsymbol{k}) \rangle e^{-\Omega_{k', k_1 k_2} t} \delta_{k', k_1 k_2} \mathrm{d}\boldsymbol{k_1} \mathrm{d}\boldsymbol{k_2},
\end{aligned} \tag{2.33}$$

which depends upon the third-order moment $\langle a_j(\boldsymbol{k})a_{j'}(\boldsymbol{k'})a_{j''}(\boldsymbol{k''})\rangle$. A similar equation can be written for the third-order moment using Equation (2.28),

$$\begin{aligned}\frac{\partial}{\partial t}&\langle a_j(\boldsymbol{k})a_{j'}(\boldsymbol{k'})a_{j''}(\boldsymbol{k''})\rangle \\ &= \epsilon \iint\limits_{\mathbb{R}^6} \mathcal{H}^{\boldsymbol{k}\boldsymbol{k_1}\boldsymbol{k_2}}_{jmn}\langle a_m(\boldsymbol{k_1})a_n(\boldsymbol{k_2})a_{j'}(\boldsymbol{k'})a_{j''}(\boldsymbol{k''})\rangle e^{-\Omega_{k,k_1k_2}t}\delta_{k,k_1k_2}\mathrm{d}\boldsymbol{k_1}\mathrm{d}\boldsymbol{k_2} \\ &\quad + \iint\limits_{\mathbb{R}^6} \mathcal{H}^{\boldsymbol{k'}\boldsymbol{k_1}\boldsymbol{k_2}}_{j'mn}\langle a_m(\boldsymbol{k_1})a_n(\boldsymbol{k_2})a_{j}(\boldsymbol{k})a_{j''}(\boldsymbol{k''})\rangle e^{-\Omega_{k',k_1k_2}t}\delta_{k',k_1k_2}\mathrm{d}\boldsymbol{k_1}\mathrm{d}\boldsymbol{k_2} \\ &\quad + \iint\limits_{\mathbb{R}^6} \mathcal{H}^{\boldsymbol{k''}\boldsymbol{k_1}\boldsymbol{k_2}}_{j''mn}\langle a_m(\boldsymbol{k_1})a_n(\boldsymbol{k_2})a_{j}(\boldsymbol{k})a_{j'}(\boldsymbol{k'})\rangle e^{-\Omega_{k'',k_1k_2}t}\delta_{k'',k_1k_2}\mathrm{d}\boldsymbol{k_1}\mathrm{d}\boldsymbol{k_2}.\end{aligned} \tag{2.34}$$

Notice that this is now dependent upon the fourth-order moments. From here, we could continue writing equations in the same way which would lead to an infinite hierarchy of moment equations. This is the fundamental problem in turbulence which has led to difficulty in finding exact solutions. In weak wave turbulence there exists a natural asymptotic closure which can be employed here. The statistical moments can be written as combinations of statistical cumulants which have the advantage of decaying sufficiently quickly to zero as the separation between the points becomes large. The moments and cumulants are related as follows:

$$\langle a_j(\boldsymbol{k})a_{j'}(\boldsymbol{k'})\rangle = \delta(\boldsymbol{k}+\boldsymbol{k'})Q^{jj'}(\boldsymbol{k},\boldsymbol{k'}), \tag{2.35}$$

$$\langle a_j(\boldsymbol{k})a_{j'}(\boldsymbol{k'})a_{j''}(\boldsymbol{k''})\rangle = \delta(\boldsymbol{k}+\boldsymbol{k'}+\boldsymbol{k''})Q^{jj'j''}(\boldsymbol{k},\boldsymbol{k''},\boldsymbol{k''}), \tag{2.36}$$

$$\begin{aligned}\langle a_j(\boldsymbol{k})a_{j'}(\boldsymbol{k'})a_{j''}(\boldsymbol{k''})a_{j'''}(\boldsymbol{k'''})\rangle &= \delta(\boldsymbol{k}+\boldsymbol{k'}+\boldsymbol{k''}+\boldsymbol{k'''})Q^{jj'j''j'''}(\boldsymbol{k},\boldsymbol{k''},\boldsymbol{k''},\boldsymbol{k'''}) \\ &\quad + \delta(\boldsymbol{k}+\boldsymbol{k'})Q^{jj'}(\boldsymbol{k},\boldsymbol{k'})\delta(\boldsymbol{k''}+\boldsymbol{k'''})Q^{j''j'''}(\boldsymbol{k''},\boldsymbol{k'''}) \\ &\quad + \delta(\boldsymbol{k}+\boldsymbol{k''})Q^{jj''}(\boldsymbol{k},\boldsymbol{k''})\delta(\boldsymbol{k'}+\boldsymbol{k'''})Q^{j'j'''}(\boldsymbol{k'},\boldsymbol{k'''}) \\ &\quad + \delta(\boldsymbol{k}+\boldsymbol{k'''})Q^{jj'''}(\boldsymbol{k},\boldsymbol{k'''})\delta(\boldsymbol{k'}+\boldsymbol{k''})Q^{j'j''}(\boldsymbol{k'},\boldsymbol{k''}).\end{aligned} \tag{2.37}$$

Notice that the fourth-order moment is written as a sum of the fourth-order cumulant and products of second-order ones. The natural closure (as described in [9, 60, 61, 55]) comes from the fact that at asymptotically large times the fourth-order cumulant does not contribute, such that, the third-order moments are essentially dependent only on second-order ones. Using this fact, Equations (2.34) and (2.35),

the third-order moment can be written as

$$
\begin{aligned}
&\langle a_j(\boldsymbol{k})a_{j'}(\boldsymbol{k'})a_{j''}(\boldsymbol{k''})\rangle \\
&\quad= \epsilon \iint_{\mathbb{R}^6} \mathcal{H}_{jmn}^{\boldsymbol{k}\boldsymbol{k_1}\boldsymbol{k_2}} \big(\langle a_m(\boldsymbol{k_1})a_n(\boldsymbol{k_2})\rangle\langle a_{j'}(\boldsymbol{k'})a_{j''}(\boldsymbol{k''})\rangle \\
&\qquad + \langle a_m(\boldsymbol{k_1})a_{j'}(\boldsymbol{k'})\rangle\langle a_n(\boldsymbol{k_2})a_{j''}(\boldsymbol{k''})\rangle \\
&\qquad + \langle a_m(\boldsymbol{k_1})a_{j''}(\boldsymbol{k''})\rangle\langle a_n(\boldsymbol{k_2})a_{j'}(\boldsymbol{k'})\rangle\Delta(\Omega_{k,k_1k_2})\delta_{k,k_1k_2}\mathrm{d}\boldsymbol{k_1}\mathrm{d}\boldsymbol{k_2} \\
&\quad + \epsilon \iint_{\mathbb{R}^6} \mathcal{H}_{j'mn}^{\boldsymbol{k'}\boldsymbol{k_1}\boldsymbol{k_2}} \big(\langle a_m(\boldsymbol{k_1})a_n(\boldsymbol{k_2})\rangle\langle a_j(\boldsymbol{k})a_{j''}(\boldsymbol{k''})\rangle \\
&\qquad + \langle a_m(\boldsymbol{k_1})a_j(\boldsymbol{k})\rangle\langle a_n(\boldsymbol{k_2})a_{j''}(\boldsymbol{k''})\rangle \\
&\qquad + \langle a_m(\boldsymbol{k_1})a_{j''}(\boldsymbol{k''})\rangle\langle a_n(\boldsymbol{k_2})a_j(\boldsymbol{k})\rangle\Delta(\Omega_{k,k_1k_2})\delta_{k,k_1k_2}\mathrm{d}\boldsymbol{k_1}\mathrm{d}\boldsymbol{k_2} \\
&\quad + \epsilon \iint_{\mathbb{R}^6} \mathcal{H}_{j''mn}^{\boldsymbol{k''}\boldsymbol{k_1}\boldsymbol{k_2}} \big(\langle a_m(\boldsymbol{k_1})a_n(\boldsymbol{k_2})\rangle\langle a_j(\boldsymbol{k})a_{j'}(\boldsymbol{k'})\rangle \\
&\qquad + \langle a_m(\boldsymbol{k_1})a_j(\boldsymbol{k})\rangle\langle a_n(\boldsymbol{k_2})a_{j'}(\boldsymbol{k'})\rangle \\
&\qquad + \langle a_m(\boldsymbol{k_1})a_{j'}(\boldsymbol{k'})\rangle\langle a_n(\boldsymbol{k_2})a_j(\boldsymbol{k})\rangle\Delta(\Omega_{k,k_1k_2})\delta_{k,k_1k_2}\mathrm{d}\boldsymbol{k_1}\mathrm{d}\boldsymbol{k_2},
\end{aligned}
\tag{2.38}
$$

where

$$
\begin{aligned}
\Delta(\Omega_{k,k_1k_2} &= \int_0^{t\gg 1/\omega} e^{i\Omega_{k,k_1k_2}t'}\mathrm{d}t' \\
&= \frac{e^{i\Omega_{k,k_1k_2}t}-1}{i\Omega_{k,k_1k_2}}.
\end{aligned}
\tag{2.39}
$$

The upper limit of the time integral $t \gg 1/\omega$ implies that the time here is much longer than the linear time scale. Now that the third-order moment has been written in terms of the second-order moment, we can introduce the density tensor (2.32) into this equation. The integration over wave vectors can be performed using the fundamental property of the Dirac delta function:

$$
\int_{-\infty}^{\infty} f(x)\delta(x-a)\mathrm{d}x = f(a). \tag{2.40}
$$

After performing the integration and simplifying, the third-order moment can be written as

$$\begin{aligned}\langle a_j(\boldsymbol{k})a_{j'}(\boldsymbol{k'})a_{j''}(\boldsymbol{k''})\rangle = \\ = 2\epsilon\Delta(\Omega_{kk'k''})\delta_{kk'k''}\Big(\mathcal{H}_{jmn}^{\boldsymbol{k-k'-k''}}q_{mj'}(\boldsymbol{k'})q_{nj''}(\boldsymbol{k''}) \\ + \mathcal{H}_{j'mn}^{\boldsymbol{k'-k-k''}}q_{mj}(\boldsymbol{k})q_{nj''}(\boldsymbol{k''}) + \mathcal{H}_{j''mn}^{\boldsymbol{k''-k-k'}}q_{mj}(\boldsymbol{k})q_{nj'}(\boldsymbol{k'})\Big).\end{aligned} \tag{2.41}$$

Substituting this into Equation (2.33), we are left with the asymptotically exact kinetic equations for wave turbulence:

$$\begin{aligned}\frac{\partial q_{jj'}(\boldsymbol{k})}{\partial t} = 4\pi\epsilon^2\iint\limits_{\mathbb{R}^6}\delta_{k,k_1k_2}\delta(\Omega_{k,k_1k_2})\mathcal{H}_{jmn}^{\boldsymbol{kk_1k_2}}\Big(\mathcal{H}_{mrs}^{\boldsymbol{k_1-k_2-k}}q_{rn}(\boldsymbol{k_2})q_{j's}(\boldsymbol{k}) \\ + \mathcal{H}_{nrs}^{\boldsymbol{k_2-k_1k}}q_{rm}(\boldsymbol{k_1})q_{j's}(\boldsymbol{k}) + \mathcal{H}_{j'rs}^{\boldsymbol{-k-k_1-k_2}}q_{rm}(\boldsymbol{k_1})q_{sn}(\boldsymbol{k_2})\Big)\,\mathrm{d}\boldsymbol{k_1}\mathrm{d}\boldsymbol{k_2},\end{aligned} \tag{2.42}$$

where we have taken the long time limit to find

$$\Delta(x) \to \pi\delta(x) + i\mathcal{P}(1/x), \tag{2.43}$$

with $\mathcal{P}$ the principal value of the integral. Equation (2.42) is valid for all wave turbulence systems where the interaction is dominated by a three-wave process. The difference between systems lies in the exact form of the function $\mathcal{H}$ which is adapted to the problem considered. Steady solutions can then be found by applying the Zakharov transform or the equation itself can be studied further. The delta functions present reveal the nature of the resonance mechanism. We need to satisfy the relations

$$\omega_k = \omega_{k_1} + \omega_{k_2}, \tag{2.44}$$

$$\boldsymbol{k} = \boldsymbol{k_1} + \boldsymbol{k_2}, \tag{2.45}$$

which we refer to as the resonance conditions.

Chapter 3

Self-similar evolution of Alfvén wave turbulence

3.1 Introduction

As previously discussed, the most commonly studied objects in wave turbulence are the spectra for the inviscid invariants, usually including the energy. The stationary states of these spectra are of primary importance and such states have been found for a variety of systems including for various regimes of MHD. The temporal evolution of the spectra preceding the formation of the stationary state is not fully understood and this is what will be discussed in the next two chapters.

In general wave turbulence systems, there are two possibilities for how the stationary state may develop. In order to characterise these two cases the concept of *capacity* must first be defined.

Definition 1. Consider a stationary spectrum describing a constant flux of an invariant ψ with density ρ_k. If the integral $\int \omega_k n_k \mathrm{d}\boldsymbol{k}$ converges at the scales toward which ψ is cascading then the stationary spectrum is said to have *finite capacity*. Otherwise, it is said to have *infinite capacity*.

For an infinite capacity system, the spectrum evolves as a propagating front from small to large wavenumbers. The stationary spectrum forms right behind this front. In the limit of a dissipative region at infinitely large wavenumber, a forced-dissipative system will take an infinitely long time to form a stationary state. The KZ spectrum would still asymptotically form at any fixed k but the front would continue to propagate infinitely. In a freely decaying system (an unforced system), the KZ spectrum would not form since any initial energy would be insufficient to fill the infinite tail.

In a finite capacity system, the KZ spectrum will form in a finite time t_* regardless of the scale at which the dissipation acts. Unlike the infinite capacity case, a finite capacity system will form the KZ spectrum even in the event of it being freely decaying. The energy provided by the initial conditions is able to fill the finite tail for a long time, but the energy in the spectrum will decrease over time. Turbulent spectra in finite capacity systems undergo three distinct self-similar evolution stages, as was shown for the case of the Leith model of hydrodynamic turbulence in [56]:

1. $\underline{t < t_*}$. Self-similar solution of the second kind manifesting itself as a propagating front reaching $k = \infty$ in a finite time t_*. The power law spectrum which forms behind the front has an anomalous power-law spectrum which is steeper than the Kolmogorov (or, more generally, KZ) spectrum, $x_* > x_{KZ}$. Interestingly, presence or absence of forcing at low wave numbers becomes increasingly unimportant as one moves toward higher wave numbers because from the point of view of the self-accelerating tail the low wave numbers are "frozen". Of course in reality there exists dissipation at very high wave numbers (due to finite viscosity and resistivity omitted in equation (3.9), and the evolution ceases to be self-similar near these scales.

2. $\underline{t_* < t < t_* + t_{max}}$. Reflection wave from large to small wavenumbers leaving the KZ spectrum in its wake. Such a wave is also self-similar at the wave numbers much less than the dissipation wave numbers.

3. $\underline{t > t_* + t_{max}}$. In presence of a statistically stationary forcing, a steady KZ spectrum forms after the reflected wave reaches the minimal (i.e. initial) wave numbers. In absence of forcing, however, there exist a third self-similar stage describing a gradual decay of the KZ spectrum with the inertial range shrinking toward smaller k (i.e. with the dissipation wave numbers getting smaller).

The first two stages are shown qualitatively in Figure 3.1. In the current chapter and the following chapter, Alfvén wave turbulence is studied. The wave turbulence theory for Alfvén waves was developed by Galtier *et. al.* [27]. In Alfvén wave turbulence there is a direct energy cascade from low to high wavenumbers in which the stationary energy spectrum is found to be $E^{(1D)}_{k_\perp} \sim k_\perp^{-2}$. Therefore, in order to describe the capacity of the system, one must find the convergence of the integral

$$\int_0^{k_\perp} \omega_{k_\perp} n_{k_\perp} \mathrm{d}\boldsymbol{k}_\perp = \int_0^{k_\perp} E_{k_\perp} \mathrm{d}k_\perp \tag{3.1}$$

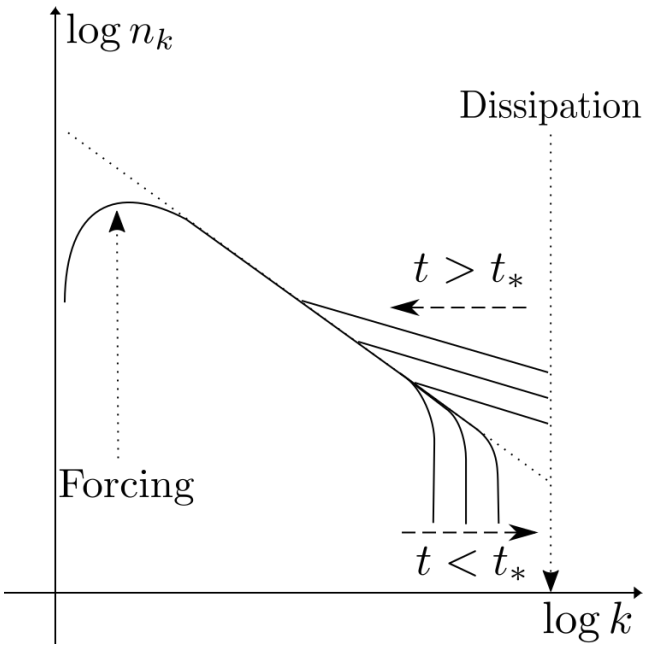

Figure 3.1: Formation of the stationary spectrum. An anomalous spectrum (steeper than KZ) forms behind a propagating front for $t < t_*$. The KZ spectrum forms at $t > t_*$ as a reflected wave which propagates from the dissipative scale.

as $k_\perp \to \infty$. The integral for Alfvén wave turbulence is then

$$\int_0^{k_\perp} k_\perp^{-2} \mathrm{d}k_\perp = -\frac{1}{k_\perp}\bigg|_{k_\perp \to \infty} \to 0. \tag{3.2}$$

Thus it is found that Alfvén wave turbulence is a finite capacity system.

3D MHD turbulence in an incompressible conducting fluid embedded in a strong uniform magnetic field consists of a large set of weakly interacting Alfvén waves.

The full kinetic equations are derived and given in [27] and results in a kinetic equation of the form 2.42. The full derivation is very long and so for brevity just a summary of the main results is given here. The full wave kinetic equations can be simplified using the limit of strong anisotropy $k_\perp \gg k_\parallel$ such that the Elsässer energy spectra of the Alfvén waves evolve according to the following integro-differential equations

$$\begin{aligned} \frac{\partial E^\pm(k_\perp, k_\parallel)}{\partial t} &= \tfrac{\pi\epsilon^2}{B_0} \iint\limits_{\Delta_k} \cos^2\theta_2 \sin\theta_1 \tfrac{k_\perp}{k_{1\perp}} E^\mp(k_{1\perp}, 0) \\ &\quad \times \left[k_\perp E^\pm(k_{2\perp}, k_\parallel) - k_{2\perp} E^\pm(k_\perp, k_\parallel)\right] \end{aligned} \tag{3.3}$$

where θ_2 is the angle between $\mathbf{k}_\perp$ and $\mathbf{k}_{2\perp}$, and θ_1 is the angle between $\mathbf{k}_\perp$ and $\mathbf{k}_{1\perp}$. Note the absence of delta-functions in this equation which in general enforce the local conservation of energy. In deriving Equation 3.3, similar methods to those used in Section 5.4.2 have been used to reduce the kinetic equation by integrating out the delta functions. This is made easier here by the fact that in Alfvén waves, one of the wave modes in any resonant triad belongs to the $2D$ state in which $\omega_k \sim k_\parallel = 0$. This means that in any triad, the energy is conserved within two co-propagating waves, which mathematically results in a symmetry of the integrand which can be exploited. It is possible to revisit the full kinetic equations given in [27] and show the detailed energy conservation, and this argument is not affected by the algebraic manipulations involved in deriving 3.3.

Equation (3.3) reveals a fundamental property of Alfvén wave turbulence, namely that the evolution of $E^\pm$ is always mediated by the slow mode $k_\parallel = 0$ [23]. Thus, the nonlinear dynamics are not affected by the dependence on the parallel wavenumber and so $k_\parallel$ can be treated as an external parameter. Assuming that the perturbations of the external magnetic field are sufficiently small, there is no evolution in the parallel direction and the evolution in the perpendicular plane becomes identical to the purely $2D$ turbulence [54]. The energy spectrum then separates as $E^\pm(k_\perp, k_\parallel) = E^\pm(k_\perp) f_\pm(k_\parallel)$ with a time-independent (set by initial conditions) parallel part $f_\pm(k_\parallel)$. The transverse energy spectrum $E^\pm(k_\perp, t)$ then evolves according to the following equation [27, 55, 23]

$$\begin{aligned}\frac{\partial E^\pm(k_\perp)}{\partial t} &= \frac{\pi\epsilon^2}{B_0} \iint_{\Delta_k} \cos^2\theta_2 \sin\theta_1 \frac{k_\perp}{k_{1\perp}} E^\mp(k_{1\perp}) \\ &\quad \times \left[k_\perp E^\pm(k_{2\perp}) - k_{2\perp} E^\pm(k_\perp)\right]. \end{aligned} \tag{3.4}$$

The exact finite flux solutions of Equation (3.4) for the stationary energy spectra are

$$E^\pm(k_\perp) \sim k_\perp^{n_\pm} \tag{3.5}$$

with

$$n_+ + n_- = -4. \tag{3.6}$$

An often considered case is the one in which there is no directional independence such that $E = E^+ = E^-$ in which case the energy spectrum scaling is

$$E(k_\perp) \sim k_\perp^{-2}. \tag{3.7}$$

It is this case which is considered here and so for what follows we are able to drop

the $\pm$ signs. Furthermore we choose to use the $2D$ energy spectrum $n_{k\perp}$ rather than the $1D$ spectrum $E_{k\perp}$. The $2D$ spectra are given by [55]

$$n_{k\perp} = \frac{1}{2\pi k_\perp} E_{k\perp}. \tag{3.8}$$

We are interested only in the spectrum in the plane transverse to the external magnetic field and so for simplicity of notation we drop the perpendicular signs. Inserting (3.8) into Equation (3.4) leads to the following kinetic equation for the $2D$ transverse energy spectrum

$$\frac{\partial n(k,t)}{\partial t} = \iint\limits_{\Delta_k} W(k,k_1,k_2)\, n(k_1)\, [n(k_2) - n(k)]\, dk_1 dk_2, \tag{3.9}$$

where $k = |\mathbf{k}_\perp|$, $k_1 = |\mathbf{k}_{1\perp}|$, $k_2 = |\mathbf{k}_{2\perp}|$. The integration area Δ_k is determined by the triangle inequalities,

$$\Delta_k = \{(k_1,k_2) \,:\, (k \le k_1 + k_2) \cap (k_1 \le k + k_2) \cap (k_2 \le k_1 + k)\}\,. \tag{3.10}$$

This is sketched in figure 3.1. The interaction coefficient is

$$W(k,k_1,k_2) = kk_2\, \cos^2\theta_2 \sin\theta_1, \tag{3.11}$$

where θ_2 is the angle between $\mathbf{k}$ and $\mathbf{k}_2$, and θ_1 is the angle between $\mathbf{k}$ and $\mathbf{k}_1$. Thus,

$$\cos^2\theta_2 = \left(\frac{k^2 - k_1^2 + k_2^2}{2kk_2}\right)^2, \quad \sin\theta_1 = \frac{\sqrt{2(k^2k_1^2 + k^2k_2^2 + k_1^2k_2^2) - k^4 - k_1^4 - k_2^4}}{2kk_1}.$$

Equation (3.9) has a two stationary power-law solutions: $n(k) \sim k^0$ corresponding to a thermodynamic equilibrium and $n(k) \sim k^{-3}$ corresponding to the Kolmogorov-Zakharov (KZ) state with constant flux of energy from small to large wave numbers k.

Numerous numerical studies of MHD turbulence have been performed [45, 65, 47] which show energy spectra confirming the Galtier spectrum when the weak wave turbulence regime is accessed. We are not aware of any previous DNS studies which have concentrated on the pre-stationary state of the energy spectra. Doing so would be difficult due to the speed at which this process occurs making observation difficult. Experimental studies of MHD turbulence tend to use astrophysical data. Numerical simulations have been compared with data from the solar wind [12] which match well with the strong turbulence prediction but do not realise the wave turbulence theory.

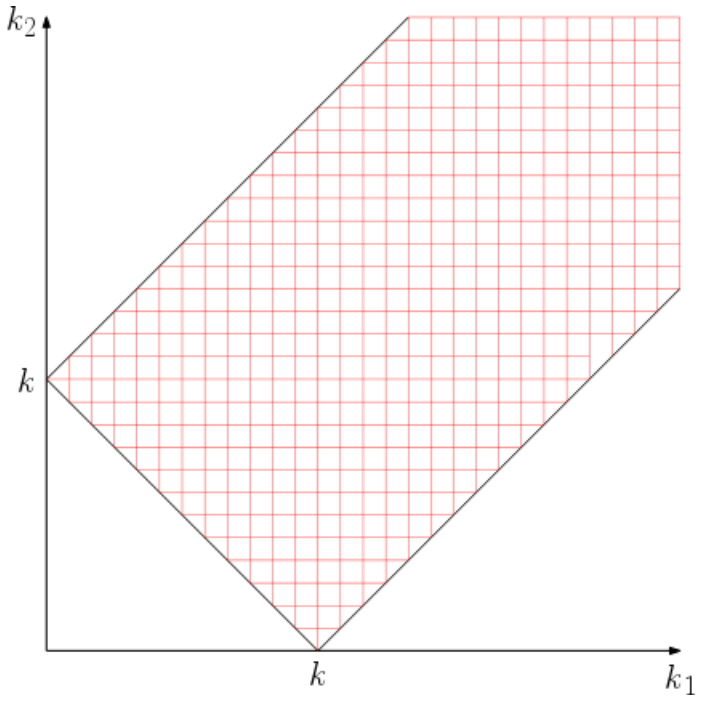

Figure 3.2: The integration area Δ_k.

Indirect evidence of Alfvén wave turbulence has been observed in the magnetosphere of Jupiter [73] and direct evidence has been observed in the solar magnetic field above active regions [1]. Such experimental results are unable to locate the pre-stationary state discussed in this paper. When analysing data from astrophysical objects, it is difficult to identify which stage the spectrum is currently in so it is difficult to view the fast pre-stationary phase.

The aim of this chapter is to study the transient self-similar behaviour discovered in the numerical experiments of [27]. The self-similar solutions are similar to the ones analysed in [14, 13, 31, 79] for the nonlinear diffusion models of Leith type [40]: they have a propagating front which accelerates explosively, reaching $k = \infty$ in a finite time t_*. The main feature of such self-similarity is that the scaling exponents cannot be found by dimensional considerations and from the existence of conservation laws. In particular, the low-wavenumber asymptotic of the self-similar spectrum is a power law with an anomalous (non-Kolmogorov) exponent. Following the Zeldovich-Raizer terminology, this type of behaviour is usually called a self-similarity of the second kind [85, 86]. The high-wavenumber boundary condition for the self-similar solution in the nonlinear diffusion equation is a sharp front – with the solution being identically equal to zero beyond a finite support. We deal with an integro-differential equation for which there exist no finite support solutions. Thus,

the question about the boundary conditions at the high wavenumbers has to be readdressed.

In the present chapter we argue that the correct boundary conditions for the self-similar solution in the considered kinetic-equation model are: (i) power-law asymptotic at low wave numbers (with an exponent x^* determined by the nonlinear eigenvalue problem) and (ii) the fastest decay at large wave numbers within the class of positive functions. We show that the fastest decay at infinity also takes form of a power law, and we predict a simple relation between the power law exponents in the vicinities of zero and infinity. We further predict the following integral relationship between the shape of the self-similar function $f(\eta)$ (defined below in (3.13)) and exponent x^*

$$D = \int_0^\infty f(\eta)\eta^3 d\eta = \frac{8}{\pi(4-x^*)\left[(x^*-1)+\sqrt{(x^*-1)^2+1}\right]}. \tag{3.12}$$

By numerical simulations, we find $f(\eta)$ and the exponent x^*, and confirm the above-mentioned integral relationship. With an accuracy of about one percent we find $x^* = 3.8$, which compares with $x^* \approx 3.33$ previously obtained by numerical simulation of the time-dependent kinetic equation (3.9)) in [27]. The reason for the discrepancy is not yet known, but we suspect that it is related to the logarithmic discretisation used in [27] that may not have resolved well the structure of the propagating front of the spectrum.

3.2 Self-similar solutions and the nonlinear eigenvalue problem

Before studying the self-similar solutions of Alfvén wave turbulence, it is necessary to first describe what we mean by such solutions. For this the conventions of Barenblatt, Raizer and Zeldovich are followed [5, 85, 86]. Self-similar solutions are ones in which the spatial distribution of the dependent variables remains similar to itself at all times during the development. Such solutions, though first studied as a means of reducing partial differential equations into ordinary differential equations, are used to describe intermediate asymptotic behaviour, i.e. the behaviour far away from the initial and/or boundary conditions such that the details of these conditions no longer affect the behaviour. Self-similar solutions of the first kind are ones in which the similarity variables can be established by dimensional analysis and the conservation laws. If this is not possible, then the self-similarity is of the second kind, in which

a nonlinear eigenvalue problem must be solved to define the similarity variables.

We look for self-similar solutions of the second kind in the form

$$n(t,k) = \frac{1}{\tau^a} f(\eta), \quad \eta = \frac{k}{\tau^b}, \quad \tau = t^* - t. \tag{3.13}$$

Making the substitution (3.13) into Equation (3.9), the interaction coefficient transforms as

$$\begin{aligned} W(k,k_1,k_2) \quad &= \tfrac{(k^2-k_1^2+k_2^2)^2}{8k_1k_2k^2}\sqrt{2(k^2k_1^2+k^2k_2^2+k_1^2k_2^2)-k^4-k_1^4-k_2^4} \\ &\to \tfrac{(\eta^2-\eta_1^2+\eta_2^2)^2}{8\eta_1\eta_2\eta^2}\tau^{2b}\sqrt{2(\eta^2\eta_1^2+\eta^2\eta_2^2+\eta_1^2\eta_2^2)-\eta^4-\eta_1^4-\eta_2^4}, \end{aligned} \tag{3.14}$$

the time differential is

$$\frac{\partial n(t,k)}{\partial t} \to a\tau^{-a-1} + b\eta\tau^{-a-1}f'(\eta), \tag{3.15}$$

and the integral becomes

$$\mathrm{d}k_1\mathrm{d}k_2 \to \tau^{2b}\mathrm{d}\eta_1\mathrm{d}\eta_2. \tag{3.16}$$

Equation (3.9) then becomes

$$\tau^{-a-1}\left[af(\eta)+b\eta f'(\eta)\right] = \iint\limits_{\Delta_\eta} \tau^{4b-2a} W(\eta,\eta_1,\eta_2) f(\eta_1)\left[f(\eta_2)-f(\eta)\right]\mathrm{d}\eta_1\mathrm{d}\eta_2 \tag{3.17}$$

In order to eliminate τ, we need to impose the condition $a = 1 + 4b$. A second condition on a and b arises from the fact that at $\eta = 0$, the function $f(\eta)$ should behave as a power law. As seen in Figure 3.1, the area of integration at $\eta = 0$ is null and so the right hand side becomes zero. Substituting in power law solutions η^{-x}, we then have

$$a\eta^{-x} - bx\eta^{-x} = 0, \tag{3.18}$$

which gives $x = a/b$. Then the self-similar shapes $f(\eta)$ obey the following equation,

$$xf + \eta f' = \frac{1}{b}\iint\limits_{\Delta_\eta} W(\eta,\eta_1,\eta_2) f(\eta_1)[f(\eta_2)-f(\eta)]d\eta_1\eta_2. \tag{3.19}$$

where

$$x = \frac{a}{b}, \quad b = \frac{1}{x-4},$$

and Δ_η is given by (3.10) where k, k_1, k_2 are replaced by η, η_1, η_2 respectively.

3.2.1 Boundary conditions

Equation (3.19) has to be complimented with boundary conditions at $\eta \to 0$ and $\eta \to \infty$. Based on our experience with the self-similar solutions of the Leith-type nonlinear PDE models [14, 31, 79], we postulate the condition on the right boundary as

$$f(\eta) \to \eta^{-x} \quad \text{for} \quad \eta \to 0. \tag{3.20}$$

Three remarks are due here.

1. Our system is scale-invariant because the interaction coefficient is a homogeneous function

$$W(\lambda\eta, \lambda\eta_1, \lambda\eta_2) = \lambda^2 W(\eta, \eta_1, \eta_2). \tag{3.21}$$

   Hence, if $f(\eta)$ is a solution of equation (3.19) satisfying condition (3.20) then $\tilde{f}(\eta) = \lambda^{-4} f(\lambda\eta)$ is also a solution – it clearly satisfies condition $\tilde{f}(\eta) \to \lambda^{-4}\eta^{-x}$ for $\eta \to 0$. Thus it is enough to consider condition (3.20) without a pre-factor in front of the power law.

2. The self-similar formulation with the boundary condition (3.20) is self consistent only if x corresponds to convergence of the integral in (3.19) at $\eta_1 \to 0$ and $\eta_2 \to 0$ i.e. only if $x < 4$, see Section 3.3.

3. As $\eta \to 0$, the right-hand side of equation (3.19) becomes vanishingly small compared to each of the terms on the left-hand side for $x < 4$, which ensures that $f = \eta^{-x}$ satisfies this equation.

The second boundary condition is the condition on the right boundary. In the Leith-type PDE models, this condition was that $f(\eta) \equiv 0$ for $\eta \geq \eta^*$ for some constant η^* and that the energy flux turns into zero at $\eta = \eta^*$ [14, 31]. There is only one value of x, $x = x^*$, for which such a boundary condition can be satisfied, and finding x^* constitutes the nonlinear eigenvalue problem to be solved. The self-similar solution corresponding to $x = x^*$ is the only one that forms asymptotically at large k in the initial value problem of the evolution equation under consideration with initial data in a finite support.

Notice that finite-support solutions are impossible for the integral equation (3.19). Indeed, suppose that $f(\eta) \equiv 0$ for $\eta \geq \eta^*$ for some constant η^*. Then for some η outside of the support but sufficiently close to its boundary there exist η_1 and η_2 in Δ_η such that the integrand in the right hand side of (3.19) is finite and positive. Hence, equation (3.19) cannot be satisfied in this case.

It is however natural to think that the self-similar solution chosen by the evolution will correspond to $x = x^*$ for which $f(\eta)$ is positive everywhere and tends to zero at $\eta \to \infty$ in a fastest way among the solutions with different values of x. This is the second boundary condition which we postulate. This constitutes the nonlinear eigenvalue problem of finding $x = x^*$ for which this boundary condition is satisfied simultaneously with the condition at $\eta \to 0$.

The condition that the solution must remain positive for all η arises from the positivity of $n(k,t)$ which is preserved by the kinetic equation (3.9). Note that not for all x are the self-similar solutions positive. In fact, $x = x^*$ separates the values of x for which the solution is positive from the values for which it crosses zero at some η. Detecting when such zero-crossings disappear will be exploited by us for finding x^* numerically.

3.3 Convergence of the integral

3.3.1 Region $\eta_1 \ll \eta, \eta_2$

Let us introduce new variables κ_1 and θ_1:

$$\eta_1 = \eta\,\kappa_1, \tag{3.22}$$

$$\eta_2 = \sqrt{\eta^2 + \eta_1^2 - 2\eta\eta_1\cos\theta_1} = \eta\sqrt{1 + \kappa_1^2 - 2\kappa_1\cos\theta_1} = \eta\,\kappa_2. \tag{3.23}$$

Then $\kappa_1 \in [0,\infty]$, $\theta_1 \in [0,\pi]$ and we have

$$
\begin{aligned}
St &= \iint\limits_{\Delta_k} W(\eta,\eta_1,\eta_2)\, f(\eta_1)\,[f(\eta_2)-f(\eta)]\,\mathrm{d}\eta_1\mathrm{d}\eta_2 \\
&= \int\limits_0^{\eta}\int\limits_{\eta-\eta_1}^{\eta+\eta_1} W(\eta,\eta_1,\eta_2)\, f(\eta_1)\,[f(\eta_2)-f(\eta)]\,\mathrm{d}\eta_1\mathrm{d}\eta_2 \\
&\quad + \int\limits_{\eta}^{\infty}\int\limits_{\eta_1-\eta}^{\eta+\eta_1} W(\eta,\eta_1,\eta_2)\, f(\eta_1)\,[f(\eta_2)-f(\eta)]\,\mathrm{d}\eta_1\mathrm{d}\eta_2 \\
&= \eta^4 \int\limits_0^{1}\int\limits_0^{\pi} W(1,\kappa_1,\kappa_2)\, f(\eta\kappa_1)\left[f(\eta\sqrt{1+\kappa_1^2-2\kappa_1\cos\theta_1})-f(\eta)\right]\frac{\partial\kappa_2}{\partial\theta_1}\mathrm{d}\theta_1\mathrm{d}\kappa_1 \\
&\quad + \eta^4 \int\limits_1^{\infty}\int\limits_0^{\pi} W(1,\kappa_1,\kappa_2)\, f(\eta\kappa_1)\left[f(\eta\sqrt{1+\kappa_1^2-2\kappa_1\cos\theta_1})-f(\eta)\right]\frac{\partial\kappa_2}{\partial\theta_1}\mathrm{d}\theta_1\mathrm{d}\kappa_1 \\
&= \eta^4 \int\limits_0^{\infty}\int\limits_0^{\pi} V_{1\kappa_1\theta_1}\, f(\eta\kappa_1)\left[f(\eta\sqrt{1+\kappa_1^2-2\kappa_1\cos\theta_1})-f(\eta)\right]\mathrm{d}\theta_1\mathrm{d}\kappa_1, \qquad (3.24)
\end{aligned}
$$

where

$$
W(1,\kappa_1,\kappa_2) = \kappa_2\,\cos^2\theta_2\sin\theta_1 = \kappa_2\frac{(1-\kappa_1\cos\theta_1)^2}{\kappa_2^2}\sin\theta_1, \qquad (3.25)
$$

$$
\frac{\partial\kappa_2}{\partial\theta_1} = \frac{\kappa_1\sin\theta_1}{\kappa_2}, \qquad (3.26)
$$

and

$$
V_{1\kappa_1\theta_1} = W(1,\kappa_1,\kappa_2)\frac{\partial\kappa_2}{\partial\theta_1} = \frac{\kappa_1\sin^2\theta_1(1-\kappa_1\cos\theta_1)^2}{1+\kappa_1^2-2\kappa_1\cos\theta_1}. \qquad (3.27)
$$

Let us consider a contribution to the integral St that comes from the region $\kappa_1 \ll 1$. We will call it St_1. We get the expansions

$$
V_{1\kappa_1\theta_1} = \kappa_1\sin^2\theta_1 + O(\kappa_1^3), \qquad (3.28)
$$

and

$$
\begin{aligned}
&f\left(\eta\sqrt{1+\kappa_1^2-2\kappa_1\cos\theta_1}\right)-f(\eta) \\
&\quad = -\kappa_1\eta\frac{\partial f(\eta)}{\partial\eta}\cos\theta_1 + \frac{1}{2}\kappa_1^2\left(\eta\frac{\partial f(\eta)}{\partial\eta}\sin^2\theta_1 + \eta^2\frac{\partial^2 f(\eta)}{\partial\eta^2}\cos^2\theta_1\right) + O(\kappa_1^3). \qquad (3.29)
\end{aligned}
$$

Note that for validity of the expansion (3.29) for values $\eta_1 \sim 1 \ll \eta$, function $f(\eta)$ must be supra-exponential, i.e. satisfying $|f'(\eta)| \ll |f(\eta)|$.

The term with $\cos\theta_1$ in (3.29) is annihilated by integration over θ_1 as result of a symmetry with respect to the centre of $[0,\pi]$. After integrating over θ_1 we get

$$St_1 = \eta^4 \int_0^\infty \int_0^\pi V_{1\kappa_1\theta_1}\, f(\eta\kappa_1) \left[f(\eta\sqrt{1+\kappa_1^2-2\kappa_1\cos\theta_1}) - f(\eta) \right] \mathrm{d}\theta_1 \mathrm{d}\kappa_1$$
$$\approx \frac{\pi}{16} \left[3\eta \frac{\partial f(\eta)}{\partial \eta} + \eta^2 \frac{\partial^2 f(\eta)}{\partial \eta^2} \right] \int_0^\infty f(\eta\kappa_1)\eta^4\kappa_1^3 \mathrm{d}\kappa_1. \tag{3.30}$$

For solutions with asymptotics $f \to \eta^{-x}$ for $\eta \to 0$, we have the convergence condition

$$x < -4. \tag{3.31}$$

3.3.2 Region $\eta_2 \ll \eta, \eta_1$

Here, it is convenient to use the variables κ_2 and θ_2:

$$\eta_2 = \eta\,\kappa_2, \tag{3.32}$$

$$\eta_1 = \sqrt{\eta^2+\eta_2^2-2\eta\eta_2\cos\theta_2} = \eta\sqrt{1+\kappa_2^2-2\kappa_2\cos\theta_2} = \eta\,\kappa_1 \tag{3.33}$$

with $\kappa_2 \in [0,\infty]$ and $\theta_2 \in [0,\pi]$. So

$$St = \iint_{\Delta_k} W(\eta,\eta_1,\eta_2)\, f(\eta_1)\,[f(\eta_2)-f(\eta)]\,\mathrm{d}\eta_1\mathrm{d}\eta_2$$
$$= \int_0^\eta \int_{\eta-\eta_1}^{\eta+\eta_1} W(\eta,\eta_1,\eta_2)\, f(\eta_1)\,[f(\eta_2)-f(\eta)]\,\mathrm{d}\eta_1\mathrm{d}\eta_2$$
$$+ \int_\eta^\infty \int_{\eta_1-\eta}^{\eta+\eta_1} W(\eta,\eta_1,\eta_2)\, f(\eta_1)\,[f(\eta_2)-f(\eta)]\,\mathrm{d}\eta_1\mathrm{d}\eta_2$$
$$= \eta^4 \int_0^\infty \int_0^\pi V_{1\theta_2\kappa_2}\, f\left(k\sqrt{1+\kappa_2^2-2\kappa_2\cos\theta_2}\right) [f(\eta\kappa_2)-f(\eta)]\,\mathrm{d}\theta_2\mathrm{d}\kappa_2, \tag{3.34}$$

where

$$\frac{\partial\kappa_1}{\partial\theta_2} = \frac{\kappa_2\sin\theta_2}{\kappa_1},$$

and

$$V_{1\theta_2\kappa_2} = \frac{\kappa_2^2 \cos^2\theta_2 \sin\theta_2}{\sqrt{1+\kappa_2^2-2\kappa_2\cos\theta_2}} \sin\theta_1 = \frac{\kappa_2^3 \cos^2\theta_2 \sin^2\theta_2}{1+\kappa_2^2-2\kappa_2\cos\theta_2}.$$

Let us consider a contribution to the integral St that comes from the region $\kappa_2 \ll 1$. We will call it St_2. We get again the expansions:

$$V_{1\theta_2\kappa_2} = \kappa_2^3 \cos^2\theta_2 \sin^2\theta_2 + O(\kappa_2^4), \tag{3.35}$$

and

$$f\left(\eta\sqrt{1+\kappa_2^2-2\kappa_2\cos\theta_2}\right) = f(\eta) - \kappa_2\eta\frac{\partial f(\eta)}{\partial\eta}\cos\theta_2 + O(\kappa_2^2), \tag{3.36}$$

where, again, $f(\eta)$ is assumed to be supra-exponential. After integrating over θ_2 we have

$$\begin{aligned} St_2 &= \eta^4 \int_0^\infty \int_0^\pi V_{1\theta_2\kappa_2}\, f\left(\eta\sqrt{1+\kappa_2^2-2\kappa_2\cos\theta_2}\right)\left[f(\eta\kappa_2)-f(\eta)\right]\mathrm{d}\theta_2\mathrm{d}\kappa_2 \\ &\approx \frac{\pi}{8} f(\eta)\int_0^\infty f(\eta\kappa_2)\,\eta^4\kappa_2^3\mathrm{d}\kappa_2. \end{aligned} \tag{3.37}$$

The integral is the same as for the region $\eta_1 \ll \eta, \eta_2$, and therefore it is convergent again when $x < 4$.

3.3.3 Region $\eta_1, \eta_2 \gg \eta$.

For completeness, let us consider convergence of the integral at the upper end of the integration domain, $\eta_1, \eta_2 \gg \eta$. For the low-η asymptotics this would mean $\eta_1, \eta_2 \sim 1 \gg \eta$, whereas for the high-$\eta$ tail we have $\eta_1, \eta_2 \gg \eta \gg 1$. Then we assume in equations (3.24) and (3.27) that $\kappa_1 \gg 1$ and Taylor expands in $\kappa_1^{-1} \le \varepsilon \ll 1$. This gives for contributions with $\kappa_1 \ge \varepsilon^{-1}$:

$$St_3 \approx \eta^4 \int_{\varepsilon^{-1}}^\infty \int_0^\pi V_{1\kappa_1\theta_1}\, f(\eta\kappa_1)\left[f(\eta\kappa_1)-f(\eta)\right]\mathrm{d}\theta_1\mathrm{d}\kappa_1, \tag{3.38}$$

$$V_{1\kappa_1\theta_1} \approx \kappa_1 \sin^2\theta_1 \cos^2\theta_1 + O(1), \tag{3.39}$$

$$\sqrt{1+\kappa_1^2-2\kappa_1\cos\theta_1} \approx \kappa_1 - \cos\theta_1 + O\left(\kappa_1^{-1}\right). \tag{3.40}$$

Integration over θ_1 gives $\pi/8$. For decaying $f(\eta)$ we have

$$St_3 \approx \frac{\pi}{8}\eta^4 \int\limits_{\varepsilon^{-1}}^{\infty} \kappa_1\, f(\eta\kappa_1)\,[f(\eta\kappa_1) - f(\eta)]\,\mathrm{d}\kappa_1$$

$$\approx -\eta^2 f(\eta)\frac{\pi}{8} \int\limits_{\eta\varepsilon^{-1}}^{\infty} \eta_1\, f(\eta_1)\mathrm{d}\eta_1. \tag{3.41}$$

For convergence of this integral $f(\eta)$ must decay faster than $1/\eta^2$.

This condition is satisfied at $\eta \ll 1$ end if $x > 2$ and at the tail $\eta \gg 1$ if $\lambda < -2$. Both inequalities are true for the solution of the nonlinear eigenvalue problem since $-\lambda^* > x^* \approx 3.8$.

3.4 Large-η asymptotics

Finding the exponent x^* analytically is difficult and probably even impossible. The same is true even for the simplest Leith-type PDE models. However, important relations between this quantity and the other properties of function $f(\eta)$ can be established via considering the large-η asymptotics of this function.

First of all, let us consider a possibility that at the $\eta \gg 1$ tail of $f(\eta)$ the interaction is local, i.e. that the leading order contribution to the integral of (3.19) comes from $\eta_1, \eta_2 \sim \eta$, and not from the regions $\eta_1 \ll \eta, \eta_2$, $\eta_2 \ll \eta, \eta_1$ or $\eta_1 \approx \eta_2 \gg \eta$. In this case $f(\eta)$ must be bound between two power laws: $f(\eta) > const/\eta^4$ (for convergence at $\eta_1 \ll \eta, \eta_2$ and $\eta_2 \ll \eta, \eta_1$) and $f(\eta) < const/\eta^2$ (for convergence at $\eta_1 \approx \eta_2 \gg \eta$); see Section 3.3. So let us take $f(\eta) = C\eta^y$ with $-4 < y < -2$ and $C = \mathrm{const}$. Then equation (3.19) becomes

$$(x+y)\eta^y = \frac{C}{b} \iint\limits_{\Delta_1} W(\eta, \eta_1, \eta_2)\eta_1^y(\eta_2^y - \eta^y)\mathrm{d}\eta_1\mathrm{d}\eta_2. \tag{3.42}$$

This can then be rewritten using the variables

$$\kappa_1 = \eta_1/\eta \quad \text{and} \quad \kappa_2 = \eta_2/\eta \tag{3.43}$$

to give

$$x + y = C\eta^{y+4}\frac{1}{b} \iint\limits_{\Delta_1} W(1, \kappa_1, \kappa_2)\kappa_1^y[\kappa_2^y - 1]d\kappa_1\kappa_2. \tag{3.44}$$

Because of the pre-factor η^{y+4} the right-hand side tends to infinity as $\eta \to \infty$. Thus

this equation can only be satisfied when the integral is zero, i.e. when y corresponds to the stationary KZ solution. But this solution must be rejected because it does not conserve energy – the energy flux is constant on this solution, and the energy is lost at $\eta \to \infty$ at a constant rate. Therefore, the interaction at the $\eta \gg 1$ tail of $f(\eta)$ is nonlocal. Nonlocal interaction with region $\eta_1 \approx \eta_2 \gg \eta$ implies slowly decaying tails with $f(\eta) > const/\eta^2$. Such spectra contain infinite energy $2\pi \int_0^\infty kn(k,t)\,dk$ and, therefore, cannot develop out of a finite-energy initial data. Thus, the nonlocal interaction takes place with the large-scale regions $\eta_1 \ll \eta, \eta_2$ and $\eta_2 \ll \eta, \eta_1$.

3.4.1 Absence of exponential and super-exponential tails

Consider first the region $\eta_1 \ll \eta, \eta_2$ and suppose that the main contribution comes from the scales $\eta_1 \sim 1$. Here we have the second small parameter $\sigma = \eta_2 - \eta$ such that within Δ_η we have $|\sigma| \le \eta_1 \sim 1 \ll \eta$. Taylor expanding the interaction coefficient, we have

$$W(\eta, \eta_1, \eta_2) = \eta^2 \sqrt{1 - \frac{\sigma^2}{\eta_1^2}} + \eta^2 o(\eta_1^2) + \eta^2 o(\sigma^2), \tag{3.45}$$

and equation (3.19) becomes

$$xf + \eta f' \approx \frac{\eta^2}{b} \int_0^\infty f(\eta_1) d\eta_1 \int_{-\eta_1}^{\eta_1} \sqrt{1 - \frac{\sigma^2}{\eta_1^2}}\, [f(\eta+\sigma) - f(\eta)]\, d\sigma. \tag{3.46}$$

Suppose that the tail of $f(\eta)$ is decaying so rapidly that $|\eta_1 f'(\eta)|$ is not small compared to $|f(\eta)|$ so that one cannot Taylor expand the square bracket in the above equation. This is the case, e.g., for the exponential and super-exponential functions, $f(\eta) \sim e^{-\mu\eta^d}$ with $\mu = const \sim 1$ and $d \ge 1$. Then the first term on the left-hand side of (3.46) can be neglected,

$$f' \approx \frac{\eta}{b} \int_0^\infty f(\eta_1) d\eta_1 \int_{-\eta_1}^{\eta_1} \sqrt{1 - \frac{\sigma^2}{\eta_1^2}}\, [f(\eta+\sigma) - f(\eta)]\, d\sigma. \tag{3.47}$$

Substituting the exponential function ($d = 1$) into Equation (3.47) gives

$$-\mu^2 = \frac{\eta}{b} \int_{-\eta_1}^{\eta_1} \sqrt{1 - \frac{\sigma^2}{\eta_1^2}}\, [f(\eta+\sigma) - f(\eta)]\, d\sigma. \tag{3.48}$$

The left hand side is a constant whereas the right hand side is a linear function of η, thus the equation is clearly not satisfied in this case.

For $d > 1$ the second term in the square bracket is sub-dominant and can be neglected. Since $b < 0$, we have in this case

$$\begin{aligned} bf' &\approx \eta \int_0^\infty f(\eta_1) d\eta_1 \int_{-\eta_1}^{\eta_1} \sqrt{1 - \frac{\sigma^2}{\eta_1^2}}\, f(\eta+\sigma) d\sigma \\ &> \eta \int_0^\infty f(\eta_1) d\eta_1 \int_{-\eta_1}^{0} \sqrt{1 - \frac{\sigma^2}{\eta_1^2}}\, f(\eta+\sigma) d\sigma \\ &> \eta f(\eta) \int_0^\infty f(\eta_1) d\eta_1 \int_{-\eta_1}^{0} \sqrt{1 - \frac{\sigma^2}{\eta_1^2}}\, d\sigma = \frac{\pi}{4} \eta f(\eta) \int_0^\infty f(\eta_1) \eta_1 d\eta_1 \\ &= \infty, \end{aligned} \tag{3.49}$$

since $f(\eta_1) \to \eta_1^{-x}$ with $x > 2$ for $\eta_1 \to 0$. Thus, we arrive at an inequality which is false and, therefore, the exponential and super-exponential tails are not possible. Taking into account the region $\eta_2 \ll \eta, \eta_1$ would not change this conclusion because the respective contribution is strictly positive.

3.4.2 Power-law decay at $\eta \gg 1$

For supra-exponential tails, such that $|f'(\eta)| \ll |f(\eta)|$, e.g. when $f(\eta) \sim e^{-\mu\eta^d}$ with $\mu = const \sim 1$ and $0 < d < 1$ or $f(\eta) \sim \eta^{-y}$ with $y > 0$, the square brackets in equation (3.46) can be Taylor expanded in $\eta_1 \sim \sigma \sim 1 \ll \eta$. Similarly, the integrand of (3.19) can be expanded in $\eta_2 \sim \rho = \eta_1 - \eta \sim 1 \ll \eta$. The sum of the respective contributions from the regions $\eta_1 \ll \eta, \eta_2$ and $\eta_2 \ll \eta, \eta_1$ (expressions (3.30) and (3.37) respectively, see Section 3.3) leads to the following ODE,

$$xf + \eta f' = N^{-1} \left[3\eta f' + \eta^2 f'' + 2f \right], \tag{3.50}$$

where

$$N = \frac{16b}{\pi D} < 0 \quad \text{and} \quad D = \int_0^\infty f(\eta_1) \eta_1^3 \, d\eta_1. \tag{3.51}$$

We should consider N to be a given constant which makes this ODE linear and easy to solve. Note that the integral D is convergent at $\eta_1 \to 0$ since $f(\eta_1) \to \eta_1^{-x}$ with $x < 4$. Convergence at $\eta_1 \to \infty$ is assumed for now but will be checked *a posteriori*. It requires that $f(\eta) < const\, \eta^{-4}$ at $\eta \to \infty$. Such a convergence on both ends of the integration region implies that the main contribution in the integral D comes from the region $\eta_1 \sim 1$, which is consistent with the Taylor expansion used.

Let us introduce

$$N^*(x) = -2\left[(x-1) + \sqrt{(x-1)^2+1}\right] < 0. \tag{3.52}$$

For $N \neq N^*$, equation (3.50) has two fundamental power-law solutions:

$$f = \eta^{\lambda_1} \quad \text{and} \quad f = \eta^{\lambda_2}, \tag{3.53}$$

with $\lambda_1 \neq \lambda_2$:

$$\lambda_1 = -1 + \frac{N}{2} - \frac{1}{2}\sqrt{N^2 + 4N(x-1) - 4}, \tag{3.54}$$

and

$$\lambda_2 = -1 + \frac{N}{2} + \frac{1}{2}\sqrt{N^2 + 4N(x-1) - 4}. \tag{3.55}$$

For $N = N^*$, the exponents of the power laws degenerate, $\lambda_1 = \lambda_2 = \lambda^*$, and the fundamental solutions become

$$f = \eta^{\lambda^*} \quad \text{and} \quad f = \eta^{\lambda^*} \ln \eta. \tag{3.56}$$

The linear combination of these solutions can be written in the form

$$f = C\eta^{\lambda^*} \ln(\eta_0/\eta) \tag{3.57}$$

with some constants C and η_0 (the latter being positive) and

$$\lambda^* = -1 + \frac{N^*}{2}. \tag{3.58}$$

We can see that solution (3.57) crosses zero at $\eta = \eta_0$ excepting for the case $\eta_0 \to \infty$, in which case one simply has $f = C\eta^{\lambda^*}$.

3.4.3 The tail corresponding to the solution with $x = x^*$

The nonlinear eigenvalue problem we have formulated requires finding $x = x^*$ for which the tail of $f(\eta)$ decays in the fastest way while remaining positive.

For $N < N^*$, the exponents λ_1 and λ_2 are complex. The corresponding real-valued solutions have infinitely many zero crossings and, therefore, cannot correspond to the solution of the nonlinear eigenvalue problem.

The solutions that stay positive for all η are only possible for $N \geq N^*$. These are the power laws, the steepest among which corresponds to the lowest value of N, namely $N = N^*$, and this is the solution that corresponds to $x = x^*$. Choosing the

solution that remains positive in this case, we finally have:

$$f(\eta) = \eta^{\lambda^*}, \quad \lambda^* = -1 + \frac{N^*(x^*)}{2} = -x^* - \sqrt{(x^*-1)^2+1}. \tag{3.59}$$

Here we have used

$$N^*(x^*) = -2\left[(x^*-1) + \sqrt{(x^*-1)^2+1}\right]. \tag{3.60}$$

Now we can check the consistency of our approach based on the Taylor expansion which requires convergence at infinity of the integral (3.51) defining N. The condition for this is $\lambda^* < -4$ which means $x^* > 7/5$. Since $x^* > 2$, this consistency condition is satisfied.

Equation (3.60) combined with (3.51) leads to the prediction of the relationship (3.12) between x^* and $f(\eta)$.

$$D = \int_0^\infty f(\eta)\eta^3 d\eta = \frac{8}{\pi(4-x^*)\left[(x^*-1) + \sqrt{(x^*-1)^2+1}\right]}. \tag{3.61}$$

This prediction will be put to test via numerical simulations in the next Section.

3.5 Numerical simulations

3.5.1 Transformation of equation

Self-similar solutions have been found by numerical simulation of the governing equation. Equation (3.19) can be transformed via the substitution $g(\eta) = f(\eta)\eta^x$ in order to simplify the boundary condition and cancel one of the terms on the left hand side. In terms of the new function $g(\eta)$, the equation to be solved is now

$$g'(\eta) = \frac{1}{8b}\iint_{\Delta_\eta} W(\eta,\eta_1,\eta_2)\eta^{x-1}\eta_1^{-x} g(\eta_1)[\eta_2^{-x} g(\eta_2) - \eta^{-x} g(\eta)]d\eta_1\eta_2, \tag{3.62}$$

with the interaction coefficient $W(\eta,\eta_1,\eta_2)$ defined as in (3.11). The left boundary condition is then

$$g(\eta) \to 1 \quad \text{for} \quad \eta \to 0. \tag{3.63}$$

3.5.2 Set-up

It was chosen to use an iterative method to solve equation (3.62). The equation is written as

$$g'_{n+1}(\eta) = \frac{1}{8b} \iint_{\Delta_\eta} W(\eta, \eta_1, \eta_2) \eta^{x-1} \eta_1^{-x} g_n(\eta_1) [\eta_2^{-x} g_n(\eta_2) - \eta^{-x} g_n(\eta)] d\eta_1 \eta_2. \quad (3.64)$$

In order to perform the iteration, we require a method for evaluating the derivative and a method for evaluating the integral.

Evaluating the integral

To calculate the two-dimensional integral, the method described in [41] is employed. The integral solved in that reference was of a similar type with the same boundary conditions. The method is deviated from by the discretisation δ, which is chosen to be linear rather than logarithmic. The logarithmic discretisation allows for a wider range of wavenumbers to be computed, but we suspect that this comes at the cost of not well resolving the propagating front of the system. This also differs from the methodology in [27] which retained the logarithmic discretisation.

The method for integration goes as follows. First, the integration area is broken up into squares of length δ_η as illustrated in Figure 3.5.2. For each square, the fraction which lies inside the integration region is calculated. Call this fraction β. The integrand is then calculated at the centre of each square and then multiplied by $\beta\delta_\eta^2$. This is then summed for all the squares.

Evaluating the derivative

In order to approximate the derivative, a forward first order method is chosen

$$g'_{n+1}(\eta) = \frac{g_{n+1}(\eta + \delta) - g_{n+1}(\eta)}{\delta}. \quad (3.65)$$

Notice that the $n + 1$ iteration is chosen for both terms in the approximation. A number of other approximations were also tried including second-order approximations. The first-order approximation was chosen to reduce the computational cost. Backward approximations and approximations involving a combination of the $n+1$ and n iteration were ruled out due to the method not converging to a solution.

Using the methods described for evaluating the integral and differential,

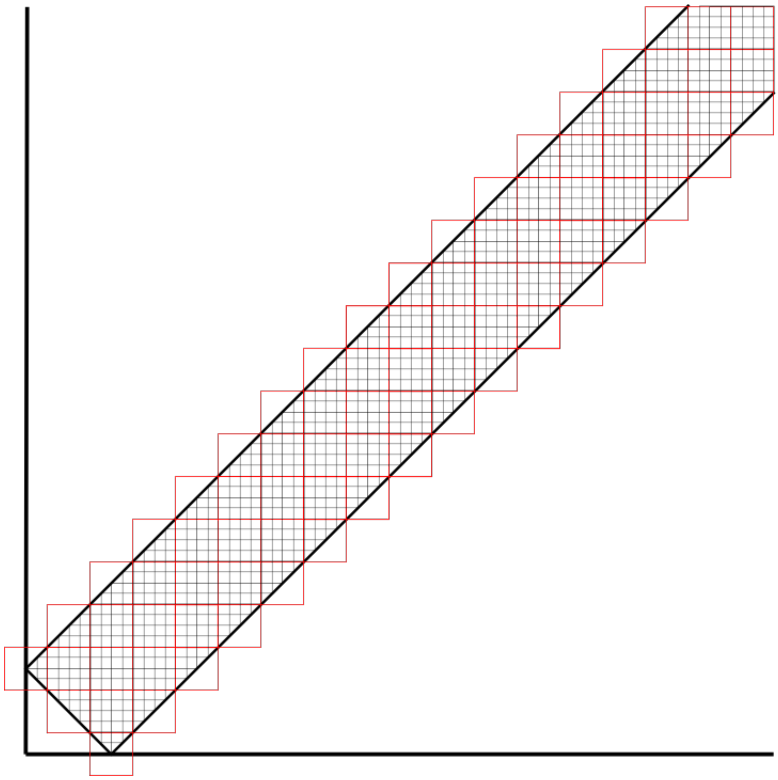

Figure 3.3: Splitting of the region of integration into squares.

equation (3.62) is solved by the iterative scheme

$$\frac{g_{n+1}(\eta+\delta)-g_{n+1}(\eta)}{\delta} = \frac{1}{8b}\iint_{\Delta_\eta} W(\eta,\eta_1,\eta_2)\eta^{x-1}\eta_1^{-x}g_n(\eta_1)[\eta_2^{-x}g_n(\eta_2)-\eta^{-x}g_n(\eta)]d\eta_1\eta_2. \tag{3.66}$$

The initial function $g_0(\eta)$ is chosen to be an indicator function on the set $\{0,1\}$ and the iteration is performed until the function $g(\eta)$ converges.

In order for the iteration procedure described to converge to a solution, two additional adjustments must be made. Firstly, the iteration procedure described will not converge to a solution if the range of η's considered begins at 0. This is due to the fact that the integrand becomes extremely large as η_1 and η_2 approach zero. We therefore introduce a further parameter $\eta_{\min}$.

It was found that as the iteration were performed, the solution became unstable at high η. This instability is then fed back into the following iteration thus increasing the level of instability. Applying a moving average filter at the upper half of the range of η was found to mitigate this issue and resulted in a convergent solution.

It should be noted that the iteration procedure does not converge to a solution on the whole domain but instead on a sub-domain containing the first two thirds of the η's. We attribute this to the truncation of the area over which we integrate illustrated in Figure 3.1. As η gets closer to $\eta_{\max}$, the rectangle becomes wider but more of the region with $\eta_1, \eta_2 > \eta_{\max}$ gets lost.

3.5.3 Parameters

The solution found by the iteration procedure is sensitive to the choice of parameters used. We have the following key parameters; the discretisation δ, the maximum similarity variable $\eta_{\max}$ and the minimum similarity variable $\eta_{\min}$. The convergence should be checked as

1. $\delta \to 0$,
2. $\eta_{\max} \to \infty$,
3. $\eta_{\min} \to 0$.

Convergence testing of the solution in terms of the three parameters was performed as follows:

1. The value of $\eta_{\max}$ and $\eta_{\min}$ are initially fixed.

2. δ is made progressively smaller until the solution converges.

3. $\eta_{\min}$ is then progressively decreased, with step 2 being re-performed at each value of $\eta_{\min}$ until the solution is converged in both $\eta_{\min}$ and δ.

4. $\eta_{\max}$ is progressively increased, once again the convergence in $\eta_{\min}$ and δ is checked at each value.

5. Once this is complete, the solution will be converged in the limiting values of each of the three parameters.

The code itself has been written in C++ and utilises MPI for parallelization. The code is parallelized in the η variables in which the whole domain is split up into P sub-domains where P is the number of processors. In order to ensure that each processor has a domain of an equal size, the maximum wavenumber is adjusted such that it is divisible by P. The two-dimensional integral was performed in serial because at each η the integral requires information from every η_1 and η_2. Even so, parallelization in one variable allowed for much faster computation than a serial code would allow.

Providing that $\eta_{\max}$ is large enough to resolve the decay of the function, increasing it further has no effect on the shape of the solution. We have chosen the moderate value $\eta_{\max} = 15$ in order to reduce computational cost. There is a greater sensitivity on the solution to the value of $\eta_{\min}$ due to the singularity of the integrand at zero η_1 and η_2. Experimentally, the decay of $g(\eta)$ is steeper for smaller values of $\eta_{\min}$. Obviously, the smaller $\eta_{\min}$ is made, the smaller δ must be chosen, and thus the larger the computational cost. This constraint is more severe for the convergence of the solution at small η's. However, as we approach larger values of η where the function is closer to zero, we do find good convergence. For identifying the value of x^* and for comparing with the theory developed in the previous section, this is the region of our interest. The remaining parameters used for what follows are $\eta_{\min} = 0.00625$ and $\delta = 0.0015625$.

3.5.4 Identifying x^*

The solution which corresponds to $x = x^*$ is one which stays positive for all η and the fastest decaying. From our simulations we find

$$x^* = 3.80 \pm 0.01. \tag{3.67}$$

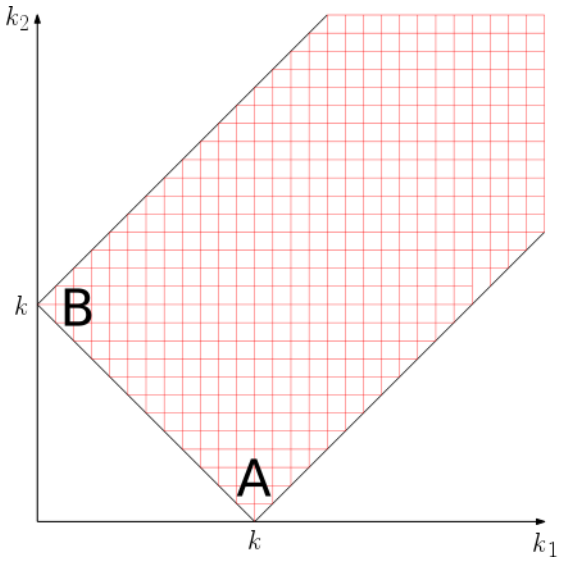

Figure 3.4: The integration area. The integrand becomes very large in regions A and B.

This is plotted in Figure 3.5.4 along with the solution for $x = 3.33$, *i.e.* the exponent found by Galtier *et. al* in [27]. The solution for $x = 3.33$ can be seen to cross zero, thus violating one of the conditions for a valid solution.

The reason for the difference between the value of x^* in this work and the one found by Galtier *et. al* in [27] is not known and would require further work to clarify. We postulate that the reason may be due to the logarithmic discretisation used in [27]. The integrand becomes very large as η_1 and η_2 enter the regions A and B in Figure 3.5.4. Looking at region B, it can be shown that there is a symmetry around the line $\eta_2 = \eta$ such that the integrand at points equidistant from this line are equal and of opposite sign. Therefore, if the discretisation is linear, the integrand will not blow up in region B since there will be cancellation of the extreme values. However, if a logarithmic discretisation is used, then the symmetric values are not resolved and so the value of the integrand in region B is exaggerated. A similar argument is valid in region A.

The solution found for $x = x^* = 3.80$ can then be compared to the theory developed in Section 3.4. Substituting x^* into equation (3.60), we find

$$N^*(x^*) = -11.55. \tag{3.68}$$

This can be compared with the value of N found for the simulation with $x = 3.8$,

$$N_{x=3.8} = -11.23, \tag{3.69}$$

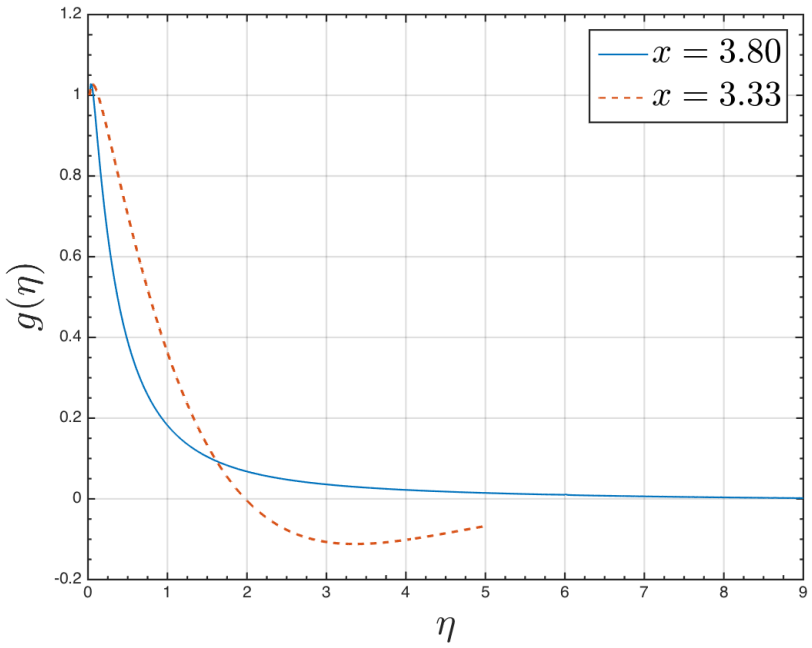

Figure 3.5: The solution for $x = x^*$ compared with the solution for $x = 3.33$, the previously reported value of x^*.

which was found using relations (3.51). This is accurate within under 3% and since N^* corresponds to a power law tail, this can be seen as some verification of this hypothesis.

From (3.58) we expect the tail to behave as

$$g(\eta) = C\eta^{-2.97}. \tag{3.70}$$

We have tried to fit this prediction with our numerical solution but only a small range for the tail is available and in this range the prediction does fit in a small region only. While this fit is not conclusive, it is at least consistent with the prediction. This power law fit is shown in Figure 3.5.4 along with two further power laws for an eye guide. An exponential and super-exponential fits were also attempted. They did not prove to be consistent with our numerics.

The spectrum for $x = x^*$ is plotted again in Figure 3.5.4, transformed back into the $f(\eta)$ variables so that is can be compared more easily with the prediction. It is also compensated by the Kolmogorov-Zakharov spectrum to show the absence of such a spectrum at this point. Also plotted is η^{x^*}. We see that at large scales the spectrum approaches the x^* scaling prediction as expected.

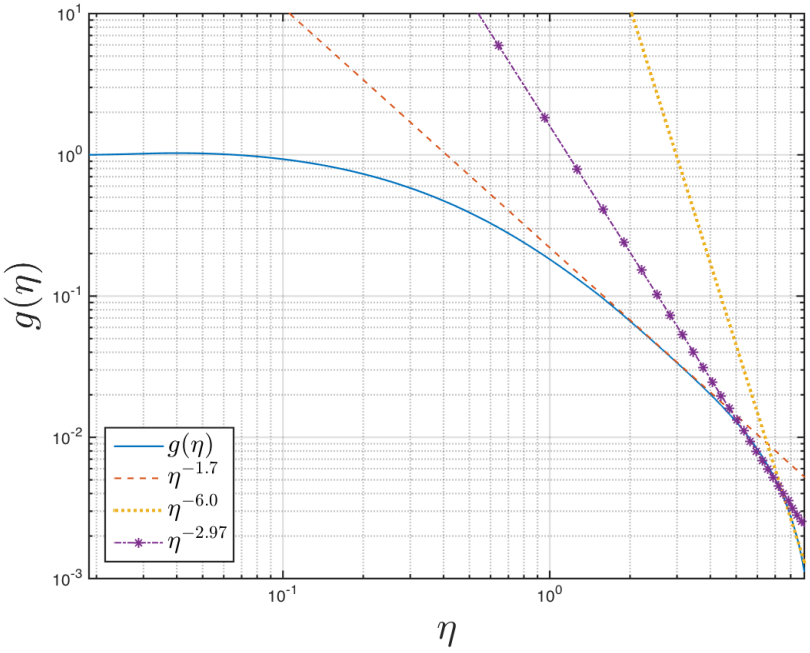

Figure 3.6: Power law fits compared to the solution for x^*. Two power laws are fitted as a guide, these seem to fit in two small regions. The theoretical prediction is in between these two guides.

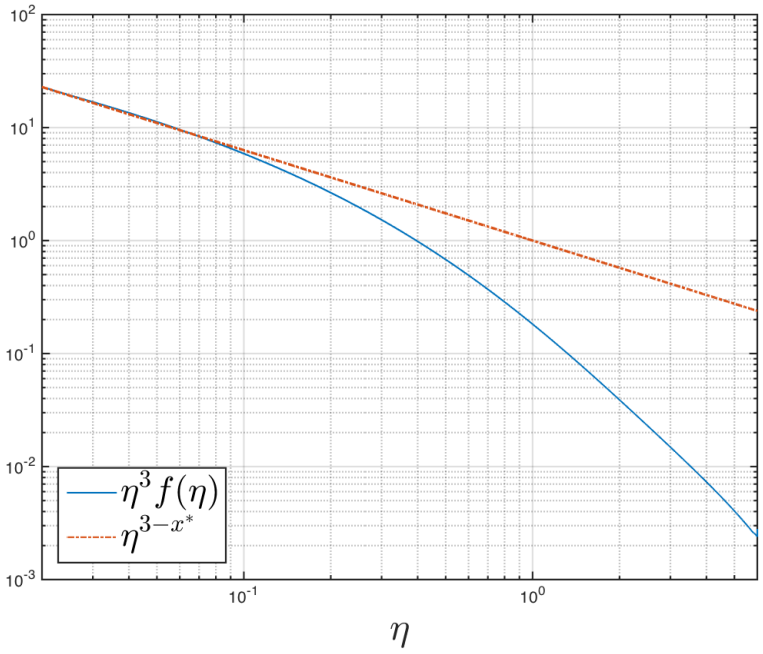

Figure 3.7: The spectrum found for x^* compensated by the Kolmogorov-Zakharov spectrum η^{-3}.

3.6 Conclusions

In this chapter, we considered self-similar solutions of the integro-differential kinetic equation (3.9) describing the MHD wave turbulence. Such self-similar solutions are of the second kind, which, by definition, means that the self-similarity parameters can not be uniquely fixed by a dimensional analysis based on a conservation law. Namely, there remains a single parameter which depends on the shape of the self-similar solution globally. This parameter was to be found by solving a nonlinear eigenvalue problem, i.e. matching the solution to relevant boundary conditions at the two ends of the interval of the self-similar variable: in our case $\eta \to 0$ and $\eta \to \infty$. The boundary conditions were to be chosen from the consideration that the respective solution is asymptotically approached as $t \to t^*$ (with some $t^* < \infty$) by the solution of the initial value problem with initial data in the finite range of wave numbers.

We postulated the following boundary conditions defining the nonlinear eigenvalue problem of the self-similar solutions. At $\eta \to 0$, the self-similar solution must tend to a power-law asymptotics, $f(\eta) \to \eta^{-x}$. The second boundary condition is that at $\eta \to \infty$ one must satisfy $f(\eta) \to 0$ where the decay to zero is the fastest

among the solutions corresponding to different parameters x in the class of positive functions $f(\eta)$. The respective value $x = x^*$ and the respective function $f(\eta)$ comprise the solution of the nonlinear eigenvalue problem. Our conjecture (yet unproven) is that the postulated boundary value problem does yield a self-similar solution which is asymptotically approached as $t \to t^*$ (with some $t^* < \infty$) by the solution of the initial value problem with initial data in the finite range of wave numbers.

We also proved that the tail of $f(\eta)$ at $\eta \to \infty$ cannot be exponentially or super-exponentially decaying. Instead, the tail is shown to be a power law with the index λ^* related to x^* as in (3.59). This leads to the prediction of a relation (3.12) between x^* and the integral of the solution $f(\eta)$ which was confirmed by numerical simulations.

The value x^* depends on the global shape of $f(\eta)$ rather than its asymptotics at the boundaries $\eta \to 0$ and $\eta \to \infty$, and, perhaps, it cannot be found analytically. Our numerical solution of the stated nonlinear eigenvalue problem yields the value $x^* = 3.80 \pm 0.01$.

We believe that the nonlinear eigenvalue problem formulated in the present paper and the methods of analysing the large-η asymptotics can be applied to other kinetic equations in Wave Turbulence and to the Smoluchowski kinetic equation and similar integro-differential equations.

Chapter 4

Reflected wave solution of Alfvén wave turbulence

4.1 Introduction

In the last chapter, the development of the stationary spectrum in Alfvén wave turbulence was discussed. The last chapter focussed on the first stage of evolution in which the energy spectrum evolves as a self-similar solution of the second kind. In such solutions, the similarity variables cannot be fixed by a conservation law but instead they are found as the result of a nonlinear eigenvalue problem. This eigenvalue problem was solved numerically by matching the solution to the relevant boundary conditions at either side of the interval of the self-similar variable, i.e. at $\eta \to 0$ and $\eta \to \infty$. This first stage only tells part of the story and a description of the stage immediately following this one is needed to tell the complete story.

In this chapter, the second self-similar evolution stage of the weak MHD turbulence is investigated using numerical simulation. This stage consists of a reflection wave propagating from large to small wavenumbers leaving the KZ spectrum in its wake and a power law asymptotic k^{-x_*} at low wavenumbers. Naturally, there must exist a transition scale k_{tr} between these two scalings which moves towards lower k. This stage is relevant only for the finite time in which k_{tr} reaches the largest scales of the system. As in the previous stage, the reflection wave stage is described by a self-similar solution. However, unlike in self-similar solutions of the second kind, the similarity indices a and b are not to be found by solving a nonlinear eigenvalue problem. Nor are they uniquely determined by the energy conservation law as per self-similar solutions of the first kind. Instead the asymptotical behaviour arising from the pre-t_* self-similar solution is imposed at the small-η end of the post-t_*

similarity interval, and this fixes the similarity indices. The asymptotic imposed at small η is the power law η^{-x_*} which was identified in the first stage of the turbulent spectra evolution. This type of self-similarity does not fit into the Zeldovich-Raizer classification [85] and, therefore, it was called a self-similar behaviour of the third kind in [56] where it was first studied within the Leith model of hydrodynamic turbulence.

The basic equation used to study this second stage is the same kinetic equation as was used in the first stage. This is reproduced here for clarity. The transverse spectrum $n(k,t)$ evolves according to the following kinetic equation [27, 55, 23],

$$\frac{\partial n(k,t)}{\partial t} = \iint\limits_{\Delta_k} W(k,k_1,k_2)\, n(k_1)\,[n(k_2) - n(k)]\, dk_1 dk_2, \tag{4.1}$$

where $k = |\mathbf{k}|$, $k_1 = |\mathbf{k}_{1\perp}|$, $k_2 = |\mathbf{k}_{2\perp}|$. The integration area Δ_k is determined by the triangle inequalities,

$$\Delta_k = \{(k_1,k_2) \,:\, (k \le k_1 + k_2) \wedge (k_1 \le k + k_2) \wedge (k_2 \le k_1 + k)\}\,. \tag{4.2}$$

The interaction coefficient is

$$W(k,k_1,k_2) = kk_2\, \cos^2\theta_2 \sin\theta_1, \tag{4.3}$$

where θ_2 is the angle between $\mathbf{k}$ and $\mathbf{k}_2$, and θ_1 is the angle between $\mathbf{k}$ and $\mathbf{k}_1$. Therefore,

$$\cos^2\theta_2 = \left(\frac{k^2 - k_1^2 + k_2^2}{2kk_2}\right)^2, \quad \sin\theta_1 = \frac{\sqrt{2(k^2k_1^2 + k^2k_2^2 + k_1^2k_2^2) - k^4 - k_1^4 - k_2^4}}{2kk_1}.$$

4.2 Self-similar solutions of the third kind

Let us start by formulating the problem for the time period right after t_*. We look for self-similar solutions of Equation (4.1) in the form

$$n(t,k) = \frac{1}{\tau^a} f(\eta), \quad \eta = \frac{k}{\tau^b}, \quad \tau = t - t_*. \tag{4.4}$$

Note that the only difference with (3.13), although a very important one, is the sign in the expression for τ. Substituting into the kinetic equation gives

$$\frac{1}{\tau^{a+1}}(af + b\eta f') = -\iint\limits_{\Delta_\eta} \frac{\tau^{4b}}{\tau^{2a}} W(\eta,\eta_1,\eta_2) f(\eta_1)[f(\eta_2) - f(\eta)] d\eta_1 d\eta_2, \tag{4.5}$$

where Δ_η and $W(\eta, \eta_1, \eta_2)$ are given by (4.2) and (4.3) respectively, with k, k_1, k_2 replaced with η, η_1, η_2. In order to eliminate τ, we impose the condition $a = 1 + 4b$. For $\eta \to 0$, the right-hand side of equation (4.5) should become negligible compared to each of the terms on the left-hand side (*i.e.* the nonlinear wave interaction becomes vanishing). This condition along with the boundary condition $f(\eta) \to \eta^{-x_*}$, where $x_* \approx 3.80$ is the exponent of the self-similar solution of the second kind found in [6] for $t < t^*$, allows us to fix $x_* = a/b$ and, therefore, indices a and b. Specifically they are found to be

$$a = \frac{x_*}{x_* - 4} \approx -19, \quad b = \frac{1}{x_* - 4} \approx -5, \tag{4.6}$$

and the integro-differential equation governing the self-similar solution is

$$x_* f + \eta f' = -(x_* - 4) \iint_{\Delta_\eta} W(\eta, \eta_1, \eta_2) f(\eta_1)[f(\eta_2) - f(\eta)] d\eta_1 d\eta_2. \tag{4.7}$$

The self-similar indices a and b have been fixed without using a conservation law or by solving a nonlinear eigenvalue solution. We thus suggest that this solution is distinct from either the self-similar solutions of the first or second kind.

4.2.1 Boundary conditions

Equation (4.7) must be supplemented with boundary conditions at $\eta \to 0$ and $\eta \to \infty$. The reflected wave immediately follows the self-similar solution of the second kind which had power law solution η^{-x_*} and propagates from large to small wave numbers leaving the KZ spectrum in its wake. This suggests the following two boundary conditions:

$$f(\eta) \to \eta^{-x_*} \quad \text{for} \quad \eta \to 0, \tag{4.8}$$

$$f(\eta) \to c\eta^{-x_{KZ}} \quad (\text{with } x_{KZ} = 3) \quad \text{for} \quad \eta \to \infty, \tag{4.9}$$

where c is a positive constant.

Note that the interaction coefficient in equation (4.7) is a homogeneous function

$$W(\lambda\eta, \lambda\eta_1, \lambda\eta_2) = \lambda^2 W(\eta, \eta_1, \eta_2). \tag{4.10}$$

Supposing that $f(\eta)$ is a solution of the equation satisfying both of the boundary conditions then $f(\eta) = \lambda^{-4} f(\lambda\eta)$ is also a solution satisfying the boundary conditions. This means that we can rescale the solution to eliminate the pre-factor in front of one of the two power laws in (4.8) and (4.9) . We choose to consider condition (4.8) without the pre-factor leaving condition (4.9) with a pre-factor c to be found.

Identification of this pre-factor constitutes a nonlinear eigenvalue problem, namely solving equation (4.7) with the specified boundary conditions. The parameter to be found from this is not however one of the similarity parameters a and b as per the definition of Zeldovich-Raizer [85], and so we do not consider the problem to be self-similarity of the second kind.

The boundary condition (4.8) is consistent with the self-similar formulation provided that there is convergence of the integral as $\eta_1 \to 0$ and $\eta_2 \to 0$ and condition (4.9)—at $\eta_1, \eta_2 \to \infty$. Proof of such convergence is identical to the analysis in Section 3.3. The condition for convergence is $x_* < 4$ at $\eta_1 \to 0$ and $\eta_2 \to 0$ and $x_* > 2$ at $\eta_1, \eta_2 \to \infty$. Both conditions are clearly satisfied for $x = x_* = 3.8$ and $x = x_{KZ} = 3$.

4.3 Numerical simulations

4.3.1 Set up

Solutions of equation (4.7) have been found numerically. The equation is first transformed via the substitution $g(\eta) = f(\eta)\eta^{x_*}$ in order to desingularise the boundary condition (4.9). The equation governing the self-similar solutions in terms of this new function is then

$$g'(\eta) = -(x_* - 4) \iint_{\Delta_\eta} W(\eta, \eta_1, \eta_2)\eta^{x_*-1}\eta_1^{-x_*} g(\eta_1)[\eta_2^{-x_*} g(\eta_2) - \eta^{-x_*} g(\eta)]d\eta_1 d\eta_2, \tag{4.11}$$

with the two boundary conditions now given by

$$g(\eta) \to 1 \quad \text{for} \quad \eta \to 0, \tag{4.12}$$

$$g(\eta) \to c\eta^{x_*-3} \quad \text{for} \quad \eta \to \infty. \tag{4.13}$$

Equation (4.11) is solved using an iterative procedure

$$g'_{n+1}(\eta) = -(x_*-4) \iint_{\Delta_\eta} W(\eta, \eta_1, \eta_2)\eta^{x_*-1}\eta_1^{-x_*} g_n(\eta_1)[\eta_2^{-x_*} g_n(\eta_2) - \eta^{-x_*} g_n(\eta)]d\eta_1 d\eta_2, \tag{4.14}$$

where the derivative is replaced by its discretised version:

$$g'_{n+1}(\eta) = \frac{g_{n+1}(\eta + \delta\eta) - g_{n+1}(\eta)}{\delta\eta}. \tag{4.15}$$

The two-dimensional integral was calculated in the method outlined by Leith [41]. The two dimensional domain (η_1, η_2) is broken into squares of side δ_η. The proportion of each square that is enclosed in the integration region $\Delta\eta$ is then calculated. This fraction is then multiplied by the value of the integrand at the centre of the square. Unlike Leith, we have chosen to use a linear discretisation as opposed to a logarithmic one. Doing so sacrifices the long range attainable using a logarithmic discretisation. However we believe that such a discretisation may not resolve well the propagating front central to this work.

The domain of η's over which the iteration is performed is broken down into two sub-domains. The first part of the domain is allowed to evolve freely according to the iteration procedure. The final part of the domain is not computed: it is forced to abide by the functional form (4.13). Picking this sub-domain to be large relative to the total range alleviates the issues which arise from truncating the area of integration Δ_η at a maximum wavenumber k_{max}. If the area is not large enough, the solution is found to diverge as the iterative procedure is performed due to the nonlocal nature of the contributions to the integral in the right-hand side. Without the inclusion of the forced sub-domain, it was found that at high values of η, the function g oscillates between large positive and negative values. As the iteration procedure continues, these large values feed back into the calculation of the new function g at lower η causing fast divergence to infinity. Including the forced sub-domain alleviates this issue and seems valid due to the boundary conditions we are considering for the reflected wave solution.

The initial condition is chosen as

$$g_0(\eta) = 1 + c\eta^{x_*-3}, \tag{4.16}$$

where $x_* = 3.8$ is used. This initial condition satisfies both of the boundary conditions.

One could think of the most straightforward strategy of iterating the specified numerical routine at many different *fixed* values of c and choosing the ultimate value of c based on the condition that the iterations converge to a smooth solution. It turns out that following this strategy it is practically impossible to identify such a value of c because even slight deviations in c lead to very fast divergence of the iterations. Thus, we have devised a different solution strategy which turned out to be successful.

Namely, the pre-factor c is given an initial value but is allowed to change between iterations by an adaptive algorithm in order to converge to a final value.

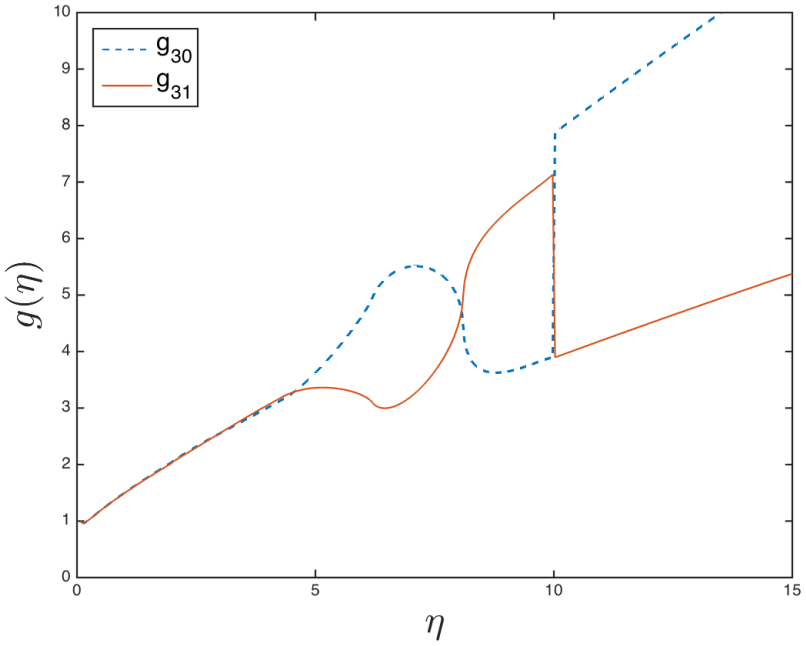

Figure 4.1: Two subsequent iterations showing how the value of c is adjusted between iterations.

This adaptive algorithm can be demonstrated by Figure 4.1 which shows two subsequent iterations of a run with $\eta = [0, 40]$. The functional form (4.13) is imposed for $\eta \geq 10$ and looking at the first iteration shown by the dashed line, we see a jump between the function before this point and the function from this point. The next value of c is chosen so that it would ensure a continuous function $f(\eta)$. It can then be estimated as

$$c = \lim_{\delta\eta \to 0} g(\eta)\eta^{3-x_*}|_{\eta=10-\delta\eta}. \tag{4.17}$$

This new value of c is then used for the next iteration and given a long enough run will converge to a single value. The value of $\delta\eta$ in this estimate is taken to be equal to the spacing between the adjacent points of the discretised η variable.

4.3.2 Convergence

We have three parameters in our method which may affect the value of c found and thus it must be checked that the result converges as each parameter is taken to its respective limit. The parameters in question are the maximum wavenumber $\eta_{\max}$, the wavenumber at which the stationary spectrum is imposed η_{cut} and the discretisation $\delta\eta$. The cut off wavenumber η_{cut} is considered as a fraction of $\eta_{\max}$.

Numerous runs of the iteration procedure have been performed to test the effect of each of these parameters. The least computationally intensive runs were performed with $\eta_{\max} = 20$ and $\delta\eta = 0.1$. Runs were performed at this resolution for different values of η_{cut} which was increased until the found value of c converged. Fixing $\eta_{\max}$, the value of $\delta\eta$ was then decreased several times and runs were again performed for different values of η_{cut} until c was satisfactorily converged in both η_{cut} and $\delta\eta$. Finally, the maximum wavenumber was increased and runs were performed with each combination of η_{cut} and $\delta\eta$.

4.3.3 Results

In each of our runs, the iteration procedure was continued until the error given by

$$e_n = \frac{\|g_{n+1}(\eta) - g_n(\eta)\|}{\|g_{n+1}(\eta)\|} \tag{4.18}$$

satisfies $e_n < 0.005$ where the norm is the $L2$ norm.

The results from the simulations described in 4.3.2 are presented in table 4.1. Considering each run with $\eta_{\max}$ and $\delta\eta$ fixed, we see that the value of c converges to one or two decimal places as η_{cut} is increased. The value of c also converges to two decimal places as $\delta\eta$ is decreased. This pattern is also observed for $\eta_{\max} = 30$ and $\eta_{\max} = 40$. Furthermore, comparing the results for each $\eta_{\max}$ with $\delta\eta = 0.025$, we again see convergence of the solution.

From the results presented, we conclude that $c = 0.59$. This solution is plotted in Figure 4.2 along with the KZ spectrum $0.59\eta^{x_*-3}$. The upper range of η's show a convergence towards the KZ solution $f(\eta) = \eta^{-3}$ as is expected from the formulation of the self-similar solution.

4.4 Conclusions

In this paper we have considered the self-similar solution for the spectrum of the Alfvén wave turbulence corresponding to the time $t_* < t < t_* + t_{max}$, where t_* is the time at which the spectral front characterising the first stage of self-similarity reaches $k = \infty$ and $t_* + t_{max}$ is the time at which the Kolmogorov-Zakharov solution fills the wavenumber space down to the initially excited wavenumber k_0. These new solutions are similar to ones previously found in the Leith model of hydrodynamic turbulence [56] and like those solutions, do not fit into the existing classification of self-similar solutions of Zeldovich and Raizer. Following [56], we call these self-similar solutions of the third kind. These solutions are ones in which the self-similar indices are not

Table 4.1: The value of c obtained for runs of the iteration procedure for various combinations of the parameters.

$\eta_{\max}$	$\delta\eta$	$\eta_{\text{cut}}/\eta_{\max}$	c
20	0.1	0.3	0.470
	0.1	0.4	0.438
	0.1	0.5	0.426
	0.1	0.6	0.424
	0.05	0.3	0.628
	0.05	0.4	0.615
	0.05	0.5	0.607
	0.05	0.6	0.608
	0.025	0.3	0.633
	0.025	0.4	0.622
	0.025	0.5	0.611
	0.025	0.6	0.611
30	0.1	0.3	0.414
	0.1	0.4	0.407
	0.1	0.5	0.402
	0.1	0.6	0.402
	0.05	0.3	0.616
	0.05	0.4	0.600
	0.05	0.5	0.592
	0.05	0.6	0.592
	0.025	0.3	0.623
	0.025	0.4	0.602
	0.025	0.5	0.594
	0.025	0.6	0.594
40	0.1	0.3	0.411
	0.1	0.4	0.403
	0.1	0.5	0.399
	0.1	0.6	0.399
	0.05	0.3	0.607
	0.05	0.4	0.595
	0.05	0.5	0.587
	0.05	0.6	0.587
	0.025	0.3	0.612
	0.025	0.4	0.598
	0.025	0.5	0.590
	0.025	0.6	0.590

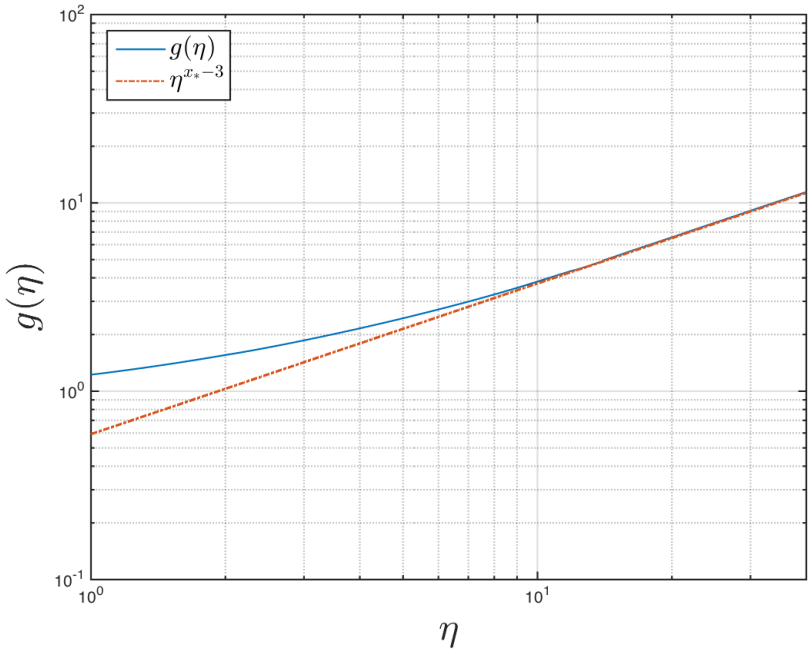

Figure 4.2: The self-similar solution $g(\eta)$ to equation (4.11) compared with the Kolmogorov-Zakharov solution.

fixed by either a conservation law or by solving a nonlinear eigenvalue problem, but instead are determined by imposing asymptotics at one end of the similarity interval based on the solution for the preceding self-similar stage.

While the similarity indices have been fixed without needing to solve a nonlinear eigenvalue problem, the constant c in front of the KZ power law at the $\eta \to \infty$ end of the similarity interval is found by a different type of eigenvalue problem. Without this constant, the boundary condition cannot be fully defined and so finding the self-similar solution depends upon also identifying this constant.

Here, we have found the constant c and the self-similar solution by numerically solving the integro-differential equation describing the self-similar dynamics. This solution represents the second stage (post-t_*) of the evolution of the turbulent spectrum in Alfvén wave turbulence. The first (pre-t_*) stage is described by self-similar solutions of the second kind which were studied in a previous paper [6]. In absence of forcing, there is also a third and final self-similar stage in which the KZ spectrum, after being fully formed at the second stage, gradually decays as a whole. All of the three stages were studied in the Leith model of hydrodynamic turbulence [56], and it is likely that the general picture also applies to other finite-capacity turbulent systems. Studying these solutions in other finite-capacity systems may

provide interesting areas of future research.

Chapter 5

Rotating MHD turbulence

5.1 Introduction

Astrophysical flows are generally electrically charged prompting the use of MHD for describing their dynamics. Such flows are often accompanied by large scale magnetic fields which results in the existence of a rich zoo of linear waves. This has motivated the use of weak wave turbulence theory when studying MHD systems [27, 25, 22, 54, 74]. Wave turbulence is the study of the long-time statistical nature of weakly nonlinear dispersive waves [84, 55]. Weak wave turbulence applies to linear waves which are weakly nonlinear. In most physical situations however, there is a coexistence of strongly nonlinear coherent structures and weakly nonlinear waves. Another way of describing the condition for the applicability of weak wave turbulence is that it is when the timescale of the linear waves is much shorter than the nonlinear timescale. The state where these two timescales are of the same order over a wide range of scales is known as critical balance which was introduced in the context of MHD by Goldreich [29].

Along with the presence of a mean magnetic field, astrophysical flows often undergo rotation about their axis. Rotating MHD then has wide application including planetary flows, stellar flows and accretion discs. The addition of the Coriolis force from rotation adds to the various other dynamical consideration. It is therefore useful to define a measure of the importance of the Coriolis force relative to these other effects. This can be achieved by the Rossby number:

$$Ro = \frac{U_0}{L_0 \Omega_0}, \tag{5.1}$$

where U_0, L_0 and Ω_0 are the typical velocity, length scale and rotation rate respectively. The Rossby number is the ratio of the advection term and the Coriolis force

in the Navier-Stokes equations. Small Rossby numbers thus correspond to flows in which the rotation is of significant importance as is the case for planetary flows in which $Ro \sim 0.1$ [75]. Large planets may have even smaller numbers with $Ro \sim 10^{-6}$ being suggested for the Earth [71].

There have been various numerical studies of the effects of rotation in hydrodynamic turbulence, for example [50, 51, 77]. The theoretical groundwork for the weak wave turbulence regime has been developed by Galtier [21]. A prediction for the energy spectrum $E(k) \sim k_\perp^{-5/2}$ was found which is applicable when the linear waves (inertial waves in this case) dominate the nonlinear effects. A prediction based on critical balance was found in Schekochihin and Nazarenko [74] which gives the energy spectrum as $E(k) \sim k_\perp^{-5/3}$. More recently a weak wave turbulence theory has been developed for rotating MHD [24]. Predictions were made for the energy spectra in two asymptotic regions; $kd = kb_0/\Omega_0 \to \infty$ and $kd \to 0$. As $kd \to \infty$, the linear waves collapse onto the Alfvén waves resulting in a k^{-2} spectrum as first found in Galtier [27]. In the $kd \to 0$ limit, the left polarised waves (inertial waves) and the right polarised waves (magnetostrophic waves) decouple such that the inertial waves contain most of the kinetic energy and the magnetostrophic waves contain most of the magnetic energy. The kinetic energy spectrum is therefore the same as for rotating hydrodynamic turbulence while the magnetic energy spectrum is also found to be $E(k) \sim k_\perp^{-5/2}$ which is incidentally similar to the electron MHD case [25].

In this chapter, we present numerical simulations of rotating MHD. First, the weak wave turbulence theory is outlined including a phenomenological derivation of the kinetic and magnetic energy spectra. Furthermore a new prediction is found based on the critical balance argument. These predictions are then compared to two simulations which show agreement with the predictions. Finally, the kinetic equation is discussed. Two regimes are considered, one in which the inertial waves and the magnetostrophic waves are completely decoupled and another in which there is coupling between the modes.

5.2 Rotating MHD

5.2.1 Governing equations

Incompressible MHD under solid body rotation and in the presence of a uniform background magnetic field is considered. The governing equations are given by

$$\frac{\partial \boldsymbol{u}}{\partial t} + 2\boldsymbol{\Omega_0} \times \boldsymbol{u} + \boldsymbol{u} \cdot \boldsymbol{\nabla} \boldsymbol{u} = -\nabla P_* + \boldsymbol{b_0} \cdot \nabla \boldsymbol{b} + \boldsymbol{b} \cdot \nabla \boldsymbol{b} + \nu \nabla^2 \boldsymbol{u}, \tag{5.2}$$

$$\frac{\partial \boldsymbol{b}}{\partial t} + \boldsymbol{u} \cdot \nabla \boldsymbol{b} = \boldsymbol{b_0} \cdot \nabla \boldsymbol{u} + \boldsymbol{b} \cdot \nabla \boldsymbol{u} + \eta \nabla^2 \boldsymbol{b}, \tag{5.3}$$

$$\nabla \cdot \boldsymbol{u} = 0, \tag{5.4}$$

$$\nabla \cdot \boldsymbol{b} = 0, \tag{5.5}$$

where $\boldsymbol{v}$ is the velocity, P_* is the total pressure, $\boldsymbol{b}$ is the magnetic field normalised to a velocity, $\boldsymbol{b_0}$ is the uniform normalised magnetic field, Ω_0 is the rotation rate and ν and η are the kinematic viscosity and magnetic diffusivity respectively. For the remainder of this chapter we shall assume that the axis of rotation is equal to the direction of the background magnetic field such that

$$\boldsymbol{\Omega_0} = \Omega_0 \hat{\boldsymbol{e}}_{\parallel}, \qquad \boldsymbol{b_0} = b_0 \hat{\boldsymbol{e}}_{\parallel}, \tag{5.6}$$

where $\hat{\boldsymbol{e}}_{\parallel}$ is a unit vector. The different regimes of rotating MHD which will be discussed here can be accessed by asymptotics in the magneto-inertial length d defined by

$$d = \frac{b_0}{\Omega_0}. \tag{5.7}$$

The magneto-inertial length gives a way to determine the strength of the ratio between the Lorentz-Laplace force and the Coriolis force. Looking at this ratio dimensionally we find

$$\mathcal{D} = \frac{|\boldsymbol{b_0} \cdot \nabla \boldsymbol{b}|}{|2\boldsymbol{\Omega_0} \times \boldsymbol{u}|} \sim \frac{b}{u} \frac{d}{l}. \tag{5.8}$$

When $\mathcal{D}$ is large, the Lorentz-Laplace force is dominant and when it is very small the Coriolis force is dominant. Assuming that u and b are known, the size of $\mathcal{D}$ can be determined using d/l, or equivalently, kd in Fourier space.

Linear waves in rotating MHD are circularly polarized and dispersive. The general solution for the frequency is given by

$$\omega \equiv \omega_\Lambda^s = \frac{s k_\parallel \Omega_0}{k} \left(-s\Lambda + \sqrt{1 + k^2 d^2} \right), \tag{5.9}$$

where $s = \pm 1$ defines the directional polarity such that we always have $sk_\parallel > 0$ and $\Lambda = \pm s$ gives the circular polarity with $\Lambda = s$ indicating right polarization and $\Lambda = -s$ left polarization. The linear waves can be considered in the limits $kd \to \infty$ and $kd \to 0$. In the small scale limit ($kd \to 0$), the frequency of the right and left polarized waves collapse onto the Alfvén wave frequency. In this limit the turbulence properties can therefore be studied as Alfvén wave turbulence for which there exists a large body of work, for example [29, 27, 26, 74, 47]. In the large scale limit ($kd \to 0$), the right and left polarized waves are the pure magnetostrophic

waves and the pure inertial waves respectively. The frequencies are given by

$$\omega_M \equiv \omega_s^s = \frac{sk_\parallel kdb_0}{2}, \tag{5.10}$$

$$\omega_I \equiv \omega_{-s}^s = \frac{2s\Omega_0 k_\parallel}{k}. \tag{5.11}$$

In the inertial wave branch, the turbulence properties are equal to the inertial wave turbulence properties in hydrodynamics as studied previously [21].

The magnetostrophic branch can be described by a single equation if we assume a balance between the Coriolis and Lorentz-Laplace forces [18]. Following this assumption, the nonlinear evolution of the magnetic field under relatively strong rotation and uniform magnetic field can be described by the magnetostrophic equation

$$\frac{\partial \boldsymbol{b}}{\partial t} = -\frac{d}{2}\nabla \times [(\nabla \times \boldsymbol{b}) \times (\boldsymbol{b} + \boldsymbol{b_0})] + \eta \nabla^2 \boldsymbol{b}. \tag{5.12}$$

This equation will be used to study the wave turbulence properties for the magnetostrophic waves.

5.2.2 Weak wave turbulence

The weak theory for rotating MHD was developed by Galtier [24]. The derivation will not be reproduced here but the results which provide context to our numerical simulations will be discussed. We turn our attention to the large scale limit $kd \to 0$. In this limit and assuming that nonlinear interactions occur locally in k-space it can be shown that the inertial waves decouple from the magnetostrophic waves. A discussion of this decoupling and identification of a coupled regime can be found in the final section in this chapter. Furthermore in this limit, the inertial waves contain all of the kinetic energy and the magnetostrophic waves contain all of the magnetic energy. Both the inertial wave turbulence and the magnetostrophic wave turbulence are found to become anisotropic such that $k_\perp \gg k_\parallel$.

The weak wave turbulence theory applies when the dynamics are dominated by the linear waves. In terms of time scales this implies that the period of the linear waves is much shorter than the nonlinear eddy turnover time

$$\tau_l \ll \tau_{nl}. \tag{5.13}$$

Looking first at the momentum equation (5.2), the nonlinear time scale is

$$\tau_{nl} \sim \frac{1}{k\widetilde{U}} \tag{5.14}$$

where $\widetilde{U}$ is the wave amplitude and the period of the inertial waves is

$$\tau_I \sim (\omega_I)^{-1} = \frac{k}{2s\Omega_0 k_\parallel}. \tag{5.15}$$

We require the transfer time in order for a phenomenological derivation of the energy spectrum. If we assume that after N stochastic collisions, the cumulative effect may be regarded as a random walk, then we can use [34, 37]

$$\tau_{tr} \sim \frac{\tau_{nl}^2}{\tau_\omega}. \tag{5.16}$$

Then, assuming a stationary state in which the kinetic energy flux per unit mass ϵ^u, is independent of scale we find

$$\begin{aligned} \epsilon^u &\sim \frac{E^u}{\tau_{tr}} \\ &\sim \frac{E^u(k_\perp, k_\parallel)k_\perp k_\parallel}{\tau_{tr}}. \end{aligned} \tag{5.17}$$

Then making use of $\widetilde{U}^2 \sim E(k_\perp, k_\parallel)k_\perp k_\parallel$ and the anisotropic assumption $k_\perp \gg k_\parallel$ we have, following some algebra

$$E^u(k_\perp, k_\parallel) \sim \sqrt{\epsilon^u \Omega_0} k_\perp^{-5/2} k_\parallel^{-1/2}. \tag{5.18}$$

To study the magnetostrophic waves, we look at the magnetostrophic equation (5.12). The nonlinear time scale is

$$\tau_{nl} \sim \frac{1}{k_\perp^2 d\widetilde{B}} \tag{5.19}$$

and the period of magnetostrophic waves is given by

$$\tau_M \sim (\omega_M)^{-1} = \frac{2}{sk_\parallel k d b_0}. \tag{5.20}$$

Performing the same analysis as for the kinetic energy spectrum, we find the magnetic energy spectrum

$$E^b(k_\perp, k_\parallel) \sim \sqrt{\frac{\epsilon^b b_0}{d}} k_\perp^{-5/2} |k_\parallel|^{-1/2}. \tag{5.21}$$

The same phenomenology can be applied to the other inviscid invariant of rotating MHD, the hybrid helicity. This will not be discussed in detail here since we

choose to concentrate on the energy spectra. The hybrid helicity may give rise to an inverse cascade and so would be an interesting topic for future study with possible insight into a dynamo process.

5.2.3 Strong wave turbulence

In strong wave turbulence, one assumes that the energy spectrum saturates when the nonlinear interaction time becomes of the same order as the linear wave period over a wide range of turbulent scales [55]. Such states are known as a critical balance (CB) as introduced in MHD turbulence by Goldreich [29]. It has been proposed that CB provides a universal scaling conjecture for determining the spectra of strong turbulence in anisotropic wave systems [59]. The weak wave turbulence prediction applies under the condition

$$\frac{\tau_\omega}{\tau_{nl}} \ll 1. \tag{5.22}$$

Assuming anisotropy we have $k \sim k_\perp$ so that this ratio for inertial waves and magnetostrophic waves becomes

$$\frac{\tau_\omega}{\tau_{nl}} \sim \frac{k_\perp^2 \widetilde{U}}{k_\parallel \Omega_0} \quad \text{and} \quad \frac{\tau_\omega}{\tau_{nl}} \sim \frac{k_\perp \widetilde{B}}{k_\parallel b_0} \tag{5.23}$$

respectively. Clearly both of these ratios grow as $k_\perp$ increases and so there will be some scale at which the weak wave turbulence assumption is broken and where the critical balance assumption becomes relevant.

In the classical Kolmogorov spectrum of turbulence [35], the system is isotropic and highly nonlinear such that the transfer time is simply the nonlinear timescale. When waves are present there is an additional time scale, the period of the linear waves. The critical balance assumption

$$\tau_{tr} \sim \tau_\omega \sim \tau_{nl} \tag{5.24}$$

provides the additional scaling required to perform a heuristic derivation of the energy spectrum.

To derive the kinetic energy spectrum in the critical balance regime we shall again turn our attention to the momentum equation. The nonlinear time scale and the linear wave period are again given by (5.14) and (5.15) respectively. Balancing these time scales as per (5.24) gives

$$\widetilde{U} \sim \frac{\Omega_0 k_\parallel}{k_\perp^2}. \tag{5.25}$$

The kinetic energy flux is then found to be

$$\begin{aligned} \epsilon^u &\sim \frac{\widetilde{U}^2}{\tau_{tr}} \\ &\sim \widetilde{U}^3 k_\perp \\ &\sim \frac{\Omega_0^3 k_\parallel^3}{k_\perp^5}, \end{aligned} \tag{5.26}$$

which when rearranged gives the wavenumber scaling for the critical balance

$$k_\parallel \sim (\epsilon^u)^{1/3} \Omega_0^{-1} k_\perp^{5/3}. \tag{5.27}$$

Using relations (5.25) and (5.27) we can derive the kinetic energy spectrum

$$\begin{aligned} E^u(k_\perp) &\sim \frac{\widetilde{U}^2}{k_\perp} \\ &\sim (\epsilon^u)^{2/3} k_\perp^{-5/3}. \end{aligned} \tag{5.28}$$

The magnetic energy spectrum can be calculated similarly using the magnetostrophic equation in which the nonlinear time scale and the linear wave period are given by (5.19) and (5.20) respectively. Equating these two time scales gives a scaling for the wave amplitude as

$$\widetilde{B} \sim \frac{k_\parallel b_0}{k_\perp} \tag{5.29}$$

and the magnetic energy flux as

$$\epsilon^b \sim \frac{\widetilde{B}^2}{\tau_{tr}}. \tag{5.30}$$

The critical balance scaling for the wavenumbers is thus

$$k_\parallel \sim (\epsilon^b)^{1/3} b_0^{-1} d^{-1/3} k_\perp^{1/3}, \tag{5.31}$$

which leads to the magnetic energy spectrum

$$E^b(k_\perp) \sim \left(\frac{\epsilon^b}{d}\right)^{2/3} k_\perp^{-7/3}. \tag{5.32}$$

5.2.4 Domain of validity for weak wave turbulence

Weak wave turbulence relies upon the time scale separation between the linear time scale and the nonlinear time scale. It assumes that the nonlinear time scale is much

longer than the period of the linear waves. A result of this is that the weak wave turbulence approach is valid under the condition that the ratio of linear time period to nonlinear time scale is much smaller than one, i.e.

$$\frac{\tau_\omega}{\tau_{nl}} \ll 1. \tag{5.33}$$

In rotating MHD, there are two linear waves corresponding to different dispersion relations and we have defined different nonlinear times to each, given by Equation (5.14) for the inertial waves and Equation (5.19) for the magnetostrophic waves. Therefore, in order for the weak wave turbulence theory to apply, the following two relations must hold:

$$\chi^u = \frac{\tau_I}{\tau^u_{nl}} \sim \frac{k_\perp^2 \widetilde{U}}{k_\parallel \Omega_0}, \tag{5.34}$$

$$\chi^b = \frac{\tau_M}{\tau^b_{nl}} \sim \frac{k_\perp \widetilde{B}}{k_\parallel b_0}. \tag{5.35}$$

It is clear from these relations that the ratio will vary with the wavenumber and thus may not be uniformly valid across the domain. The dependence of both χ^u and χ^b can be estimated using the weak wave turbulence predictions along with $\widetilde{U} \sim \sqrt{2E^u(k_\perp, k_\parallel)k_\perp k_\parallel}$ and $\widetilde{B} \sim \sqrt{2E^b(k_\perp, k_\parallel)k_\perp k_\parallel}$. One then finds,

$$\chi^u \sim \left(\frac{\sqrt{\epsilon^u}}{\Omega_0}\right)^{1/2} k_\parallel^{-3/4} k_\perp^{5/4}, \tag{5.36}$$

$$\chi^b \sim \left(\frac{\sqrt{\epsilon^b}}{b_0 d}\right)^{1/2} k_\parallel^{-3/4} k_\perp^{1/4}. \tag{5.37}$$

Both χ^u and χ^b grow as $k_\perp$ increases and so there will be some scale at which the weak wave turbulence assumption is broken and where the critical balance assumption becomes relevant. Such a transition from weak to strong wave turbulence has been observed in numerical simulations of Alfvén wave turbulence [46] and Hall MHD turbulence [48].

5.2.5 Transition from weak to strong wave turbulence

Assuming a state in which the weak wave turbulence regime is valid at small perpendicular wave numbers, one would expect a transition to strong wave turbulence at some critical perpendicular wave number. The kinetic energy spectrum at low perpendicular wavenumber should thus correspond to the scaling (5.18) whilst scaling as (5.28) at large perpendicular wavenumbers. Similarly, for the magnetic energy

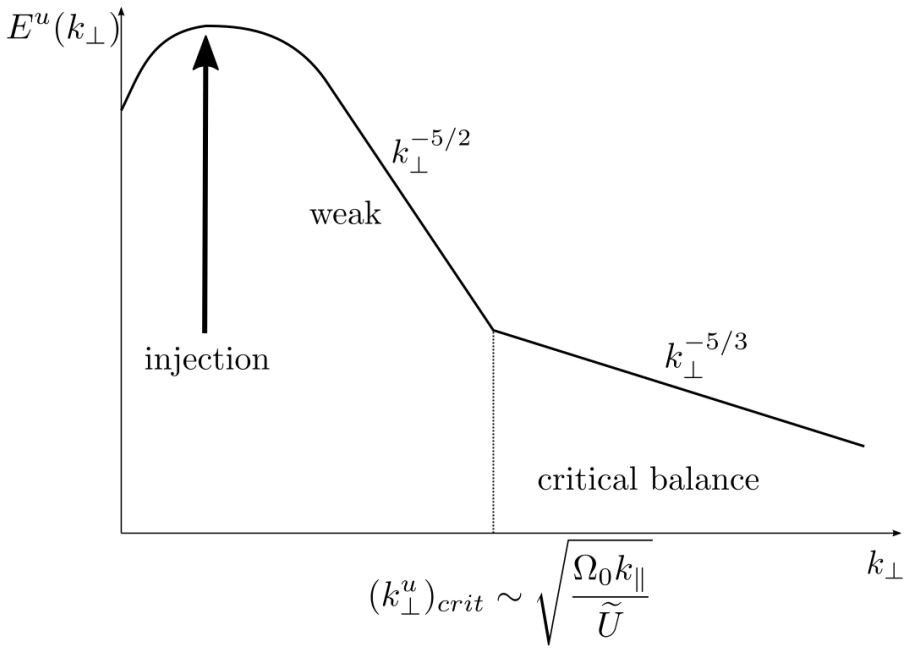

Figure 5.1: A sketch of the predicted kinetic energy spectrum in rotating MHD showing a transition from weak to strong wave turbulence at a critical value of the perpendicular wavenumber.

spectrum we would expect a transition from (5.21) to (5.32).

One can estimate the location that this transition will occur using Equations (5.34) and (5.35). A sketch of the predicted kinetic and magnetic energy spectra are given in figures 5.1 and 5.2.

5.3 Numerical simulations

5.3.1 Set-up

The rotating MHD equations (5.2)–(5.5) were solved numerically using the Fourier pseudospectral code GHOST [30, 49, 52]. Time integration is performed by a second order Runge-Kutta scheme and the 2/3 rule is employed for dealiasing. An isotropic initial condition of velocity and magnetic field fluctuations with random phases was chosen and we consider a decaying turbulence to avoid any artefacts from any forcing. A hyperviscosity and hyperdiffusivity was used such that the viscous and diffusive terms are $\nu\nabla^6\boldsymbol{u}$ and $\eta\nabla^6\boldsymbol{b}$ respectively. The initial kinetic and magnetic energy entered into the system are given by E^k_{init} and E^b_{init} respectively and the simulation is performed in a period box of resolution N^3.

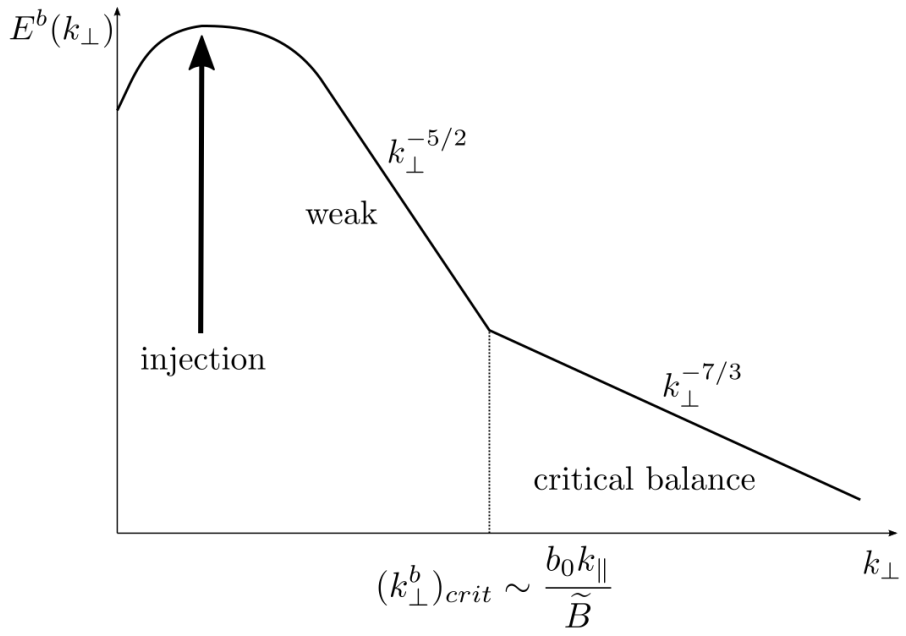

Figure 5.2: A sketch of the predicted magnetic energy spectrum in rotating MHD showing a transition from weak to strong wave turbulence at a critical value of the perpendicular wavenumber.

In order to access the two regimes of rotating MHD turbulence, namely the weak wave turbulence and critical balance regimes, one must take careful consideration of the parameters used. In both cases we are interested in the large scale limit

$$kd = k\frac{b_0}{\Omega_0} \to 0 \tag{5.38}$$

and the limit of small Rossby number

$$Ro \sim \frac{kU}{\Omega_0} \to 0. \tag{5.39}$$

The difference between the weak and strong turbulence regimes is controlled by the ratios of linear wave period to nonlinear turnover time given by Equation (5.23). These ratios should be very small in the weak turbulence limit and of the order 1 in the critical balance.

5.3.2 Simulation A

First we consider simulation A. The parameters used for the simulation can be found in Table 5.1. An isotropic initial condition was chosen in the range $k = [2, 4]$. The

Simulation	N	b_0	Ω_0	E^k_{init}	E^b_{init}	ν	η
A	512	50	1000	20.0	209.0	10^{-12}	10^{-12}
B	128	50	1000	2.9	3.2	10^{-10}	10^{-10}

Table 5.1: Parameters used in the numerical simulations.

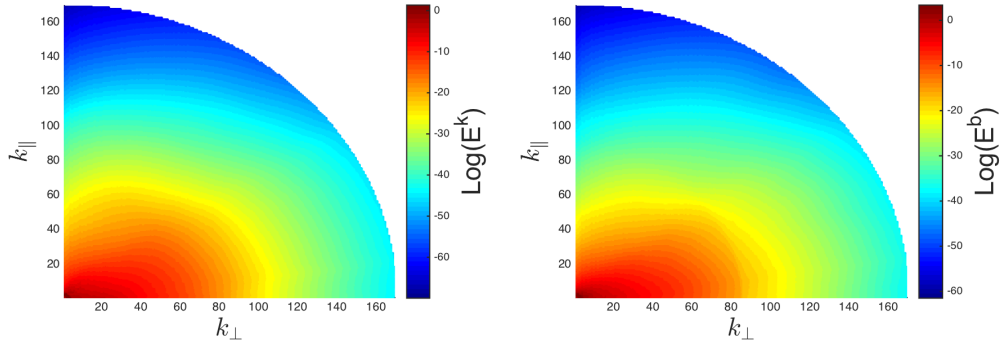

Figure 5.3: $2D$ energy spectra for the (a) kinetic and (b) magnetic energies from simulation A.

simulation has been performed in a periodic box of spatial resolution 512^3. After application of the $N/3$ rule for dealiasing, this gives a maximum wavenumber of 170. The parameter kd therefore ranges from 0 to 8.5. This is only moderately small for much of the wavenumber range and thus complete decoupling of the magnetic and kinetic energies may not be achieved. However, it is sufficiently far from the opposite limit $kd \to \infty$ for this simulation to consider inertial and magnetostrophic waves.

In both the weak and strong turbulence derivations, anisotropy is assumed such that $k_\perp \ll k_\parallel$. In order to check the validity of this assumption, we plot the $2D$ energy spectrum in $k_\perp$ and $k_\parallel$. The spectra for both the kinetic and magnetic energy can be seen in Figure 5.3. In both cases we see a preferential transfer of energy along $k_\perp$ as is predicted by the anisotropic assumption.

Figure 5.4 shows the one-dimensional axisymmetric energy spectra for the kinetic and magnetic energy. The spectra are integrated over $k_\parallel$. The kinetic energy spectrum is compensated by the critical balance prediction $k_\perp^{-5/3}$ and is plotted alongside the weak wave turbulence prediction $k_\perp^{-5/2}$. Similarly, the magnetic energy spectrum is compensated by $k_\perp^{-7/3}$ (the critical balance prediction) and is plotted alongside $k_\perp^{-5/2}$ (the weak wave turbulence prediction). In each case, distinguishing between the two predictions is difficult due to their similarity. In order to establish whether the spectra are due to weak or strong turbulence we must look at the spatio-temporal properties of the turbulence.

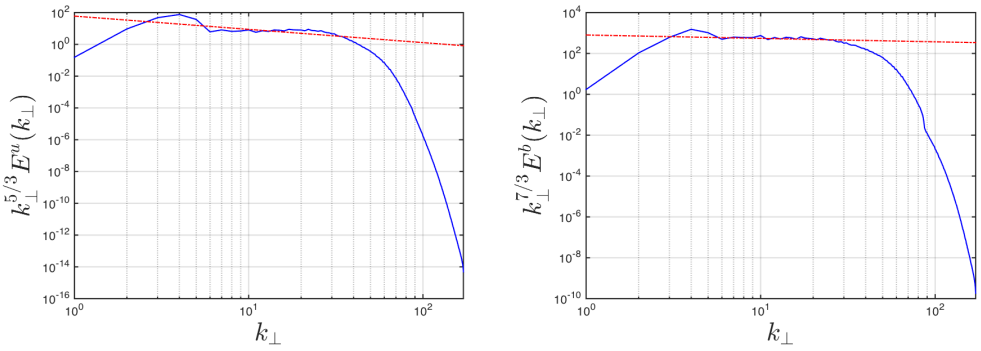

Figure 5.4: Compensated axisymmetric energy spectra for the (a) kinetic and (b) magnetic energies for simulation A. The dotted line indicates the weak wave turbulence prediction for comparison.

A common method to detect linear waves is to compute and analyse the spatio-temporal spectrum [42] which gives the energy in the $k_\perp - \omega$ plane. This can then be compared with the dispersion relation of the linear waves. Computing the spatio-temporal spectrum requires simultaneous space and time Fourier transforms and thus data must be recorded about the spatial properties at each time point. In order to resolve all the waves present, the sampling frequency must be at least twice as large as the frequency of the fastest waves in the system and the total acquisition time must be larger than both the slowest wave period and the turnover time of the slowest eddies. These requirements result in a high storage space requirement which proved restrictive for the resolution of simulation A. The spatio-temporal spectra have therefore been calculated using a truncated resolution 256^3 and data is collected for a fixed $k_\parallel = 3$. The time scales can be estimated using (5.14), (5.15), (5.19) and (5.20). For $\widetilde{U}$ and $\widetilde{B}$, we can make use of $\widetilde{U} \sim \sqrt{2E^u(k_\perp, k_\parallel)k_\perp k_\parallel}$ and $\widetilde{B} \sim \sqrt{2E^b(k_\perp, k_\parallel)k_\perp k_\parallel}$ and the kinetic and magnetic energy spectra shown in Figure 5.4. The time scales are plotted in Figure 5.5 where $k_\parallel$ has been fixed at 3. Ignoring the dissipative region, we can see that the smallest time scale is approximately 10^{-4} corresponding to the inertial wave at $k_\perp = 1$ and the largest time scale is 10 corresponding to the nonlinear time scale of the magnetostrophic equation at $k_\perp = 1$.

Given the estimates of the time scales, it is also possible to estimate the ratios of nonlinear time to linear wave period, χ^u and χ^b. It is clear that both χ^u and χ^b are dependent upon the perpendicular wave number $k_\perp$. The dependence is predicted by Equation (5.34) for the inertial waves and Equation (5.35) for the magnetostrophic waves. These predictions are plotted by the red dotted lines and

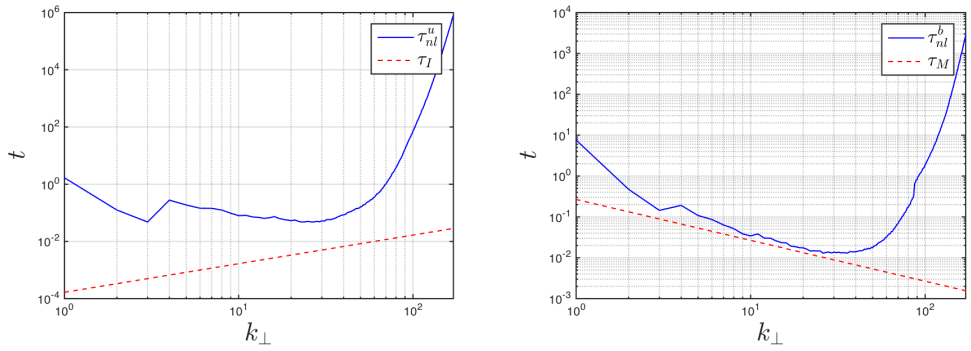

Figure 5.5: *Left:* The nonlinear time scale as given by the momentum equation and the time period of inertial waves from simulation A. *Right:* The nonlinear time scale as given by the magnetostrophic equation and the time period of magnetostrophic waves from simulation A.

we see that the actual values of χ^u and χ^b match well with the predictions. We see that χ^u is at all $k_\perp$ less than 0.1. This would seem to be sufficiently small for the weak wave turbulence to be relevant. In comparison, χ^b is larger, being of the order 0.5. Thus the turbulence for magnetostrophic waves is likely to be stronger. It is still necessary to check for linear waves using the spatio-temporal spectra.

Resolving every mode in our system would require a high number of files and so we have chosen to use an acquisition frequency of $\delta t = 0.001$ and $T = \delta t = 0.511$. This resolves all of the magnetostrophic waves and the inertial waves for $k_\perp > 5$. In Figures 5.7 and 5.8 we plot the spatio-temporal spectra for the kinetic and magnetostrophic energy respectively. In order to avoid spectral leakage, a Hamming window is applied before computation of the temporal Fourier transform. The spectra are calculated at a fixed $k_\parallel = 3$ and overlayed with the inertial and magnetostrophic wave dispersion relations. The color map is normalised to the maximum value of the spectrum at each $k_\perp$. In the weak wave turbulence regime, one would expect the kinetic and magnetic energy to accumulate on the dispersion relations for the linear waves. In a critical balance regime however, the dispersion relation acts as a boundary with the energy filling the region below it [78]. In Figure 5.8 we see that the magnetic energy behaves exactly like this with the energy filling the area in $k_\perp - \omega$ space between the two polarities of the magnetostrophic dispersion relation. In Figure 5.7 we see that the kinetic energy behaves similarly at high wavenumbers but does not fill the region at small wavenumbers. The ratio of time scales increases with $k_\perp$. The weak wave turbulence prediction is therefore more relevant as small wavenumbers. At small wavenumbers, there is a build up of kinetic energy around $\omega = 0$ in addition to a concentration of energy along the

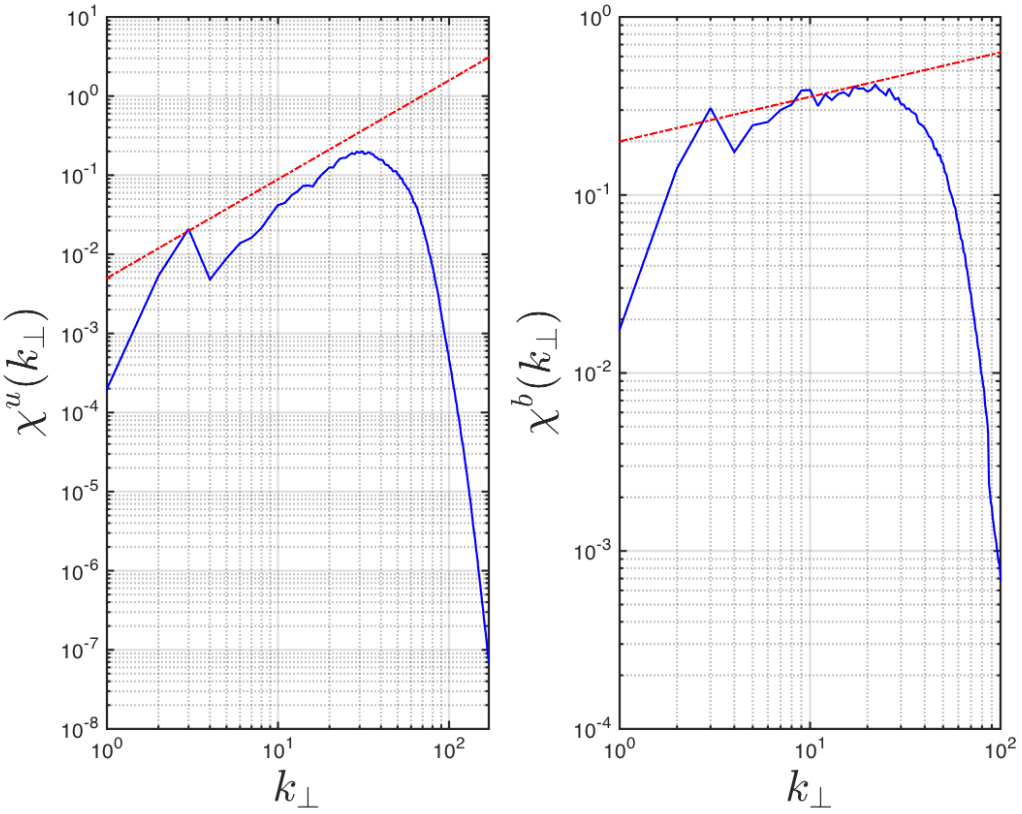

Figure 5.6: *Left:* The ratio of nonlinear time scale to time period of inertial waves in simulation A. The dotted line is the prediction of the $k_\perp$ dependence. *Right:* The ratio of nonlinear time scale to time period of magnetostrophic waves in simulation A. The dotted line is the prediction of the $k_\perp$ dependence.

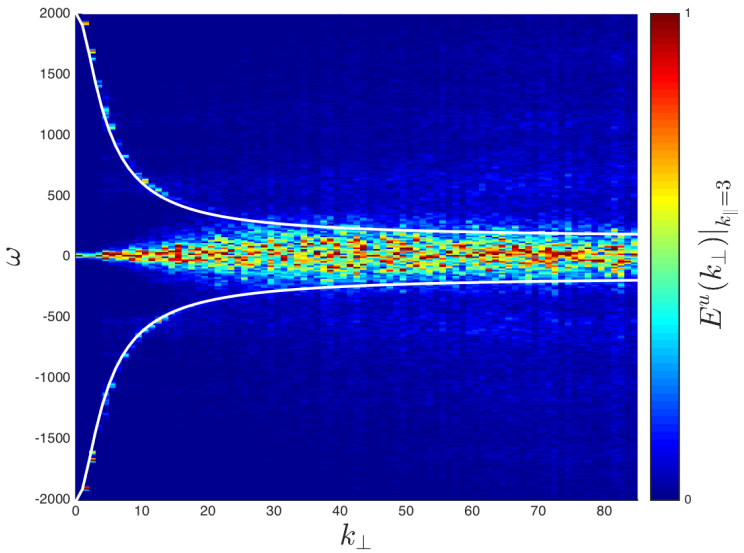

Figure 5.7: Spatio-temporal spectrum for the kinetic energy for simulation A. The white lines indicate the dispersion relation for inertial waves.

dispersion relation for inertial waves. This suggests the presence of both waves and vortices.

In Figures 5.9 we plot the amplitude of the vorticity and current both in the $k_\perp$ plane and the $x - k_\parallel$ plane. In the perpendicular plane, we see a collection of small scale structures both in the current and in the vorticity. This is evidence of the presence of vortex lines and current sheets. We also see that the structures are stretched in the parallel direction as expected for an anisotropic state. Combined with the $2D$ spectra in Figure 5.3, we have strong evidence for the anisotropic assumption which both the weak and strong turbulence predictions are based upon.

In simulation A we have verified the anisotropic assumption with the $2D$ energy spectra and by observing the vorticity and current in the perpendicular plane and a plane along $k_\parallel$. Energy spectra have been plotted for the kinetic and magnetic energy which have been compared with both the weak and strong turbulence predictions. Distinguishing between the two is difficult and thus spatio-temporal spectra and the ratio of nonlinear to linear time scales have been investigated. For the magnetostrophic waves, the ratio of time scales is of the order 0.5 and the spatio-temporal spectrum shows no indication of linear waves. Thus we conclude that the magnetic energy spectrum is most likely a result of strong turbulence. For the inertial waves, the ratio of time scales is smaller, peaking at 0.1. The spatio-temporal spectrum shows the presence of both inertial waves and vortices. This suggests that

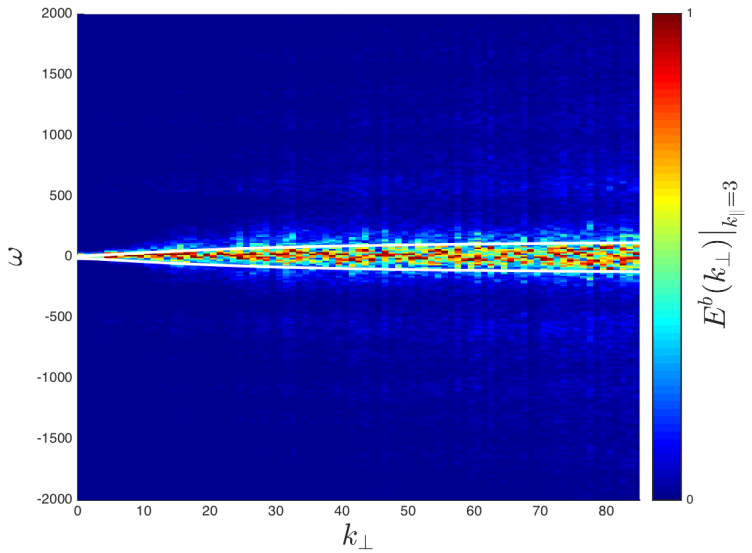

Figure 5.8: Spatio-temporal spectrum for the magnetic energy for simulation A. The white lines indicate the dispersion relation for magnetostrophic waves.

the kinetic energy spectrum is more likely to be a result of weak wave turbulence.

5.3.3 Simulation B

Simulation B is performed at a smaller resolution of 128^3. The initial condition is once again isotropic and concentrated in the range $k = [2, 4]$. However, the energy input to the system is much smaller than in simulation A. The full parameters can be seen in Table 5.1. As before, we can check the ratios of linear to nonlinear time scales χ^u and χ^b to verify that the weak wave turbulence condition $\tau_\omega \ll \tau_{nl}$ is met. These ratios are plotted in Figure 5.10. For both the inertial and magnetostrophic waves we see that the ratio is very small so that the time period of linear waves is faster than the nonlinear time scale. This suggests that the weak wave turbulence theory is valid for both inertial and magnetostrophic waves.

Once again we search for linear waves by plotting the spatio-temporal spectra of the kinetic and magnetic energy. As before they are plotted for fixed $k_\parallel = 3$. The spatio-temporal spectra for the kinetic energy is plotted in Figure 5.11. The white lines indicates the positive and negative polarities of the inertial wave dispersion relation. The energy can be seen to accumulate along these lines suggesting the presence of inertial waves. The magnetic energy spectrum is shown in Figure 5.12 where the white lines are the two polarities of the magnetostrophic wave dispersion relation. Once again the energy accumulates along the dispersion relation as is the

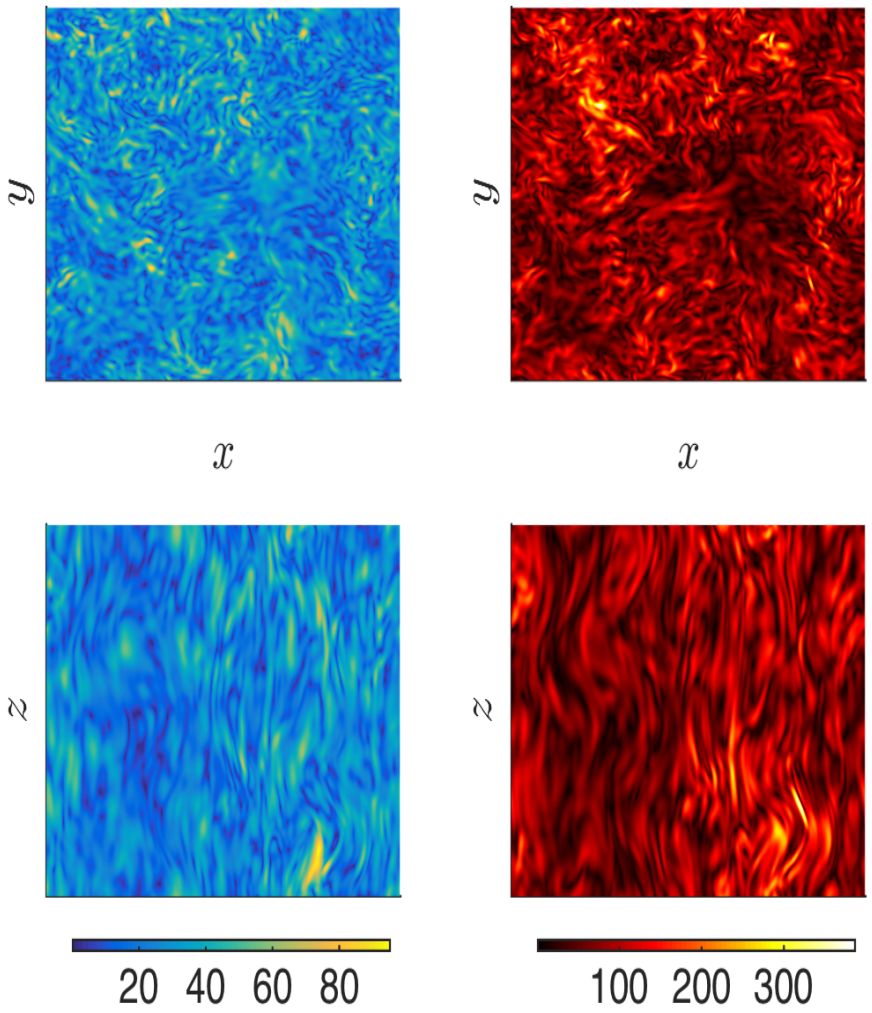

Figure 5.9: *Left:* vorticity amplitude in the $k_\perp$ plane and the $x - k_\parallel$ plane. *Right:* current amplitude in the $k_\perp$ plane and the $x - k_\parallel$ plane.

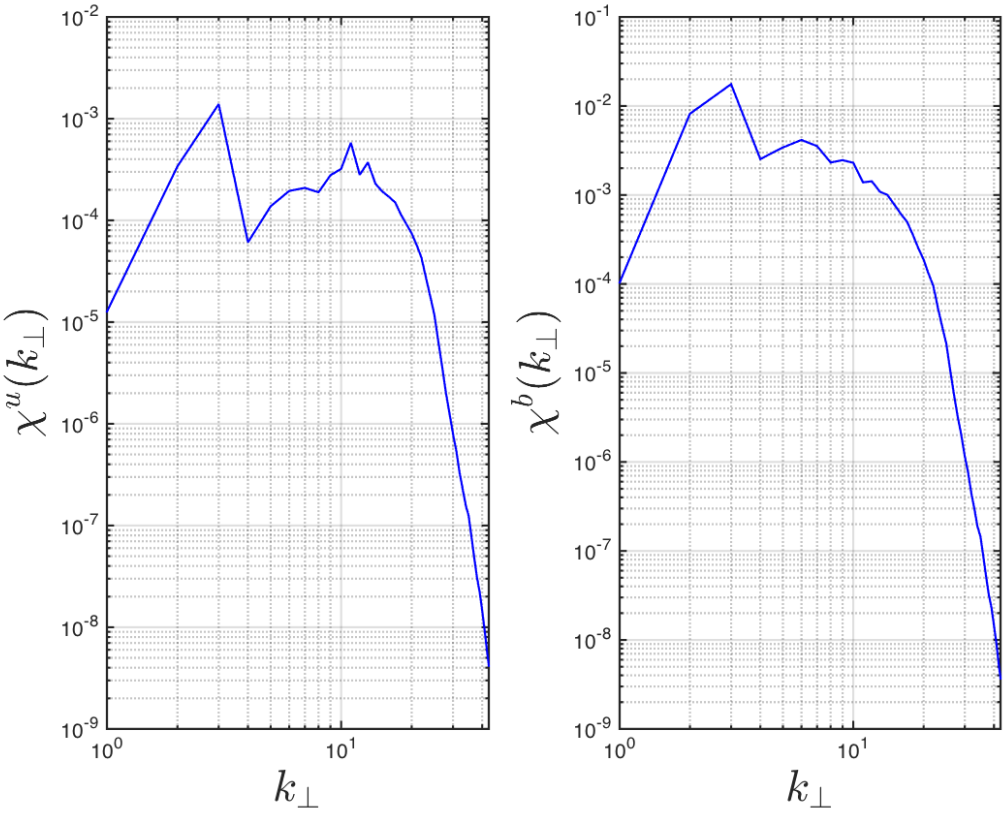

Figure 5.10: *Left:* The ratio of nonlinear time scale to time period of inertial waves in simulation B. The dotted line is the prediction of the $k_\perp$ dependence. *Right:* The ratio of nonlinear time scale to time period of magnetostrophic waves in simulation B. The dotted line is the prediction of the $k_\perp$ dependence.

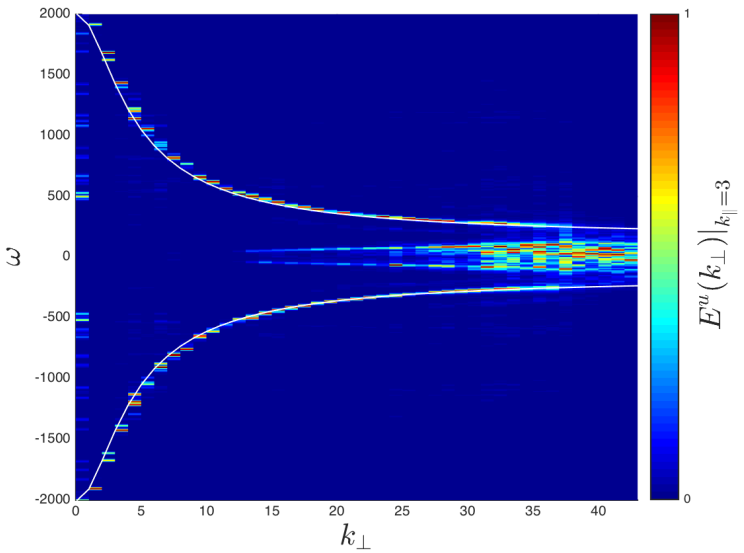

Figure 5.11: Spatio-temporal spectrum for the kinetic energy for simulation B. The white lines indicate the dispersion relation for inertial waves.

signature of linear waves.

From Figures 5.10, 5.11 and 5.12 we can safely say that linear waves are the dominant structures in simulation B. In order to compare to the weak wave turbulence predictions, we look at the axisymmetric energy spectra plotted in Figure 5.13. Each spectra is compensated by the weak wave turbulence prediction $k_\perp^{-5/2}$ so that a horizontal line would correspond to the prediction. We see that both the kinetic and magnetic energy spectra are much steeper than predicted by the weak wave turbulence theory. They are also steeper than the critical balance phenomenology predicts. The reason for such steep spectra could be due to a "frozen turbulence" as first found by Pushkarev and Zakharov [67, 68]. This occurs when the nonlinear resonance broadening is much less than the spacing between the modes in the period box which can be caused by small wave amplitudes. When this happens, only waves that are in exact resonance can interact and thus transfer energy, resulting in a non cascading wave system. This highlights the difficulty in achieving numerical simulations of weak wave turbulence systems which by definition require small amplitude waves. In order to overcome this problem, one could reduce the spacing between the Fourier modes or increase the total number of modes whilst also increasing the forcing region.

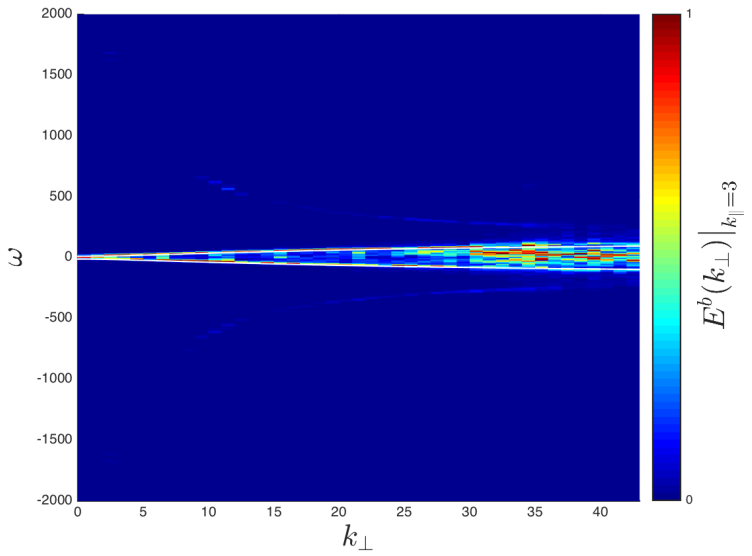

Figure 5.12: Spatio-temporal spectrum for the magnetic energy for simulation B. The white lines indicate the dispersion relation for magnetostrophic waves.

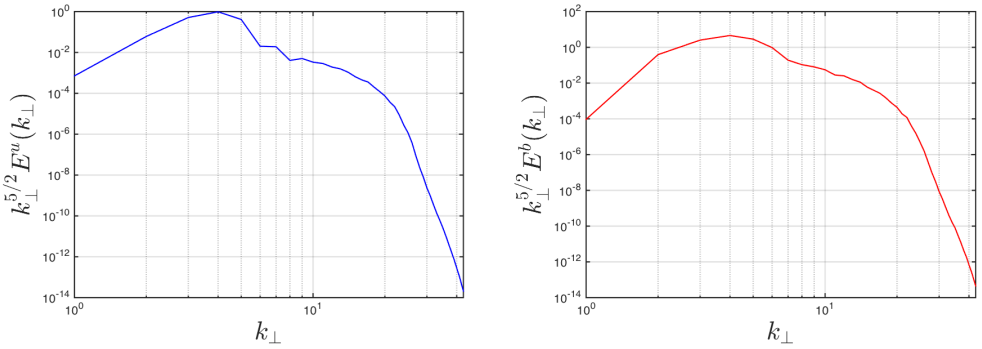

Figure 5.13: Compensated axisymmetric energy spectra for the (a) kinetic and (b) magnetic energies for simulation B.

5.4 Coupling between waves

The full derivation of the weak wave turbulence theory has been omitted here since it is very lengthy and has already been described clearly by Galtier [24]. The main result from the weak wave turbulence theory is the predictions for the scaling of the turbulent spectra. These have been discussed already but now I shall discuss the kinetic equation from which these predictions were found. The full kinetic equation is

$$\begin{aligned}\frac{\partial n^s_\Lambda(\boldsymbol{k})}{\partial t} = \frac{\pi\epsilon^2 d^4}{64 b_0^2}\iint \sum_{\substack{\Lambda_1,\Lambda_2\\ s_1,s_2}} \left(\frac{\sin\psi_k}{k}\right)^2 k^2 k_1^2 k_2^2 (\Lambda k + \Lambda_1 k_1 + \Lambda_2 k_2)^2 \\ \times (\xi^s_\Lambda)^2 (\xi^{s_1}_{\Lambda_1})^2 (\xi^{s_2}_{\Lambda_2})^2 \left(\frac{\xi^{-s_2}_{\Lambda_2} - \xi^{-s_1}_{\Lambda_1}}{k_\parallel}\right)^2 \left(\frac{\omega^s_\Lambda}{1+(\xi^{-s}_\Lambda)^2}\right) \\ \times \left(2 + (\xi^{-s}_\Lambda)^2 (\xi^{-s_1}_{\Lambda_1})^2 (\xi^{-s_2}_{\Lambda_2})^2 - (\xi^{-s}_\Lambda)^2 - (\xi^{-s_1}_{\Lambda_1})^2 - (\xi^{-s_2}_{\Lambda_2})^2\right)^2 \\ \times \left[\frac{\omega^s_\Lambda}{\{1+(\xi^{-s}_\Lambda)^2\} n^s_\Lambda(\boldsymbol{k})} - \frac{\omega^{s_1}_{\Lambda_1}}{\{1+(\xi^{-s_1}_{\Lambda_1})^2\} n^{s_1}_{\Lambda_1}(\boldsymbol{k_1})} - \frac{\omega^{s_2}_{\Lambda_2}}{\{1+(\xi^{-s_2}_{\Lambda_2})^2\} n^{s_2}_{\Lambda_2}(\boldsymbol{k_2})}\right] \\ \times n^s_\Lambda(\boldsymbol{k}) n^{s_1}_{\Lambda_1}(\boldsymbol{k_1}) n^{s_2}_{\Lambda_2}(\boldsymbol{k_2}) \delta(\Omega_{k,k_1 k_1}) \delta_{k,k_1 k_1} \mathrm{d}\boldsymbol{k_1} \mathrm{d}\boldsymbol{k_2}. \end{aligned} \tag{5.40}$$

The angle ψ_k refers to the angle opposite $\boldsymbol{k}$ in the triangle defined by $\boldsymbol{k} = \boldsymbol{k_1} + \boldsymbol{k_2}$, ξ^s_Λ is defined by

$$\xi^s_\Lambda = \frac{-skd}{-s\Lambda + \sqrt{1+k^2d^2}}. \tag{5.41}$$

Recall that $s = \pm$ defines the directional wave polarity and $\Lambda = \pm s$ defines the circular polarization. If $\Lambda = s$ then we are dealing with the right polarized wave which is the magnetostrophic wave in this case. The left polarized waves are given by $\Lambda = -s$ and correspond to inertial waves. Now notice that in Equation (5.40) the summation is performed over s_1, s_2, Λ_1 and Λ_2. If we sum over the Λ's only, we can break the kinetic equation into one term containing interactions between two inertial waves, one term containing the interactions between two magnetostrophic waves and one term containing the interactions between one of each wave. Solving the full kinetic equation would be extremely difficult if not impossible. Thus, one tends to reduce the equation by considering the relative size of each term to see which has the largest affect on the dynamics. Here this is performed in two different regimes to different results.

First we shall write out and reduce the different terms in the general kinetic equation by summing over Λ_1 and Λ_2 and expanding in our small parameter kd.

Consider first the equation describing the dynamics of the inertial waves ($\Lambda = -s$). Performing the summation over polarisations Λ_1 and Λ_2, the kinetic equation takes the form

$$\partial_t n^s_{-s}(\boldsymbol{k}) = A_{II} + B_{IM} + C_{MM}, \tag{5.42}$$

where A_{II} gives the contribution from inertial-inertial wave interactions, B_{IM} gives the contribution from inertial-magnetostrophic wave interactions and C_{MM} gives the contribution from magnetostrophic-magnetostrophic interactions. Now, to leading order in kd we have the following expansions

$$\xi^s_{-s} \to -\frac{skd}{2}, \tag{5.43}$$

$$\xi^s_s \to -\frac{2s}{kd}, \tag{5.44}$$

$$(\xi^s_{-s})^2 \to \frac{k^2d^2}{4}, \tag{5.45}$$

$$(\xi^s_s)^2 \to \frac{4}{k^2d^2}, \tag{5.46}$$

$$\frac{1}{1+(\xi^s_{-s})^2} \to 1, \tag{5.47}$$

$$\frac{1}{1+(\xi^s_s)^2} \to \frac{k^2d^2}{4}, \tag{5.48}$$

$$\omega^s_s \to \frac{sk_\parallel kdb_0}{2} = \omega_M, \tag{5.49}$$

$$\omega^s_{-s} \to \frac{2s\Omega_0 k_\parallel}{k} = \omega_I. \tag{5.50}$$

Using these expansions, we write the asymptotic expressions for the terms in Equation (5.42) as;

$$\begin{aligned} A_{II} = \frac{\pi\epsilon^2}{4b_0^2}\int \sum_{s_1,s_2} \left(\frac{\sin\psi_k}{k}\right)^2 (sk + s_1k_1 + s_2k_2)^2 \frac{(s_2k_1 - s_1k_2)^2}{k_1^2k_2^2} \\ \times \frac{k^2\omega^s_{-s}}{k_\parallel^2} n^s_{-s} n^{s_1}_{-s_1} n^{s_2}_{-s_2} \left[\frac{k^2\omega^s_{-s}}{n^s_{-s}} - \frac{k_1^2\omega^{s_1}_{-s_1}}{n^{s_1}_{-s_1}} - \frac{k_2^2\omega^{s_2}_{-s_2}}{n^{s_2}_{-s_2}}\right] \\ \times \delta\left(\Omega_{k,k_1k_2}\right)\delta_{k,k_1k_2}\mathrm{d}\boldsymbol{k}_1\mathrm{d}\boldsymbol{k}_2, \end{aligned} \tag{5.51}$$

$$B_{IM} = \frac{\pi\epsilon^2}{8b_0^2}\int \sum_{s_1,s_1} k^2 d^2 \left(\frac{\sin\psi_k}{k}\right)^2 (sk + s_1k_1 + s_2k_2)^2 \frac{(k_2^2 - k_1^2 - k^2)^2}{k_1^2}$$
$$\times \frac{\omega_{-s}^s}{k_\parallel^2} n_{-s}^s n_{-s_1}^{s_1} n_{s_2}^{s_2} \left[\frac{k^2 d^2 \omega_{-s}^s}{4n_{-s}^s} - \frac{k_1^2 d^2 \omega_{-s_1}^{s_1}}{4n_{-s_1}^{s_1}} - \frac{\omega_{s_2}^{s_2}}{n_{s_2}^{s_2}}\right]$$
$$\times \delta\left(\Omega_{k,k_1k_2}\right)\delta_{k,k_1k_2}\mathrm{d}\boldsymbol{k}_1\mathrm{d}\boldsymbol{k}_2, \tag{5.52}$$

$$C_{MM} = \frac{\pi\epsilon^2}{16b_0^2}\int \sum_{s_1,s_2} k^2 d^2 \left(\frac{\sin\psi_k}{k}\right)^2 (sk + s_1k_1 + s_2k_2)^2 (s_2k_2 - s_1k_1)^2$$
$$\times \frac{\omega_{-s}^s}{k_\parallel^2} n_{-s}^s n_{s_1}^{s_1} n_{s_2}^{s_2} \left[\frac{k^2 d^2 \omega_{-s}^s}{4n_{-s}^s} - \frac{\omega_{s_1}^{s_1}}{n_{s_1}^{s_1}} - \frac{\omega_{s_2}^{s_2}}{n_{s_2}^{s_2}}\right]$$
$$\times \delta\left(\Omega_{k,k_1k_2}\right)\delta_{k,k_1k_2}\mathrm{d}\boldsymbol{k}_1\mathrm{d}\boldsymbol{k}_2. \tag{5.53}$$

Now consider the equation describing the dynamics of the magnetostrophic wave action, n_s^s *i.e.* $\Lambda = s$. The kinetic equation will assume a similar form as for inertial waves,

$$\partial_t n_s^s(\boldsymbol{k}) = D_{MM} + E_{IM} + F_{II}. \tag{5.54}$$

The expansions given in (5.43) – (5.50) are again used to give the individual terms as;

$$D_{MM} = \frac{\pi\epsilon^2}{b_0^2}\int \sum_{s_1,s_2} \left(\frac{\sin\psi_k}{k}\right)^2 (sk + s_1k_1 + s_2k_2)^2 (s_1k_1 - s_2k_2)^2 \frac{\omega_s^s}{k_\parallel^2}$$
$$\times n_s^s n_{s_1}^{s_1} n_{s_2}^{s_2} \left[\frac{\omega_s^s}{n_s^s} - \frac{\omega_{s_1}^{s_1}}{n_{s_1}^{s_1}} - \frac{\omega_{s_2}^{s_2}}{n_{s_2}^{s_2}}\right]\delta\left(\Omega_{k,k_1k_2}\right)\delta_{k,k_1k_2}\mathrm{d}\boldsymbol{k}_1\mathrm{d}\boldsymbol{k}_2, \tag{5.55}$$

$$E_{IM} = \frac{8\pi\epsilon^2}{b_0^2}\int \sum_{s_1,s_2} \left(\frac{\sin\psi_k}{k}\right)^2 (sk + s_1k_1 + s_2k_2)^2 \frac{\omega_s^s}{k_\parallel^2 k_1^2 d^4}$$
$$\times n_s^s n_{-s_1}^{s_1} n_{s_2}^{s_2} \left[\frac{\omega_s^s}{n_s^s} - \frac{k_1^2 d^2 \omega_{-s_1}^{s_1}}{4n_{-s_1}^{s_1}} - \frac{\omega_{s_2}^{s_2}}{n_{s_2}^{s_2}}\right]\delta\left(\Omega_{k,k_1k_2}\right)\delta_{k,k_1k_2}\mathrm{d}\boldsymbol{k}_1\mathrm{d}\boldsymbol{k}_2, \tag{5.56}$$

$$F_{II} = \frac{\pi\epsilon^2}{4b_0^2}\int \sum_{s_1,s_2} \left(\frac{\sin\psi_k}{k}\right)^2 (sk + s_1k_1 + s_2k_2)^2 (s_2k_1 - s_1k_2)^2$$
$$\times \frac{\left(k^2 - k_1^2 - k_2^2\right)^2}{k_1^2 k_2^2} \frac{\omega_s^s}{k_\parallel^2} n_s^s n_{-s_1}^{s_1} n_{-s_2}^{s_2} \left[\frac{\omega_s^s}{n_s^s} - \frac{k_1^2 d^2 \omega_{-s_1}^{s_1}}{4n_{-s_1}^{s_1}} - \frac{k_2^2 d^2 \omega_{-s_2}^{s_2}}{4n_{-s_2}^{s_2}}\right]$$
$$\times \delta\left(\Omega_{k,k_1k_2}\right)\delta_{k,k_1k_2}\mathrm{d}\boldsymbol{k}_1\mathrm{d}\boldsymbol{k}_2. \tag{5.57}$$

Equations (5.42) and (5.54) and their constituent terms are valid in all cases where $kd \to 0$.

5.4.1 Decoupled Kinetic Equations

First the kinetic equation resulting in the weak wave turbulence predictions by Galtier [24] are derived. This was touched upon in that paper, but a full derivation was not given. In this regime, we assume that their is no scale separation between the inertial waves and the magnetostrophic waves. In other words, we assume that the wavenumbers are of the same order for both the inertial waves and the magnetostrophic waves. Assume for now that for both waves

$$k \sim k_{\|} \sim 1, \tag{5.58}$$

the anisotropic assumption is made later. Now if we rename our small parameter $kd \equiv \lambda$, we get the following scalings;

$$b_0 \sim \lambda, \tag{5.59}$$

$$\Omega_0 \sim 1, \tag{5.60}$$

$$\omega_s^s \sim \lambda^2, \tag{5.61}$$

$$\omega_{-s}^s \sim 1, \tag{5.62}$$

$$n_s^s \sim 1/\lambda^2, \tag{5.63}$$

$$n_{-s}^s \sim 1. \tag{5.64}$$

The scaling for the wave actions n_s^s and n_{-s}^s come from ensuring that the total energy contained within the inertial waves is of the same order as the total energy in the magnetostrophic waves. Thus we have used

$$\int \omega_{-s}^s E_{-s}^s(\boldsymbol{k}) \mathrm{d}\boldsymbol{k} \sim \int \omega_s^s E_s^s(\boldsymbol{k}) \mathrm{d}\boldsymbol{k}, \tag{5.65}$$

together with the following relation for the energy given by Galtier [24]

$$E_\Lambda^s(\boldsymbol{k}) = \left[1 + (\xi_\Lambda^{-s})^2\right] n_\Lambda^s(\boldsymbol{k}). \tag{5.66}$$

Inertial waves

Now one can use the scalings given by (5.58) – (5.64) to compare the relative magnitudes of the terms in Equation (5.42). One can immediately neglect C_{MM} due to the resonance condition $\delta\left(\Omega_{k,k_1k_2}\right)$ because,

$$\begin{aligned}\delta\left(\Omega_{k,k_1k_2}\right) &= \delta(\omega^{s}_{-s} - \omega^{s_1}_{s_1} - \omega^{s_2}_{s_2}) \\ &\approx \delta(\omega^{s}_{-s}),\end{aligned} \tag{5.67}$$

and thus the delta function is non-zero only if ω^{s}_{-s} is zero which then results in the whole term being zero. The remaining two terms scale as follows:

$$A_{II} \sim 1/\lambda^2, \tag{5.68}$$

$$B_{IM} \sim 1, \tag{5.69}$$

and thus B_{IM} is negligible and we get for the kinetic equation,

$$\begin{aligned}\partial_t n^{s}_{-s}(\boldsymbol{k}) = \frac{\pi\epsilon^2}{4b_0^2}\int \sum_{s_1,s_2}\left(\frac{\sin\psi_k}{k}\right)^2 (sk + s_1k_1 + s_2k_2)^2\,\frac{(s_2k_1 - s_1k_2)^2}{k_1^2k_2^2} \\ \times \frac{k^2\omega^{s}_{-s}}{k_\parallel^2} n^{s}_{-s} n^{s_1}_{-s_1} n^{s_2}_{-s_2}\left[\frac{k^2\omega^{s}_{-s}}{n^{s}_{-s}} - \frac{k_1^2\omega^{s_1}_{-s_1}}{n^{s_1}_{-s_1}} - \frac{k_2^2\omega^{s_2}_{-s_2}}{n^{s_2}_{-s_2}}\right] \\ \times \delta\left(\Omega_{k,k_1k_2}\right)\delta_{k,k_1k_2}\mathrm{d}\boldsymbol{k}_1\mathrm{d}\boldsymbol{k}_2.\end{aligned} \tag{5.70}$$

Magnetostrophic waves

This reasoning can now be applied to Equation (5.54) describing the magnetostrophic waves. As with the inertial waves, one term can be ignored due to the frequency resonance condition. In this case, it is E_{IM} which is zero, since

$$\begin{aligned}\delta\left(\Omega_{k,k_1k_2}\right) &= \delta(\omega^{s}_{s} - \omega^{s_1}_{-s_1} - \omega^{s_2}_{s_2}) \\ &\approx \delta(\omega^{s}_{-s_1}),\end{aligned} \tag{5.71}$$

which is again non-zero only if $\omega^{s_1}_{-s_1}$ is zero. This is a contradiction since $\omega^{s_1}_{-s_1}$ is the largest frequency. Therefore, E_{IM} is zero. The other two terms scale as;

$$D_{MM} \sim 1/\lambda^2, \tag{5.72}$$

$$F_{II} \sim 1, \tag{5.73}$$

thus, the term containing only magnetostrophic waves is dominant and the kinetic equation can be written,

$$\partial_t n_s^s(\boldsymbol{k}) = \frac{\pi\epsilon^2}{b_0^2}\int\sum_{s_1,s_2}\left(\frac{\sin\psi_k}{k}\right)^2(sk+s_1k_1+s_2k_2)^2\,(s_1k_1-s_2k_2)^2\,\frac{\omega_s^s}{k_\parallel^2}$$
$$\times\, n_s^s n_{s_1}^{s_1} n_{s_2}^{s_2}\left[\frac{\omega_s^s}{n_s^s}-\frac{\omega_{s1}^{s1}}{n_{s1}^{s1}}-\frac{\omega_{s2}^{s2}}{n_{s2}^{s2}}\right]\delta\left(\Omega_{k,k_1k_2}\right)\delta_{k,k_1k_2}\mathrm{d}\boldsymbol{k}_1\mathrm{d}\boldsymbol{k}_2. \tag{5.74}$$

We have then, that the kinetic equations for both inertial and magnetostrophic waves contain only interactions between those waves, or in other words, inertial and magnetostrophic waves are completely decoupled in the asymptotic as $kd \to 0$.

5.4.2 Coupled Kinetic Equations

In the derivation of the previous kinetic equations, it was assumed that there was no scale separation between the inertial and magnetostrophic waves. This resulted in a decoupling between the two types of wave. This decoupling is a useful property in terms of simplifying the kinetic equations and makes finding stationary solutions possible. A regime in which this decoupling did not occur such that there was a transfer of energy between the two waves would be interesting dynamically. One way to find such a regime would be to incorporate the two terms which were neglected before, *i.e.* C_{MM} and E_{IM}. These two terms are non zero if $\omega_I = \omega_{-s}^s = \frac{2\Omega_0 s k_\parallel}{k}$ and $\omega_M = \omega_s^s = \frac{sk_\parallel k d b_0}{2}$ are both of the same order of magnitude. This can be achieved if we scale the wave numbers for the inertial waves such that

$$k = \mathcal{O}(1) \quad \text{and} \quad k_\parallel = \mathcal{O}(\lambda^2), \tag{5.75}$$

i.e. the anisotropic limit. The wave numbers for the magnetostrophic waves are left unchanged so that the parallel component is still of order one. The frequencies and the wave action spectra now scale as follows

$$\omega_{-s}^s \sim \lambda^2, \tag{5.76}$$

$$\omega_s^s \sim \lambda^2, \tag{5.77}$$

$$n_{-s}^s \sim 1, \tag{5.78}$$

$$n_s^s \sim 1, \tag{5.79}$$

where once again the energy in the inertial and magnetostrophic waves is assumed to be of the same order of magnitude.

Now that the frequencies are all of the same order, no terms are zero due to the frequency resonance condition. However, B_{IM} and F_{II} are zero due to the wavenumber resonance condition. To see this, first note the following property of the Dirac delta function

$$\begin{aligned}\delta_{k,k_1k_2} &\equiv \delta(\boldsymbol{k}-\boldsymbol{k_1}-\boldsymbol{k_2}) \\ &= \delta(\boldsymbol{k}_\perp-\boldsymbol{k}_{1\perp}-\boldsymbol{k}_{2\perp})\delta(k_\parallel-k_{1\parallel}-k_{2\parallel}).\end{aligned} \tag{5.80}$$

The parallel wavenumber delta function in B_{IM} is then

$$\delta(k_\parallel-k_{1\parallel}-k_{2\parallel}) \approx \delta(k_{2\parallel}), \tag{5.81}$$

which implies that $k_{2\parallel}$ must be zero but this is the largest parallel wavenumber, hence the term is zero. The F_{II} term is zero due to the same argument. The remaining terms have the following orders of magnitude

$$A_{II} \sim 1/\lambda^2, \tag{5.82}$$

$$C_{MM} \sim 1/\lambda^2, \tag{5.83}$$

$$D_{MM} \sim 1, \tag{5.84}$$

$$E_{IM} \sim 1/\lambda^2. \tag{5.85}$$

From this we see that in this range of wave numbers, the kinetic equation for inertial waves is, to leading order

$$\begin{aligned}\partial_t n^s_{-s}(\boldsymbol{k}) = \frac{\pi\epsilon^2}{4b_0^2}\int\sum_{s_1,s_2}&\left(\frac{\sin\psi_k}{k}\right)^2(sk+s_1k_1+s_2k_2)^2\,\frac{(s_2k_1-s_1k_2)^2}{k_1^2k_2^2} \\ &\times\frac{k^2\omega^s_{-s}}{k_\parallel^2}n^s_{-s}n^{s_1}_{-s_1}n^{s_2}_{-s_2}\left[\frac{k^2\omega^s_{-s}}{n^s_{-s}}-\frac{k_1^2\omega^{s_1}_{-s_1}}{n^{s_1}_{-s_1}}-\frac{k_2^2\omega^{s_2}_{-s_2}}{n^{s_2}_{-s_2}}\right] \\ &\times\delta\left(\Omega_{k,k_1k_2}\right)\delta_{k,k_1k_2}\mathrm{d}\boldsymbol{k}_1\mathrm{d}\boldsymbol{k}_2 \\ -\frac{\pi\epsilon^2}{16b_0^2}\int\sum_{s_1,s_2}&k^2d^2\left(\frac{\sin\psi_k}{k}\right)^2(sk+s_1k_1+s_2k_2)^2\,(s_2k_2-s_1k_1)^2 \\ &\times\frac{\omega^s_{-s}}{k_\parallel^2}n^s_{-s}n^{s_1}_{s_1}n^{s_2}_{s_2}\left[\frac{\omega^{s_1}_{s_1}}{n^{s_1}_{s_1}}+\frac{\omega^{s_2}_{s_2}}{n^{s_2}_{s_2}}\right] \\ &\times\delta\left(\Omega_{k,k_1k_2}\right)\delta_{k,k_1k_2}\mathrm{d}\boldsymbol{k}_1\mathrm{d}\boldsymbol{k}_2.\end{aligned} \tag{5.86}$$

Similarly, the kinetic equation for magnetostrophic waves is

$$\partial_t n_s^s(\boldsymbol{k}) = \frac{8\pi\epsilon^2\Omega^4}{b_0^6}\int\sum_{s_1,s_2}\left(\frac{\sin\psi_k}{k}\right)^2(sk+s_1k_1+s_2k_2)^2\,\frac{\omega_s^s}{k_\parallel^2k_1^2}$$
$$\times\, n_s^s n_{-s_1}^{s_1} n_{s_2}^{s_2}\left[\frac{\omega_s^s}{n_s^s}-\frac{\omega_{s_2}^{s_2}}{n_{s_2}^{s_2}}\right]\delta\left(\Omega_{k,k_1k_2}\right)\delta_{k,k_1k_2}\mathrm{d}\boldsymbol{k}_1\mathrm{d}\boldsymbol{k}_2. \tag{5.87}$$

Note that in both of these equations, the integration is performed over $k_{1\parallel}$, $k_{2\parallel}$, $\boldsymbol{k}_{1\perp}$ and $\boldsymbol{k}_{2\perp}$. One of the parallel integrals can be performed using the $k_\parallel$ component of the $\boldsymbol{k}$-delta function and the other can be performed using the frequency delta function. We concentrate on the magnetostrophic waves to begin with. Furthermore, the frequency resonance condition gives $k_\parallel = k_{2\parallel}$, thus, writing $n_s^s(\boldsymbol{k}) = f(k_\parallel)n_\perp^M(k_\perp)$, $f(k_\parallel)$ cancels from both sides and we get the reduced form for the magnetostrophic wave equation

$$\partial_t n_\perp^M(k_\perp) = \frac{\Omega_0^3\pi\epsilon^2}{8b_0^6}\int\sum_{s_1,s_2}\frac{4k_{1\perp}^2(k_{2\perp}+k_\parallel)^2-\left(k^2-k_{1\perp}^2-(k_{2\perp}+k_\parallel)^2\right)^2}{k^4k_\parallel^2k_{1\perp}(k_{2\perp}+k_\parallel)^2s_1}$$
$$\times\left(sk-s_1k_{1\perp}+s_2(k_{2\perp}+k_\parallel)\right)^2$$
$$\times\left[\omega^M(k_\perp,k_\parallel)n_\perp^M(k_{2\perp})-\omega^M(k_{2\perp},k_\parallel)n_\perp^M(k_\perp)\right]$$
$$\times\,\omega^M(k_\perp,k_\parallel)n^I(k_{1\perp},0)\delta(\boldsymbol{k}_\perp-\boldsymbol{k}_{1\perp}-\boldsymbol{k}_{2\perp})\mathrm{d}\boldsymbol{k}_{1\perp}\mathrm{d}\boldsymbol{k}_{2\perp}. \tag{5.88}$$

Now note that the only part of this equation which depends upon the perpendicular vectors rather than merely the magnitude is the delta function, and so only this needs to be averaged over angles. This can be done using the following angular integration

$$\int\delta(k_\perp-k_{1\perp}\cos\theta_1-k_{2\perp}\cos\theta_2)\mathrm{d}\theta_1\mathrm{d}\theta_2 = S_{12k}^\perp, \tag{5.89}$$

where

$$S_{12k}^\perp = \frac{1}{2\sqrt{2\left(k_\perp^2k_{1\perp}^2+k_\perp^2k_{2\perp}^2+k_{1\perp}^2k_{2\perp}^2\right)-k_\perp^4-k_{1\perp}^4-k_{2\perp}^4}}. \tag{5.90}$$

Thus the kinetic equation for magnetostrophic waves can be written

$$\partial_t n_\perp^M(k_\perp) = \frac{\Omega_0^3\pi\epsilon^2}{8b_0^6}\int\sum_{s_1,s_2}\frac{4k_{1\perp}^2(k_{2\perp}+k_\parallel)^2-\left(k^2-k_{1\perp}^2-(k_{2\perp}+k_\parallel)^2\right)^2}{k^4k_\parallel^2k_{1\perp}(k_{2\perp}+k_\parallel)^2s_1}$$
$$\times\, k_{1\perp}k_{2\perp}S_{12k}^\perp\left(sk-s_1k_{1\perp}+s_2(k_{2\perp}+k_\parallel)\right)^2$$
$$\times\left[\omega^M(k_\perp,k_\parallel)n_\perp^M(k_{2\perp})-\omega^M(k_{2\perp},k_\parallel)n_\perp^M(k_\perp)\right]$$
$$\times\,\omega^M(k_\perp,k_\parallel)n^I(k_{1\perp},0)\delta(k_\parallel-k_{1\parallel}-k_{2\parallel})\mathrm{d}k_{1\perp}\mathrm{d}k_{2\perp}. \tag{5.91}$$

The above analysis cannot be performed on the equation for inertial waves due to the fact that the frequency resonance condition for the second term in this equation has a quadratic dependence on the $k_\parallel$ variables. It is possible to integrate over one of the parallel wave numbers using the other resonance condition, but in order to retain symmetry, it is preferable not to do so. It is however still possible to average over the angular variables using the perpendicular delta function if we first rewrite $\frac{\sin\psi_k}{k}$ in terms of magnitudes only, doing this leads to the following kinetic equation for inertial waves

$$\begin{aligned}\partial_t n^s_{-s}(\boldsymbol{k}) = \frac{\pi\epsilon^2}{4b_0^2}\int\sum_{s_1,s_2} S^\perp_{12k}\frac{4k_{1\perp}^2k_{2\perp}^2-(k_\perp^2-k_{1\perp}^2-k_{2\perp}^2)}{k_{1\perp}^3k_{2\perp}^3}\left(sk_\perp+s_1k_{1\perp}+s_2k_{2\perp}\right)^2\\ \times\left(s_2k_{1\perp}-s_1k_{2\perp}\right)^2\frac{\omega^s_{-s}}{k_\parallel^2}n^s_{-s}n^{s_1}_{-s_1}n^{s_2}_{-s_2}\left[\frac{k^2\omega^s_{-s}}{n^s_{-s}}-\frac{k_1^2\omega^{s_1}_{-s_1}}{n^{s_1}_{-s_1}}-\frac{k_2^2\omega^{s_2}_{-s_2}}{n^{s_2}_{-s_2}}\right]\\ \times\delta\left(\Omega_{k,k_1k_2}\right)\delta(k_\parallel-k_{1\parallel}-k_{2\parallel})\mathrm{d}k_{1\parallel}\mathrm{d}k_{2\parallel}\mathrm{d}k_{1\perp}\mathrm{d}k_{2\perp}\\ -\frac{\pi\epsilon^2}{16b_0^2}\int\sum_{s_1,s_2}k^2d^2k_{1\perp}k_{2\perp}S^\perp_{12k}\frac{4k_1^2k_2^2-(k_\perp^2-k_1^2-k_2^2)}{k_1^2k_2^2}\left(sk+s_1k_1+s_2k_2\right)^2\\ \times\left(s_2k_2-s_1k_1\right)^2\frac{\omega^s_{-s}}{k_\parallel^2}n^s_{-s}n^{s_1}_{s_1}n^{s_2}_{s_2}\left[\frac{\omega^{s_1}_{s_1}}{n^{s_1}_{s_1}}+\frac{\omega^{s_2}_{s_2}}{n^{s_2}_{s_2}}\right]\\ \times\delta\left(\Omega_{k,k_1k_2}\right)\delta(k_\parallel-k_{1\parallel}-k_{2\parallel})\mathrm{d}k_{1\parallel}\mathrm{d}k_{2\parallel}\mathrm{d}k_{1\perp}\mathrm{d}k_{2\perp}.\end{aligned}\tag{5.92}$$

The Equations (5.86) and (5.92) above describe the dynamics of the inertial and magnetostrophic wave action spectra in a regime where there is coupling between the two types of wave. This regime is realised when there is a scale separation between the waves such that the perpendicular wavenumber dominates the parallel wavenumber in inertial range but are of the same scale in magnetostrophic waves. It is not yet clear whether this regime has any physical relevance but it offers an interesting dynamical regime where there may be significant transfer between kinetic and magnetic energy.

5.5 Conclusions

In this section rotating MHD has been studied within the context of wave turbulence. The weak wave turbulence predictions have been discussed with the use of a phenomenological derivation. Furthermore a new prediction based on the critical balance approach has been given. Numerical simulations have then been presented with attempted to verify the predictions. In the simulation A, the energy spectra have been produced for the kinetic and magnetic energy. Distinguishing between

the prediction of weak wave turbulence and strong wave turbulence is difficult given their similar scaling properties, however with the use of the spatio-temporal spectra and the ratios of linear to nonlinear time scales, we conclude that the magnetic energy spectra is a result of a critically balanced state whereas the kinetic energy seems to contain a mixture of waves and vortices. Simulation B presents spatio-temporal spectra and ratios of time scales which indicate the dominance of linear waves in the system. The energy spectra have again been plotted. These appear to be much steeper than either of the predictions and we conclude that they are a result of a frozen turbulence *i.e.* a non cascading wave system.

In the final section, the kinetic equation has been discussed. Two regimes have been studied; one in which there is a decoupling between inertial and magnetostrophic waves and one in which there is coupling. The former regime is the one on which the weak wave turbulence predictions are based. The latter is a regime which does not yet have a clear physical relevance, but may offer interesting transfer of energy between kinetic energy and magnetic energy.

Chapter 6

Conclusions

In this thesis rotating and non-rotating MHD has been studied with specific emphasis on the Weak Wave Turbulence theory. Two introductory chapters have been included which give some historical context to the work and a fundamental understanding of both MHD and turbulence. Using a model equation, the weak wave turbulence theory has been demonstrated showing the derivation of the kinetic equation which is vital to wave turbulence.

In chapter 3 self-similar solutions of the kinetic equation have been studied. Such self-similar solutions preclude the formation of the stationary spectrum. The self-similar solutions are of the second kind which, by definition means that the self-similarity parameters cannot be uniquely defined by a conservation law. Instead, there remains a single parameter which depends on the shape of the self-similar solution. This parameter has been found by numerically solving a nonlinear eigenvalue problem. It has been proven that the tail of the self-similar solution at large η cannot be exponentially or super-exponentially decaying as is often believed in similar systems. Instead the tail is shown to behave as a power law. The formulation of the nonlinear eigenvalue problem and the methods for analysing the large η asymptotics can be applied to other kinetic equations in Wave Turbulence and to the Smoluchowski kinetic equation.

In chapter 4, the next stage in the formation of the stationary spectrum is studied. This is the reflected wave solution. As in the previous stage, this is again characterised by a self-similar solution of the kinetic equation. These self-similar solutions cannot be fixed by either a conservation law or by solving a nonlinear eigenvalue problem, but are instead determined by imposing asymptotics at one end of the similarity interval based on the solution for the preceding self-similar stage. Similar to the terminology used for other self-similar solutions, these solutions are

dubbed self-similar solutions of the third kind. While the similarity variables are able to be fixed without solving an eigenvalue problem, there remains a constant in front of the KZ power law which must be determined. This constant is found by numerically solving the integro-differential equation describing the self-similar dynamics. The solutions found in this chapter, provide further understanding of the formation of the stationary spectrum. This has application to other wave turbulence systems.

The work developed in chapters 3 and 4 could be applied to a number of other wave turbulence systems in order to build a fuller picture of how the stationary solution forms in each system.

In chapter 5 the rotating MHD system has been studied using direct numerical simulation of the governing equations. The weak wave turbulence theory for MHD has been reviewed. Furthermore scalings for the kinetic and magnetic energy spectra for strong turbulence have been derived based upon the critical balance phenomenology. These scalings have been compared to numerical simulations of rotating MHD and seem to corroborate the strong turbulence scalings. The kinetic equation itself has been analysed, including a discussion on coupled and decoupled regimes. The theory developed is based on a decoupled regime, however, a regime in which the kinetic and magnetic regimes are coupled would have potential applications to the magnetic dynamo in rotating planetary systems.

Bibliography

[1] V. I. Abramenko. Relationship between magnetic power spectrum and flare productivity in solar active regions. *Astrophys. J.*, 629:1141–1149, 2005.

[2] H. Alfvén. Existence of electromagnetic-hydrodynamic waves. *Nature*, 150:405–406, 1942.

[3] S. Annenkov and V. Shrira. New numerical method for surface waves hydrodynamics based on the zakharov equation. *J. Fluid Mech.*, 449:341–371, 2001.

[4] S. Annenkov and V. Shrira. Role of non-resonant interactions in evolution of nonlinear random water wave fields. *J. Fluid Mech.*, 561:181–207, 2006.

[5] G. I. Barenblatt and Ya B. Zeldovich. Self-similar solutions as intermediate asymptotics. *Annual Review of Fluid Mechanics*, 1972.

[6] N. K. Bell, V. Grebenev, S. Medvedev, and S. Nazarenko. Self-similar evolution of alfvén wave turbulence. *Journal of Physics A: Mathematical and Theoretical*, 50(435501), 2017.

[7] N. K. Bell and S. Nazarenko. Reflected wave solution of alfvén wave turbulence. *Journal of Physics A: Mathematical and Theoretical*, 51(40), 2018.

[8] F. Bellet, F. S. Godeferd, J. Scott, and C. Cambon. Wave turbulence in rapidly rotating flows. *J. Fluid Mech.*, 562:83–121, 2006.

[9] D. J. Benney and A. C. Newell. Random wave closures. *Studies Appl. Math.*, 48(1):29, 1969.

[10] D. J. Benney and P. Saffman. Nonlinear interaction of random waves in a dispersive medium. *Proc. R. Soc. A*, 289:301–320, 1966.

[11] D. Biskamp. *Magnetohydrodynamic turbulence*. Cambridge University Press, 2003.

[12] S. Boldyrev, J. C. Perez, J. E. Borovsky, and J. J. Podesta. Spectral scaling laws in magnetohydrodynamic turbulence simulations and the the solar wind. *The asrophysical journal letters*, 741(1), 2011.

[13] C. Connaughton and S. Nazarenko. A model equation for turbulence. *ArXiv:physics/0304044*.

[14] C. Connaughton and S. Nazarenko. Warm cascade and anomalous scaling in a diffusion model of turbulence. *Phys. Rev. Lett.*, 92(044501), 2004.

[15] M. Dobrowolny, A. Mangeney, and P. Veltri. Fully developed anisotropic hydromagnetic turbulence in interplanetary space. *Phys. Rev. Lett.*, 45(144), 1980.

[16] A Dyachenko, A. C. Newell, A. Pushkarev, and V. E. Zakharov. Optical turbulence: weak turbulence, condensates and collapsing fragments in the nonlinear schrodinger equation. *Phys. D*, 57(1-2), 1992.

[17] W. M Elsässer. The hydromagnetic equations. *Phys. Rev.*, 79:183, 1950.

[18] C. C. Finlay. Waves in the presence of magnetic fields, rotation and convection. In P. Cardin, editor, *Dynamos*, volume 88, pages 403–450. Elsevier science publishers, 2008.

[19] Falkovich. G. and A.V. Shafarenko. Non-stationary wave turbulence. *J. Nonlinear Sci.*, 1:457–480, 1991.

[20] A. A. Galeev and R. Z. Sagdeev. Review of plasma physics. In *Leontovich, M. A. (ed.)*, volume 7, page 307. Consultants Bureau, New York, 1979.

[21] S. Galtier. Weak inertial-wave turbulence theory. *Phys. Rev. E*, 68(015301), 2003.

[22] S. Galtier. Wave turbulence in incompressible hall magnetohydrodynamics. *J. Plasma Phys.*, 72(5):721–769, October 2006.

[23] S. Galtier. Wave turbulence in astrophysics. In V. Shrira and S. Nazarenko, editors, *Advances in Wave Turbulence*, volume 83 of *A*. World Scientific, 2013.

[24] S. Galtier. Weak turbulence theory for rotating magnetohydrodynamics and planetary flows. *J. Fluid Mech.*, 757:114–154, 2014.

[25] S. Galtier and A Bhattacharjee. Anisotropic wave turbulence in electron mhd. *Plasma Phys. Control Fusion*, (47):B791–B701, 2005.

[26] S. Galtier, S. Nazarenko, and A. C. Newell. On wave turbulence in mhd. *Nonlinear Processes in Geophysics*, 8(3):141–150, May 2001.

[27] S. Galtier, S. Nazarenko, A. C. Newell, and A. Pouquet. A weak turbulence theory for incompressible mhd. *J. Plasma Phys.*, 63(447), 2000.

[28] S. Galtier, S. Nazarenko, A. C. Newell, and A. Pouquet. Anisotropic turbulence of shear-alfvén waves. *Astrophys. J.*, 564, 2002.

[29] P. Goldreich and S. Sridhar. Toward a theory of interstellar turbulence. 2: strong alfvénic turbulence. *Astrophys. J.*, 438(2):763–775, 1995.

[30] D. O. Gómez, P. D. Mininni, and P. Dmitruk. Parallel simulations in turbulent mhd. *Physica Scripta*, (T116):123, 2005.

[31] V. Grebenev, S. Nazarenko, S. Medvedev, I. Schwab, and Yu. A. Chirkunov. Self-similar solution in the leith model of turbulence: anomalous power law and asymptotic analysis. *Journal of Physics A: Mathematical and Theoretical*, 47(2):025501, 2013.

[32] K. Hasselman. On the nonlinear energy transfer in a gravity wave spectrum part 1. *J. Fluid Mech.*, 12:481–500, 1962.

[33] K. Hasselman. On the nonlinear energy transfer in a gravity wave spectrum part 2. *J. Fluid Mech.*, 15:273–281, 1963.

[34] P. S. Iroshnikov. Turbulence of a conducting fluid in a strong magnetic field. *Sov. Astron.*, 7:566–571, 1964.

[35] A. N. Kolmogorov. The local structure of turbulence in incompressible viscous fluid for very large reynolds numbers. *Dokl. Akad. Nauk. SSSR*, 30:301–305, 1941.

[36] E. V. Kozik and B. V. Svistunov. Kelvin-wave cascade and decay of superfluid turbulence. *Phys. Rev. Lett.*, 92(035301), 2004.

[37] R. H. Kraichnan. Inertial range spectrum in hydromagnetic turbulence. *Phys. Fluids*, 8:1385–1387, 1965.

[38] E. A. Kuznetsov. Turbulence of ion sound in a plasma located in a magnetic field. *Sov. Phys. J. Exp. Theor. Phys.*, 35:310–314, 1972.

[39] Bo Lehnert. Magneto-hydrodynamic waves in liquid sodium. *Phys. Rev.*, 94(815), 1954.

[40] C. E. Leith. Diffusion approximation to intertial energy transfer in isotropic turbulence. *Phys. Fluids*, 10:1409, 1967.

[41] C. E. Leith. Atmospheric predictability and two-dimensional turbulence. *J. Atmospheric Sciences*, 28(2):145–161, March 1971.

[42] P. C. Leoni, P. J. Cobelli, and P. D. Mininni. The spatio-temporal spectrum of turbulent flows. *The European Physical Journal E*, 38(136), 2015.

[43] S. Lundquist. Experimental investigations of magneto-hydrodynamic waves. *Phys. Rev.*, 76(1805), 1949.

[44] V. S. L'vov, S. Nazarenko, and O. Rudenko. Bottleneck crossover between classical and quantum superfluid turbulence. *Phys. Rev. B*, 76(024520), 2007.

[45] J. Mason, F. Cattaneo, and S. Boldyrev. Numerical measurements of the spectrum in magnetohydrodynamic turbulence. *Phys. Rev. E*, 77(036403), 2008.

[46] R. Meyrand, S. Galtier, and K. Kiyani. Direct evidence of the transition from weak to strong magnetohydrodynamic turbulence. *Phys. Rev. Lett.*, 116(105002), 2016.

[47] R. Meyrand, K. Kiyani, and S. Galtier. Intermittency in weak mhd turbulence. *J. Fluid Mech.*, 770, 2015.

[48] R. Meyrand, K. Kiyani, O. D. Gurcan, and S. Galtier. Coexistence of weak and strong wave turbulence in incompressible hall magnetohydrodynamics. *arXiv:1712.10002*, 2017.

[49] P. D. Mininni and A. Pouquet. Energy spectra stemming from interactions of alfvén waves and turbulent eddies. *Phys. Rev. Lett.*, 99(254502), 2007.

[50] P. D. Mininni and A. Pouquet. Rotating helical turbulence. i. global evolution and spectral behaviour. *Phys. Fluids*, 22 (3)(035105), 2010.

[51] P. D. Mininni, D. Rosenberg, and A. Pouquet. Isotropization at small scales of rotating helically driven turbulence. *J. Fluid Mech.*, 699:263–279, 2012.

[52] P. D. Mininni, D. Rosenberg, R. Reddy, and A. Pouquet. A hybrid mpi–openmp scheme for scalable parallel pseudospectral computations for fluid turbulence. *Parallel Computing*, 37(6):316–326, 2011.

[53] D. C. Montgomery and W. H. Matthaeus. Anisotropic modal energy transfer in interstellar turbulence. *Astrophys. J.*, 447, 1995.

[54] S. Nazarenko. 2d enslaving of mhd turbulence. *New J. Phys.*, 9(307), 2007.

[55] S. Nazarenko. *Wave Turbulence*. Lecture Notes in Physics. Springer, 2011.

[56] S. Nazarenko and V. Grebenev. Self-similar formation of the kolmogorov spectrum.

[57] S. Nazarenko, A. C. Newell, and S. Galtier. Non-local mhd turbulence. *Physica D*, 2001.

[58] S. Nazarenko and M. Onorato. Wave turbulence and vortices in bose-einstein condensation. *Phys. D*, 219:1–12, 2006.

[59] S. Nazarenko and A. Schekochichin. Critical balance in magnetohydrodynamic, rotating and stratified turbulence: towards a universal scaling conjecture. *J. Fluid Mech.*, 677:134, 2011.

[60] A. C. Newell, S. Nazarenko, and L. Biven. Wave turbulence and intermittency. *Physica D*, pages 520–550, 2001.

[61] A. C. Newell and B. Rumpf. Wave turbulence. *Ann. Rev. Fluid Mech.*, 43:59–78, 2011.

[62] C. S. Ng and A Bhattacharjee. Interaction of shear-alfvén wave packets: Implication for weak magnetohydrodynamic turbulence in astrophysical plasmas. *Astrophys. J.*, 465, 1996.

[63] A. M. Obukhov. On the distribution of energy in the spectrum of turbulent flow. *Dokl. Akad. Nauk SSSR*, 32(1):22–24, 1941.

[64] R. Peierls. Zur kinetischen theorie der wärmeleitung in kristallen. *Ann. Phys.*, 395:1055–1101, 1929.

[65] J. C. Perez and S. Boldyrev. On weak and strong magnetohydrodynamic turbulence. *The asrophysical journal letters*, 672(1), 2007.

[66] E. Priest. *Magnetohydrodynamics of the sun*. Cambridge University Press, 2014.

[67] A. Pushkarev. On the kolmogorov and frozen turbulence in numerical simulation of capillary waves. *Eur. J. Mech. B/Fluids*, 18(3):345, 1999.

[68] A. Pushkarev and V. E. Zakharov. Turbulence of capillary waves – theory and numerical simulation. *Phys. D*, 135(1–2):98, 2000.

[69] O. Reynolds. An experimental investigation of the circumstances which determine whether the motion of water shall be direct or sinuous and of the law of resistance in parallel channels. *Proc. R. Soc. Lond.*, 35:84–99, 1883.

[70] L. F. Richardson. *Proc. R. Soc. Lond. Ser. A*, 110:709, 1926.

[71] P. H. Roberts and G. Belmont. On the genesis of the earth's magnetism. *Rep. Prog. Phys.*, 76 (9), 2013.

[72] Fjørtoft. On changes in the spectral distribution of kinetic energy for two-dimensional non-divergent flow. *Tellus*, 5(225), 1953.

[73] J. Saur, H. Politano, A. Pouquet, and W. H. Matthaeus. Evidence for weak mhd turbulence in the middle magnetosphere of jupiter. *Astron. astrophys.*, 386:699–708, 2002.

[74] A. Schekochichin and S. Nazarenko. Weak alfvén wave turbulence revisited. *Phys. Rev. E*, 85(3), March 2012.

[75] J. H. Shirley and R. W. Fairbridge. *Encyclopedia of Planetary Sciences*. Springer, 1997.

[76] S. Sridhar and P. Goldreich. Toward a theory of interstellar turbulence. 1: Weak alfvenic turbulence. *Astrophys. J.*, 432(2), 1994.

[77] T. Teitelbaum and P. D. Mininni. Effect of helicity and rotation on the free decay of turbulent flows. *Phys. Rev. Lett.*, 103 (1)(014501), 2012.

[78] J. M. TenBarge and G. G. Howes. Evidence of critical balance in kinetic alfvén wave turbulence simulations. *Physics of Plasmas*, 19(5), 2011.

[79] S. Thalabard, S. Nazarenko, S. Galtier, and S. Medvedev. Anomalous spectral laws in differential models of turbulence. *Journal of Physics A: Mathematical and Theoretical*, 48(28):285501, 2015.

[80] A. A. Vedenov. Theory of weakly turbulent plasma. In *Leontovich, M. A. (ed.) Reviews of Plasma Physics*, volume 3, page 229. Consultants Bureau, New York, 1967.

[81] M. Verma. Statistical theory of magnetohydrodynamic turbulence. *Phys. Rep.*, 401, 2004.

[82] L. Woltjer. On hydrodynamic equilibrium. *Proc. Natl. Acad. Sci.*, 46:833–841, 1958.

[83] V. E. Zakharov. Weak turbulence in media with decay spectrum. *J. Appl. Mech. Tech. Phys.*, 4:22–24, 1965.

[84] V. E. Zakharov, V. S. L'vov, and Falkovich. G. *Kolmogorov Spectra of Turbulence 1: Wave Turbulence*. Springer, Berlin, 1992.

[85] Ya B. Zeldovich. The morion of a gas under the action of a short time pressure (shock). *Akust. Zh. 2*, pages 25–35, 1956.

[86] Ya B. Zeldovich and Yu P. Raizer. *Physics of Shock-waves and High-temperature Phenomena*, volume 2. Academic Press, 1966.